Role of Mitochondrial Protein TCAIM in Preventing Lung Infiltration and T cell-induced Immunopathology

Inaugural-Dissertation

to obtain the academic degree

Doctor rerum naturalium (Dr. rer. nat.)

submitted to the Department of Biology, Chemistry, Pharmacy

of Freie Universität Berlin

by

Julia Stein

from Berlin

Berlin, 2024

The doctoral studies presented herein were commenced in March 2019 at Berlin Institute of Health (BIH) & Charité Universitätsmedizin Berlin under supervision of Prof. Dr. Birgit Sawitzki until July 2024.

1st Reviewer: Prof. Dr. Birgit Sawitzki, Berlin Institute of Health (BIH) & Charité Universitätsmedizin Berlin

2nd Reviewer: Prof. Dr. Rainer Haag, Freie Universität Berlin

Date of defense: 20.11.2024

Acknowledgments

First of all, I would like to thank Prof. Dr. Birgit Sawitzki for giving me the opportunity to perform my doctoral thesis in her lab and under her guidance. Dear Birgit, I appreciated your love for science, enthusiasm and strong work ethic over all those years.

I also thank Prof. Dr. Rainer Haag for reviewing my doctoral thesis.

Moreover, I would like to thank all my collaborators.

Prof. Dr. Martin Witzenrath for providing lab space for the infection experiments and offering his advice. Also, all lab-members of AG Witzenrath, AG Hocke and AG Opitz for welcoming me. Special thanks go to Birgitt, Geraldine and Peter for giving advice, sharing their experience and helping out during the infection experiments.

Dr. Sandra Kunder and Prof. Dr. Achim Gruber for providing their expertise in analysing the histology samples and guidance in choosing the areas for IMC.

Dr. Jakob Trimpert for advice and performing the HAI assay.

A big thank you goes to all the current (Adrian, Christina, Christine, Juliette, Katrin, Lev, Lucas, Manuela, Matthias, Olufemi, Peggy, Selin, Somesh, Tomislav, Zeynep) and past (Christiane, Daniela, Emma, Hannah, Inga, Katarina, Karla, Kerstin, Laia, Lucas, Maria, Martin, Laura, Sophia, Tizia) members of AG Sawitzki - for the provided help in the lab or with bioinformatics and for creating a comfortable atmosphere at work every day.

I would like to thank Olufemi, Lev and Zeynep for supporting me in my R-adventure despite their own busy schedules.

Also, thank you to Tomi, who always had an open ear and lifted the mood with his positivity. I really enjoyed our time as office neighbours.

I am very grateful for sharing the ups and downs of the last couple of weeks with Juliette. Dear Juliette, I could not have asked for a better companion and moral support.

Special thanks go to Katrin, Christine and Christina - you have been there since the beginning. All along the way I could count on you providing comfort in difficult times and celebrating with me every small and big achievement. Dear Christina, I value your critical, scientific thinking and your ambition to deliver always in the best and precise way you can. Most importantly I am thankful for your support and the companion- and friendship – I never felt alone in this experience.

I am very grateful for my friends and family, their sympathetic ear whenever needed but most importantly distracting my thoughts and forcing me to take refreshing and recreative time.

A tremendous thank you goes to my parents, who supported me in every way they could. Your endless love and belief in me, means the world to me.

Lastly I have to thank my husband Felix. Throughout this whole journey I could always rely on your optimism and confidence, when mine was low, your patience and understanding, when I introduced a bunch of “Mäuse-Männer” to our daily life for three years, your ability to know when to calm and when to push, and your unconditional love.

Without all of you, I am sure, those pages would have been empty! ♥

Declaration

Herewith I certify that I have prepared and written my thesis independently and that I have not used any sources and aids other than those indicated by me.

Julia Stein

Berlin, 2024

Summary

Seasonal outbreaks of Influenza A virus (IAV) infections repeatedly challenge the immune system, which is in charge of controlling viral replication and facilitating clearance and subsequently recovery. T cells, which are part of the adaptive immune system, provide a highly specific response towards IAV during the acute infection phase that supports viral clearance. For that, activated effector T cells migrate from the lung-draining lymph nodes (drLN) to the side of infection, where they induce cell death of infected cells. Besides effector function in the lung, the follicular T helper cell subset provides help to B cells in drLN thereby supporting plasma cell differentiation and production of neutralizing antibodies. Furthermore, memory T cells reside long term in the body and serve as protection against re-infections. Although the T cell response is crucial for virus control, it has to be tightly regulated as T cell induced immunopathology and collateral tissue damage is disadvantageous.

The protein T cell activation inhibitor, mitochondrial (TCAIM) was previously found to interfere with effector T cell differentiation and function. Yet, TCAIM overexpressing T cells were able to respond to activating stimuli by entering the proliferation cycle and reduced cytokine production. Thus, within the scope of this work, the question was addressed, if the degree of T cell activation and differentiation in TCAIM overexpressing mice is sufficient to facilitate viral clearance and to support establishment of a protective memory T cell pool. Furthermore, no *in vivo* data are available for TCAIM deficient T cells, but previous *in vitro* work showed an advantage in T cell activation under sub-optimal stimulation conditions. This raises the question, whether viral control is improved in TCAIM deficient mice.

The here presented data show an impaired lung infiltration of TCAIM overexpressing T cells upon IAV infection, which is linked to the failure to modulate CD44 and CD62L receptor expression and upregulation of genes involved in migration and effector T cell differentiation. As a functional consequence cytokine production was diminished and viral clearance delayed. Nevertheless, TCAIM overexpressing mice did recover from IAV infection and were able to respond to infection induced activation stimuli seen in undisturbed type I interferon (IFN) signalling and T cell expansion within drLN. Importantly, reduced T cell response at the side of infection prevented T cell induced immunopathology since TCAIM overexpressing mice only slightly lost weight. Surprisingly, although generation of lung homing effector and tissue resident memory T cells was impaired, neutralizing antibodies were formed which might serve as protection during re-infection. TCAIM deficient T cells were found to predominantly accumulate at the side of infection. Early upregulation of *Ifng* and genes involved in T cell activation however did not translate into increased IFN-γ production at the peak of infection and improved viral control.

In conclusion, the data within this work highlight the impact of TCAIM on T cell migration and the prevention of T cell induced immunopathology thereby proposing a beneficial role during IAV infections.

Kurzzusammenfassung

Saisonale Ausbrüche von Influenza-A-Virus-Infektionen (IAV) stellen das Immunsystem, das für die Kontrolle der Infektion und anschließenden Genesung zuständig ist, immer wieder vor Herausforderungen. T-Zellen, die Teil des adaptiven Immunsystems sind, weisen während der akuten Infektionsphase eine hochspezifische Antwort gegen IAV auf, die die Virusbeseitigung fördert. Zu diesem Zweck wandern aktivierte Effektor-T-Zellen aus den lungen-drainierenden Lymphknoten (drLN) zum Infektionsherd, wo sie den Zelltod infizierter Zellen auslösen. Neben der Effektor-Funktion in der Lunge leisten follikuläre T-Helferzellen in den drLN den B-Zellen Hilfe und fördert so die Differenzierung von Plasmazellen und die Produktion neutralisierender Antikörper. Darüber hinaus verbleiben Gedächtnis-T-Zellen langfristig im Körper und dienen als Schutz vor Reinfektionen. Obwohl die T-Zell-Antwort für die Viruskontrolle von entscheidender Bedeutung ist, muss sie streng reguliert werden, da T-Zell-induzierte Immunpathologie und kollaterale Gewebeschäden nachteilig sind.

In früheren Studien wurde bereits festgestellt, dass das Protein T cell activation inhibitor, mitochondrial (TCAIM) die Differenzierung und Funktion von Effektor-T-Zellen beeinträchtigt. Es konnte jedoch gezeigt werden, dass TCAIM-überexprimierende T-Zellen auf aktivierende Signale reagieren, da sie in den Proliferationszyklus eintraten und geringe Zytokinmengen produzierten. Im Rahmen dieser Arbeit wurde daher die Frage untersucht, ob der Grad der T-Zell-Aktivierung und -Differenzierung in TCAIM-überexprimierenden Mäusen ausreichend ist, um die Virusbeseitigung zu ermöglichen und die Bildung eines schützenden Gedächtnis-T-Zellpools zu unterstützen. Darüber hinaus liegen keine In-vivo-Daten zu TCAIM-defizienten T-Zellen vor, jedoch zeigen frühere In-vitro-Arbeiten einen Vorteil bei der T-Zell-Aktivierung unter suboptimalen Stimulationsbedingungen. Dies wirft die Frage auf, ob die Viruskontrolle in TCAIM-defizienten Mäusen verbessert ist.

Die im Rahmen dieser Arbeit präsentierten Daten zeigen eine beeinträchtigte Lungeninfiltration von TCAIM-überexprimierenden T-Zellen während einer IAV-Infektion, die mit der fehlenden Modulation der CD44- und CD62L-Rezeptorexpression und der Hochregulierung von Genen, die an der Migration und Effektor-T-Zelldifferenzierung beteiligt sind, verknüpft ist. Als funktionelle Folge wurde eine verringerte Zytokinproduktion und verzögerte Virusbeseitigung beobachtet. TCAIM überexprimierende Mäuse waren dennoch in der Lage sich von der IAV-Infektion zu erholen und konnten auf Infektionsbedingte Aktivierungssignale reagieren. Dies konnte durch die Induktion des Typ-I-Interferon (IFN) Signalweges und die T-Zell-Expansion innerhalb von drLN gezeigt werden. Bemerkenswert ist, dass die die reduzierte T-Zell-Antwort in der Lunge eine durch T-Zellen induzierte Immunpathologie verhinderte, da TCAIM-überexprimierende Mäuse nur geringfügig an Gewicht verloren. Obwohl die Bildung von infiltrierenden Effektor-T-Zellen und in der Lunge verbleibenden Gedächtnis-T-Zellen beeinträchtigt war, wurden überraschenderweise neutralisierende Antikörper gebildet, die einen

potentiellen Schutz vor einer erneuten Infektion bewirken könnten. Darüber hinaus wurde festgestellt, dass sich TCAIM-defiziente T-Zellen insbesondere am Infektionsherd anreichern. Eine frühe Hochregulierung von *Ifng* und Genen, die an der Aktivierung von T-Zellen beteiligt sind, führte jedoch nicht zu einer erhöhten IFN-γ-Produktion am Höhepunkt der Infektion und zu einer verbesserten Viruskontrolle.

Zusammenfassend lässt sich sagen, dass die Daten dieser Arbeit den Einfluss von TCAIM auf die T-Zellmigration und die Prävention von durch T-Zellen induzierter Immunpathologie hervorheben und eine positive Rolle bei IAV-Infektionen nahelegen.

Contents

List of Figures

List of Tables

Abbreviations

%	Percent
°C	Degree Celsius
µm	Micrometre
AB	Antibody
AP-1	Activating protein-1
APC	Antigen presenting cell
BAL	Broncho alveolar lavage
Bcl2	B-cell lymphoma 2
BCR	B cell receptor
BSA	Bovine serum albumin
$CaCl_2$	Calcium chloride
CCL2/7	Chemokine C-C motif ligand 2 / 7
CCR7	C-C Chemokine receptor type 7
CD	Cluster of differentiation
CD40L	CD40 ligand
cDC	Conventional DC
cDNA	Complementary DNA
CO_2	Carbon dioxide
Covid-19	Coronavirus disease 2019
Cre	Causes recombination
cRNA	Copy RNA
CTLA4	Cytotoxic T-lymphocyte-associated protein 4
CXCL2/10/13	C-X-C motif chemokine 2/10/13
CXCR3/6	CXC motif chemokine receptor 3/6
d	Day
DC	Dencritic cell
DEG	Differentially expressed genes
DNA	Deoxyribonucleic acid
drLN	draining lymph nodes
EDTA	Ethylenediaminetetraacetic acid
FcR	Fc receptor
FCS	Fetal calf serum
g	Gravitational force
g, mg, kg	Gram, milligram, kilogram
GC	Germinal centre

GO	Gene ontology
GranB	Granzyme B
GSEA	Gene set enrichment analysis
h	Hours
H&E	Haematoxylin & eosin
HA	Heamagluttinin
HAI	Heamagluttinin inhibition
HIF1α	Hypoxia inducible factor 1 alpha
IAV	Influenza A virus
IAV-spec. T cell	Infuenza A virus specific T cell
ICAM-1	Intercellular adhesion molecule-1
ICOS	Inducible T-cell co-stimulator
Id2	Inhibitor of DNA binding 2
IFITM	IFN-induced transmembrane
IFN	Interferon
IFN-γ / *Ifng*	Interferon gamma
Ig	Immunglobulin
IL-1b/2/4/12/21	Interleukin-1b/2/4/12/21
IMC	Imaging mass cytometry
IP-10	Interferon gamma-induced protein 10
IRF3, IRF7	IFN-regulatory factor 3, IFN-regulatory factor 7
ISG	IFN-stimulated genes
Itga4	Integrin alpha 4
Itgb1/7	Integrin beta 1 /7
KI	Knock-In
KLF2	Krüppel-like Factor 2
KO	Knock-out
ldrLN	Lung draining lymph node
LFA-1	Lymphocyte function-associated antigen-1
M1, M2	Matrix protein 1, matrix protein 2
MDCK	Madin-Darby canine kidney
MEM	Minimum essential medium
MERC	Mitochondrial-endoplasmic reticulum contact sides
$MgCl_2$	Magnesium chloride
MHC	Major histocompatibility complex
min	Minutes

ml, µ	Millilitre, microliter
mM	Millimolar
mTOR	Mechanistic target of rapamycin
MTORC1	mTOR complex 1
NA	Neuraminidase
NFAT	Nuclear factor of activated T-cells
NF-κB	Nuclear factor-κB
NK cell	Natural killer cell
NLRP3	NOD-, LRR- and pyrin domain-containing 3
NP	Nucleoprotein
NS1, NS2	Non structural protein 1, non structural protein 2
p.i.	Post infection
PA	Polymerase acidic protein
PAMP	Pathogen-associated molecular patterns
PB1, PB2	Polymerase basic protein1, Polymerase basic protein2
PBS	Phosphate-buffered saline
PC	Principal component
PFU	Plaque forming unit
Pp1r21r	Protein Phosphatase 1 Regulatory Subunit 21
PR8	IAV virus strain H1N1/Puerto Rico/8/1934
PRR	Pattern recognition receptors
PSGL-1	P-selectin glycoprotein ligand-1
RBC	Red blood cell
RIG-I	Retinoic acid-inducible gene I
RNA	Ribonucleic acid
ROI	Region of interest
ScRNAseq	Single cell RNA sequencing
SD	Standard deviation
SEM	Standard error of the mean
Slfn1	Schlafen1
SLO	Secondary lymphoid organ
Sqpx	Square pixel
STAT	signal transducer and activator of transcription protein
TCAIM	T cell activation inhibitor, mitochondrial
Tcm	Central memory T cell
TCR	T cell receptor

TCRb	T cell receptor beta
Tem	Effector memory T cell
Tfh	Follicular T helper cell
Th1	Type1 T helper cells
TLR3, TLR7	Toll-like receptor 3, Toll-like receptor 7
TMA	Tissue micro array
TNF	Tumor necrosis factor
Tnfrsf4	Tumor necrosis factor receptor superfamily, member 4
TOAG-1	Tolerance-associated gene 1
TRAIL	TNF-related apoptosis-inducing ligand
Treg	Regulatory T cell
Trm	Tissue resident memory T cells
UMAP	Uniform manifold approximation and projection
VCAM-1	Vascular cell adhesion molecule-1
VDAC2	Voltage-dependent anion channel 2
VLA-4	Very late activation antigen-4
Vol	Volume
vRNA	Viral ribonucleic acid
vRNP	Viral nucleoprotein
WHO	World Health Organization
Wt	Wildtype

1. Introduction

1.1 Influenza virus infection

1.1.1 Introduction and relevance of Influenza virus infections

The World Health Organization (WHO) listed lower respiratory infections as one of the top 10 causes of death in 2019. With an estimated number of 3 to 5 million severe cases and up to 650 000 annually deaths worldwide, Influenza virus infections are a major disease burden for the global community and the health system[1,2]. Virus particles are transmitted between individuals by either direct contact or by droplets produced trough sneezing or coughing and aerosol formation[3]. Most infections cause a mild illness affecting the upper respiratory tract. Symptoms include cough, sore throat, fever, headache and fatigue[4,5]. However, children under the age of 5 years, older people over the age of 65 years, obese individuals, immunocompromised patients or patients with comorbidities like heart and pulmonary diseases have a higher risk of developing a severe illness[6–8]. In those cases, the lower respiratory tract is affected and co-infections with bacterial pathogens can occur that lead to pneumonia or the acute respiratory distress syndrome, which needs medical care and hospitalization and ultimately can result in death[9].

Influenza viruses are part of the *Orthomyxoviridae* family and can be divided into four different types: A, B, C and D. Influenza A and B viruses cause severe infections in humans. In contrast, Influenza C virus is endemic in the human population but leads to only mild symptoms and Influenza D virus is restricted to primarily cattle[10–13]. Therefore, only Influenza A and B viruses contribute to the seasonal disease outburst. Influenza A virus (IAV) can be further sub-classified by the combination of its two surface glycoproteins haemagglutinin (HA) and neuraminidase (NA)[14]. In total, 16 different HA and 9 different NA are known so far. In addition, two other HA and NA were found only in bats[15,16]. In the human population IAV strains H1N1 and H3N2 are currently circulating[17].

IAV is constantly mutating and thereby generating seasonal different IAV strains that can have the ability to escape the memory functions of the human immune system. Hence, one can be repeatedly infected with different strains that have undergone small changes like point mutations in the HA or NA sequence, known as antigenic drift[18,19]. In rare cases, major changes occur through a process called antigenic shift[20]. Here, large segments of two subtypes or segments from natural animal reservoirs like aquatic birds and other avian species are exchanged and generate a novel human IAV strain[21]. Those strains have the ability to reach an epidemic or even pandemic outbreak as the human population is mostly naive towards the new strain. In the last century, four pandemic IAV strains caused a pandemic outbreak: H1N1 in the years 1918 and 2009, H2N2 in 1957 and H3N2 in 1968[22,23]. The change in seasonal circulating IAV strains arises the need for a constant adaptation of the vaccination strategies.

Thus, current vaccines are a composition of three to four different strains of IAV and IBV that are updated every year due to the prognosis of upcoming viral strains[24,25]. Vaccination efficiency ranges between 30% and 70% showing there is still a need for improved vaccines that are able to reliably protect especially risk groups from a severe IAV infection[14,26,27].

1.1.2 Structure of IAV

The IAV is a single-stranded, negative-sense RNA virus that reaches around 100 nm in its sphere form. In addition, it can be found as filaments where it is up to 20 µm long[28,29]. The viral genome consists of eight viral ribonucleic acids (vRNA) that encode ten proteins and further accessory proteins (see Fig. 1-1). The virus envelope is composed of a host-derived lipid membrane and the viral proteins HA, NA and matrix proteins 2 (M2). HA and NA are surface proteins that are located on the outer virus envelope whereas M2 is an ion channel within the membrane[30,31]. The matrix protein 1 (M1) is supporting the viral envelope from underneath[32]. Inside the virion, the viral genome is stored in eight individual viral ribonucleoprotein (vRNP) complexes. The vRNA is wrapped around several nucleoproteins (NP) and is bound as a helical hairpin by the heterotrimeric polymerase composed of the polymerase basic protein 1 and 2 (PB1, PB2) and polymerase acidic protein (PA)[33,34]. The non-structural proteins 1 and 2 (NS1, NS2) take action upon cell entry as they are able to interfere with interferon signalling in host cells[35].

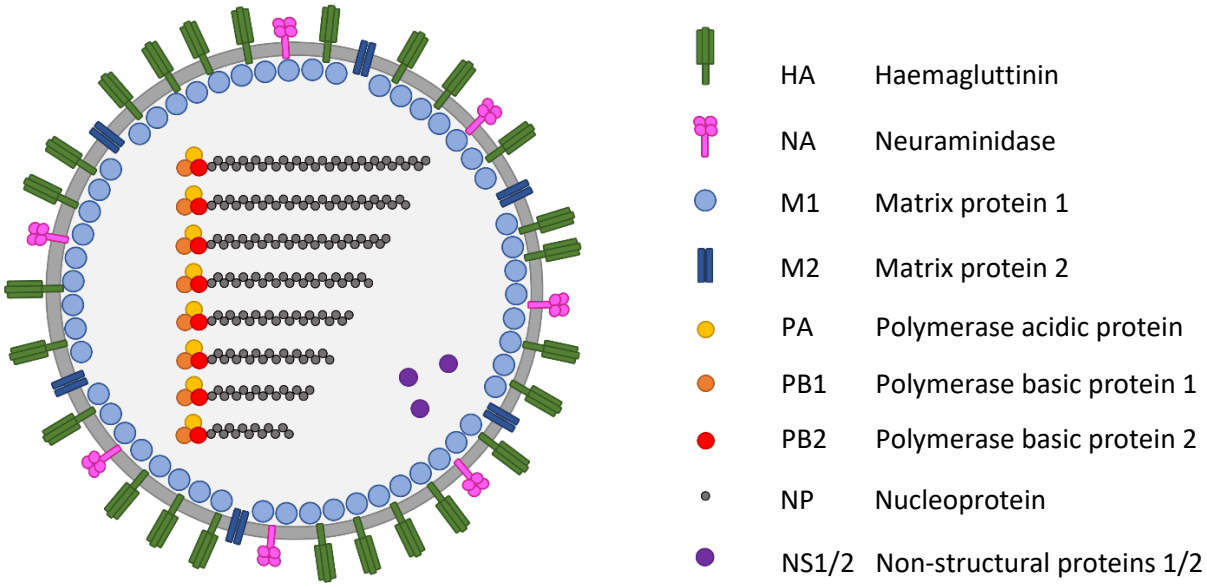

Figure 1-1 Influenza A virus (IAV) structure. *The IAV is an enveloped virus containing eight single-stranded, negative-sense RNA segments. The virus envelope is composed of the surface proteins haemagglutinin (HA), neuraminiase (NA) and the ion channel matrix protein 2 (M2). Matrix protein 1 (M1) is located at the inside of the membrane for stabilization. The eight viral genome segments are wrapped around multiple nucleoproteins (NP) and bound by the three polymerase proteins polymerase acidic protein (PA), polymerase basic protein 1 and 2 (PB1 and PB2). Also the non-structural proteins 1 and 2 (NS1 and 2) are encapsulated within the virion.*

1.1.3 IAV life cycle

Once IAV enters the respiratory tract, the viral surface protein HA binds to sialic acid residues bound to galactose on mucins of the mucosal barriers[36]. In order to avoid being captured at the mucosal sides, the sialidase function of NA cleaves off the terminal sialic acid residues and releases the virus until it reaches a host cell[37]. IAV can infect a broad range of different cells but its main target cells are the epithelial cells of the respiratory tract[25].

When the virus reaches a target cell, it scans the surface for a so far unknown sialyted receptor. The binding of HA to the receptor initiates the viral entry via endocytosis[25,38]. The low pH inside of the endosome causes the opening of the ion channel M2, which acidifies the inside of the virus and leads to the HA-mediated fusion of the viral and endosomal membranes[38,39]. The vRNP are released into the cytoplasm and utilize host cell transport pathways to reach the nucleus for replication. The vRNA is transcribed by the viral RNA polymerase in a two-step process. Fist, the negative-sense vRNA serves as a template to create the positive-sense copy RNA (cRNA). Second, the transcription of new vRNA copies is carried out using the cRNA as a template. Not only the eight genome segments have to be multiplied but also new viral proteins have to be generated for viral replication. Protein translation relies on host cell machinery. Therefore, mRNA is transcribed from vRNA templates and extended with a 5' cap derived from host cell transcripts through a process called cap snatching that primes the mRNA to be translated at the host cell ribosomes[38]. IAV uses several mechanisms to promote the translation of its own viral proteins e.g. NS1 interacts with proteins needed for pre-mRNA processing and hence reduces host cell mRNA production[40].

Newly generated vRNA and proteins translocate to the host cell membrane and are packaged into the budding virus[38]. Once virus assembly is finished, virus particles attach to the host cell due to HA surface protein binding to sialic acid residues on the cell membrane. The virus is finally released by NA cleavage function and can now spread and infect another host cell.

1.2 Immune response against IAV infections

The respiratory tract is exposed to the outside through air influx at all times. Hence, invading pathogens like IAV challenge the host repeatedly and need to be strictly controlled by the immune system. Beside mechanical barriers like the mucus layer of the respiratory tract, the immune response is mediated by humoral components and cells of the innate and adaptive immune system. The first line of defence is the innate immune system, which offers a rapid but non-specific response within hours upon infection and aims to limit viral replication and spread. Furthermore, innate immune cells activate the adaptive immune system. The adaptive immune system is slower but highly specific, as

involved cells possess antigen-specific receptors. Exerted effector function of adaptive immune cells and humoral components facilitate final viral clearance. Importantly, the adaptive immune system enables the formation of a long-lasting immunological memory that allows a faster response during a re-infection[41].

1.2.1 Innate immunity as a first line of defence

Once the IAV passes the mucus layer and infects the respiratory epithelial cells, cell intrinsic pattern recognition receptors (PRRs) detect pathogen-associated molecular patterns (PAMPs). The main PRRs for the recognition of IAV are Toll-like receptors 3 and 7 (TLR3, TLR7) which detect double-stranded and single-stranded RNA respectively in the endosomes of host cells, retinoic acid-inducible gene I (RIG-I) which recognizes 5'-triphosphate RNA in the cytosol and NLR family pyrin domain containing 3 (NLRP3) which senses cellular damage. Upon recognition of target structures, TLR3, TLR7 and RIG-I initiate signalling cascades that lead to the activation of transcription factors IFN-regulatory factor 3 (IRF3) or IFN-regulatory factor 7 (IRF7) and nuclear factor-κB (NF-κB). Those migrate into the nucleus and mediate transcription of type I interferons (IFNs)[42]. IFNs in turn bind to their respective receptors and induce transcription of IFN-stimulated genes (ISGs) or pro-inflammatory cytokines and chemokines via signal transducer and activator of transcription protein (STAT) signalling and thereby inducing an antiviral state[42,43].

ISGs are important for an early limitation of IAV progression and spread since they have antiviral activity themselves. IFN-induced transmembrane (IFITM) proteins e.g. block fusion of viral and host endosome membranes after virus entry and protein kinase R interferes with viral translation by binding to viral nucleic acids[44,45]. Studies using IFITM3-deficient mice were able to show the importance of functioning IFITM proteins as those mice had a greater morbidity since they fail to restrict IAV infection leading to severe lung pathologies[46,47].

Besides limiting viral processes, IFN also have immunoregulatory functions as they directly influences the function of immune cells. For instance, they support upregulation of chemokines like chemokine C-C motif ligand 2 (CCL2), CCL7 and interferon gamma-induced protein 10 (IP-10) that drive immune cells infiltration at the side of infection[48,49].

The IFN signalling is an important part in the establishment of a proper immune response during IAV infection. Thus, IFN signalling is an attractive target for the invading virus to dampen the host's immune response. Indeed, the viral protein NS1 is known for its anti-interferon activity[50–52].

Secretion of pro-inflammatory cytokines and for example tumor necrosis factor (TNF), Interleukin-1β (IL-1β), CCL2 or C-X-C motif chemokine 2 (CXCL2) chemokines by respiratory epithelial cells and

resident pulmonary macrophages drive the recruitment of innate immune cells like neutrophils, monocytes and natural killer (NK) cells to the site of infection[41,43]. Recruited monocytes will differentiate into inflammatory macrophages that as well as neutrophils phagocytose virus-infected cells, thereby limit spreading of virus particles in the host organism[53]. In addition to their phagocytosis function, neutrophils are also known for producing neutrophil extracellular traps which can neutralize bacteria and are also beneficial in viral infections[54–56] NK cells are mediating viral control by the lysis of infected cells. Studies showed that NK cell directly bind to viral HA proteins on the IAV envelope via their surface receptors NKp44 and NKp46 and furthermore produce pro-inflammatory cytokines like interferon gamma (IFN-γ)[57–60]. Conventional dendritic cells (cDCs) are antigen presenting cells (APCs) that are connecting the innate immune system with adaptive immune cells since they activate virus-specific T cells[43]. Viral material is taken up by cDCs, processed and presented via major histocompatibility complex (MHC) molecules on the cell surface. Antigen-loaded cDCs express C-C chemokine receptor 7 (CCR7), which drives the migration to the lymph nodes, where the antigen is presented to T cells[41,61].

1.2.2 Adaptive immunity against IAV infections

The adaptive immune system is composed of the humoral immunity mediated by antibodies produced by plasma cells that originate from B lymphocytes (B cells) and the cellular immunity carried out by T lymphocytes (T cells). B and T cells originate from hematopoietic stem cells in the bone marrow. To ensure that their specificity is not autoreactive, they undergo a selection process in which only maturation of cells that recognize nonself-antigens is promoted[62,63].

Progenitor T cells migrate from the bone marrow to the thymus for their maturation[62]. There, they undergo the processes of T cell receptor (TCR) beta chain rearrangement (β-selection), positive selection and negative selection, which ensure a functional TCR that is able to recognize foreign antigens but does not respond to self-antigens. In addition, during positive selection T cells differentiate into either the $CD4^+$ T helper cell or $CD8^+$ cytotoxic T cell subset based on their $CD8^+$ specific interaction with either MHC class I molecules or $CD4^+$ specific interaction with MHC class II molecules presented on APCs in the thymus. Only a small proportion (1-3%) will successfully complete the maturation process and become a mature, naïve T cell that migrate to the secondary lymphoid organs (SLO) now ready to encounter their specific antigen[62]. T cells (in IAV infections) will be further discussed in detail in chapter 1.3.

Progenitor B cells undergo their maturation in the bone marrow[63,64]. The maturation process is composed of immunoglobulin (Ig) rearrangement, which is part of the B cell receptor (BCR), positive

selection and negative selection. Those processes ensure that the BCR is capable of identifying nonself-antigens and is not autoreactive. After maturation, B cells migrate to the SLO. Here, they differentiate into short-lived plasmablasts via the extra-follicular pathway or they can enter the follicular pathway in the germinal centres (GC) which drives the differentiation into memory B cells and long-lived plasma cells secreting high affinity antibodies[63,64].

During the follicular pathway, B cells receive T cell help at the T-B cell border in SLO that is required for formation and entering of GC, which are transient structures, where the B cell maturation is taking place[65,66]. For this affinity maturation, follicular B cells undergo several rounds of proliferation and somatic hypermutation of the Ig variable region in the dark zone of the GCs. B cells with improved antigen specificity will be selected and favoured in light zone by interaction with follicular DCs and specialized follicular T helper cells (Tfh). Tfhs are providing co-stimulatory signals including CD40L and inducible T-cell co-stimulator (ICOS), which bind to their respective receptors on B cells, and expression of the cytokines IL-4 and IL-21. Importantly, un-helped B cells undergo apoptosis[65–67]. In addition, during class switch recombination the constant region of the Ig changes leading to the different Ig classes IgG, IgA and IgE[64,65,68].

In the extra-follicular pathway, a small population of IgM^+ B cells reside as marginal zone B cells. Those B cells are located at the marginal zone of the spleen and lymph nodes and can provide a rapid production of low affinity antibodies in a T cell-independent manner[64,68]. However, the extra-follicular response can also lead to IgG producing short-lived plasmablasts which requires Tfh help at the T-B cell border[69].

The main targets of generated antibodies are the viral surface proteins HA and NA, but there were also antibodies found directed against e.g NP[25,70]. Thus antibodies are interfering with the function of respective viral protein. For instance, neutralizing antibodies binding HA are blocking the receptor binding which prevents cell entry[70,71].

1.3 T cells in IAV infections

1.3.1 Kinetics of the T cell response during the course of infection

As mentioned earlier, antigen loaded DCs migrate to the SLO, where they arrive 2-3 days post infection, to present their virus specific antigen to T cells[72]. Upon antigen recognition, naïve IAV-specific (IAV-spec.) T cells get activated and start to proliferate and differentiate into effector T cells that leave the SLO and migrate to the side of infection[73]. The T cell accumulation in the lung peaks around days 7 -10 post infection[74,75]. After virus clearance, the effector T cell population enters the contraction phase in which most T cells undergo apoptosis. Only a small fraction of IAV-spec. T cells will remain and persist

as a long-lived memory T cell pool that offers a rapid recall response upon a secondary infection with the same IAV strain[41,76]. In murine models, a memory response up to 2 years has been observed[77]. Importantly, memory T cell were shown to also provide protection in an infection with heterologous IAV strains as viral proteins share conserved peptide sequences that can be recognized by antigen specific T cells[41]. The memory T cell population is composed of different subset: Central memory T cells mainly found in SLO (Tcm), effector memory T cells circulating to peripheral tissues (Tem) and tissue resident memory T cell that reside at the side of infection and do not enter circulation (Trm)[76].

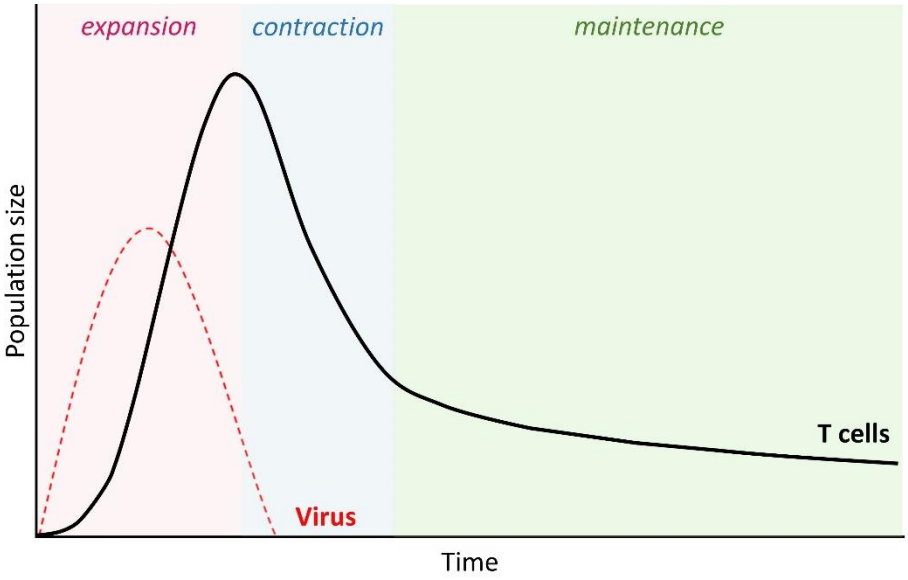

Figure 1-2 T cell kinetics during viral infections. *Schematic and simplified kinetics of the T cell response during viral infections. Upon infection, antigen specific T cell clones expand which leads to a large effector T cell population. After viral clearance, the majority of these cells undergo apoptosis in the contraction phase. Only a small population of long-lived virus specific memory T cell remain that provide protection during a secondary infection.*

1.3.2 Activation of T cells in secondary lymphoid organs

Naïve T cells are quiescent cells that localize within and circulate between the SLO until the encounter with their cognate antigen. They express the surface molecules CCR7 and L-selectin (CD62L) which drive their homing to SLO[76]. The lung draining lymph nodes (drLN) are the main side of T cell activation but studies showed that IAV-spec. T cell can also arise from the spleen although to a lesser extent[75].

The activation of naïve T cells is not dependent on only one activating stimulus but rather is a combination of signals that together overcome the activation threshold needed for full T cell activation (Fig.1-3, *left panel*). First, the viral antigen presented by APCs via their MHC molecules is recognized and bound by the TCR[72]. This binding is stabilized by CD4 or CD8 molecules respectively[78]. TCR engagement alone is not sufficient for T cell activation and drives the T cells into a functional inactive state called anergy[79]. Therefore, the second indispensable signal is the interaction of co-stimulatory molecules that strengthen and amplify the TCR signalling. The most prominent examples is CD28, which is constitutively expressed on T cells and binds to B7.1 (CD80) and B7.2 (CD86) proteins

expressed on APCs[79]. Furthermore, there are also other co-stimulatory molecules like OX40 (CD134) and ICOS which support T cell activation. In contrast, inhibitory molecules like cytotoxic T-lymphocyte-associated protein 4 (CTLA4), which competes with CD28 for binding to CD80 and CD86, are negatively regulating T cell get activation[79]. The third signal received during activation are cytokines secreted by APC that shape the T cell fate and are necessary for full effector function[80]. Once the activation threshold is reached, multiple signalling cascades lead to the expression of transcription factors like nuclear factor of activated T-cells (NFAT), NFκB or Akt1 that in turn allow proliferation and the differentiation into effector T cells[81].

1.3.3 T cell migration into the infected lung

To be able to contribute to the viral clearance at the side of infection, activated T cells have to leave the SLO, migrate to the lung, exist the vasculature and enter the infected tissue (Fig. 1-3). To prevent recirculation to the SLO , the lymph node homing receptors CD62L and CCR7 are downregulated, which is regulated by the mechanistic Target of Rapamycin (mTOR) mediated inhibition of Krüppel-like Factor 2 (KLF2)[82]. In addition to its transcriptional regulation, CD62L is shed from the cell surface via proteolytic cleavage[83–85].

Tissue migration is a multi-step process that includes T cell rolling, firm adhesion and transendothelial migration (Fig. 1-3, *right panel*). First, circulating T cell must recognize and stop at the correct tissue sides. Therefore, T cells interact with the vascular surface in a process called rolling. Reversible binding events to tissue specific adhesion receptors like selectins or components of the extracellular matrix facilitate slow rolling[86]. Upon infection, endothelial cells express E- and P-selectins that bind to selectin ligands like P-selectin glycoprotein ligand-1 (PSGL-1) on bypassing T cells[86]. In addition, chemotactic signals received via CXC motif chemokine receptor 3 (CXCR3) and CCR5 support tissue specific rolling of T cells[87,88]. One important adhesion molecule binding to E-selectins and hyaluronic acid on the endothelium is CD44, which is upregulated in activated T cells[89–91]. Cell arrest and firm adhesion is mediated by integrins. Activated T cells express lymphocyte function-associated antigen-1 (LFA-1; αLβ1) and very late activation antigen-4 (VLA-4; α4β1) that allow binding to their respective ligands intercellular adhesion molecule-1 (ICAM-1) and vascular cell adhesion molecule-1 (VCAM-1) on endothelial cells[92]. CD44 was also found to bind VLA-4, hence supporting firm adhesion[93]. For extravasation, cytoskeletal changes allow T cells to crawl and migrate through endothelial junctions[94]. In the tissue, chemokine gradients e.g. CXCL10, the ligand of CXCR3, provide local signal that drive T cell migration towards infected cells[95,96].

Besides lung migration, a subset of CD4⁺ T cells that is called Tfh provides B cell help upon infection and therefore needs to localize in SLO. CCR7 causes the localization in the T cell zone and therefore is downregulated in activated Tfh. Instead, the expression of CXCR5 upregulated[97]. The respective ligand CXCL13 is produced by stromal cell and follicular DCs which drives the migration of Tfh to the B cell zone and the GCs[98].

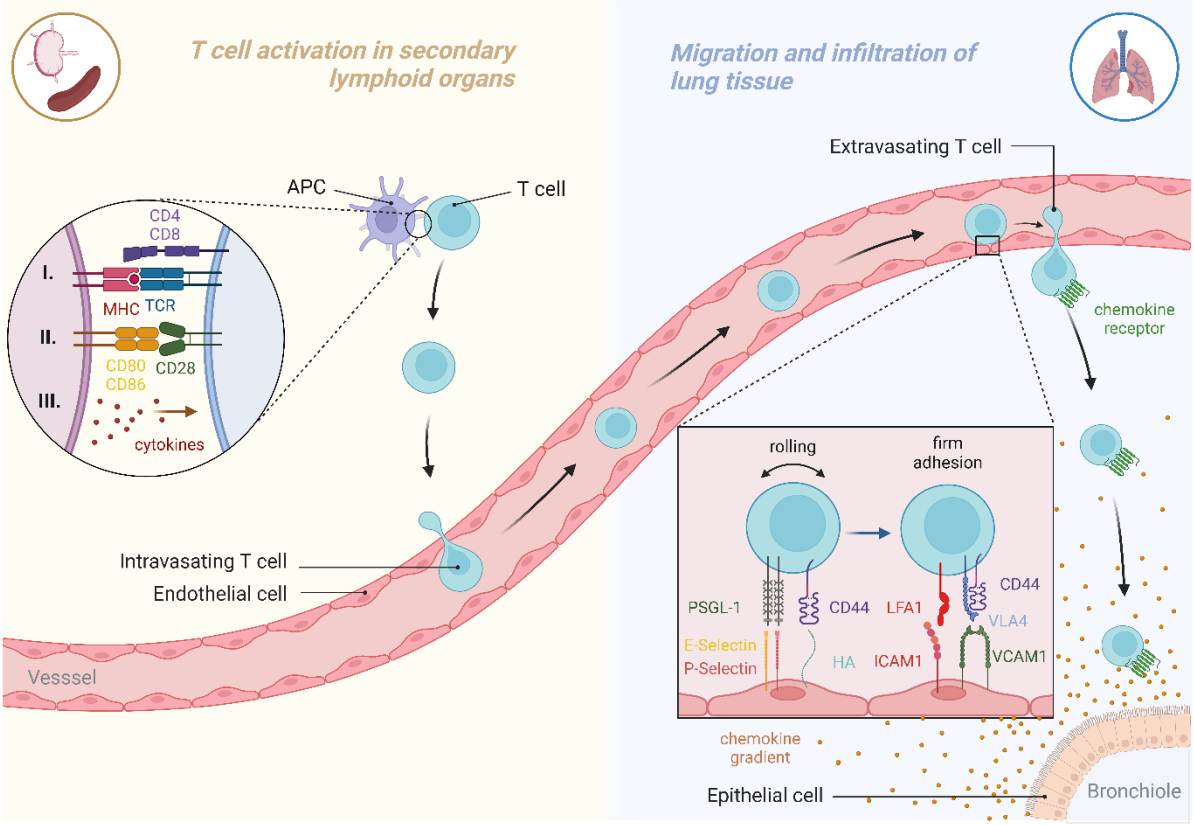

Figure 1-3 T cell activation and migration to the lung. *T cell activation (left) takes place in the secondary lymphoid organs including the spleen and draining lymph nodes. It requires* ***I*** *the presentation of cognate antigen via major histocompatibility complex (MHC) molecules on antigen presenting cells (APCs) that are bound by the T cell receptor (TCR) and stabilized by either CD4 or CD8,* ***II*** *co-stimulatory molecules e.g. CD28 binding and* ***III*** *cytokines. Upon activation, T cells are released into the blood circulation for transport to peripheral tissues. In the lung (right), T cell need to extravasate and migrate into the tissue to reach the bronchioles, the side of infection. Binding of (P-selectin glycoprotein ligand-1) PSGL-1 and CD44 to E-/P-selectin and hyaluronic acid (HA) respectively mediate rolling at the vascular surface. Integrins lymphocyte function-associated antigen-1 (LFA-1) and very late activation antigen-4 (VLA4) supported by CD44 mediate firm adhesion at the endothelium by binding to intercellular adhesion molecule-1 (ICAM-1) and vascular cell adhesion molecule-1 (VCAM-1). Chemokines gradient mediate migration throughout the lung tissue to the epithelium.*

1.3.4 Contribution of CD4⁺ T helper T cells to the antiviral immune response

The most prominent role for CD4⁺ T cells in IAV infections is to help other cells by providing activating and stimulating signals, but they also contribute to the host immune response by facilitating regulatory as well as cytotoxic functions. Distinct CD4⁺ T cell subsets carry out those diverse roles[99]. CD4⁺ T cell subsets are heterologous and play roles in many aspects of the immune response. Amongst those,

type1 T helper cells (Th1), Tfh, regulatory T cells (Treg) and cytotoxic $CD4^+$ T cells are the main populations partaking in viral infections and will be introduced in more detail hereafter.

The $CD4^+$ T cell response to viral infections is mainly comprised by the differentiation of Th1 cells, which is driven by the cytokines IFN-γ and IL-12[100]. Th1 cells are characterized by the expression of their key transcription factor T-bet and the production of the pro-inflammatory cytokines IFN-γ, IL-2 and TNF[101,102]. During IAV infection IFN-γ and CD40 ligand (CD40L) expression by Th1 cells provide activation signals for APCs[103]. In addition, secretion of IL-2 and IFN-γ by Th1 cells supports cytotoxic $CD8^+$ T cell differentiation[41]. Although the contribution of $CD4^+$ T cell help for $CD8^+$ T cell function during the acute phase is controversially described, it was shown that $CD4^+$ T cells help is important for $CD8^+$ memory T cells[104–106]. Another key role for $CD4^+$ T cells is providing help for B cell maturation and the generation of an optimal antibody response by plasma cells and thereby shaping the humoral response to IAV[99,107]. Specialized Tfh cells secrete IL-21 and IL-4 and directly interact with B cell via CD40L mediated binding of CD40 on B cells[97]. Apart from providing help, recent studies found a $CD4^+$ T cell subset that carries out cytotoxic functions including perforin mediated cytolytic activity and cytokine production[108,109]. Transfer of cytotoxic $CD4^+$ T cells mediates protection against lethal IAV doses[110]. As those cytotoxic mechanisms are the key function of $CD8^+$ T cells, they will be discussed in more detail in the next chapter.

$CD4^+$ T cell not only have pro-inflammatory functions, but a specialized subset of Tregs also contribute to the regulation of immune responses. For instance, it was shown that Tregs are beneficial in limiting tissue damage and overall pathology during IAV infections [111]. Tregs can either be generated in the thymus or develop in the periphery from conventional $CD4^+$ T cells and are characterized by the expression of the transcription factor FoxP3[112]. They suppress and regulate immune responses by e.g. production of anti-inflammatory cytokines like IL-10 or the expression of inhibitory molecules like CTLA-4[113]. Interestingly, memory Tregs were shown to control $CD8^+$ memory T cell response as depletion increased the $CD8^+$ T cell response and cytokine expression[114].

After the acute infection, an IAV-specific $CD4^+$ memory T cell pool remains that provide protection in the event of a re-encounter. In comparison to naïve T cells, memory T cells respond faster and stronger upon a secondary infection[115,116]. Interestingly, the adoptive transfer of exclusively lung resident $CD4^+$ memory T cell is sufficient to mediate protection to a lethal viral dose in naïve hosts[117,118]. In addition, the B cell help provided by memory T cells is facilitating an earlier class-switch and proliferation of B cells[119].

1.3.5 CD8$^+$ cytotoxic T cells mediate viral clearance

The main contribution of CD8$^+$ T cells to the adaptive immune response against IAV is to induce apoptosis of virus-infected cells, which restricts viral replication and spread. There are different mechanisms in which CD8$^+$ T cells mediate their cytotoxic function[120]. On the one hand, CD8$^+$ effector T cells secrete cytotoxic granules that contain perforin and a variety of granzymes[121]. Perforin is a pore-forming protein that mediates the entry of granzymes e.g. granzyme A and granzyme B (GranA, GranB) into the target cell. Granzymes are serine proteases that induce apoptosis by caspase activation that in turn initiates programmed cell death pathways within the target cell[122–124]. Furthermore, CD8$^+$ effector T cell express the transmembrane protein Fas ligand (CD95L) on the cell surface. When FAS ligand binds to its receptor Fas, apoptosis is induced in virus-infected cells [121]. A similar induction of cell death is mediated by TNF-related apoptosis-inducing ligand (TRAIL) interaction[125]. In addition to directly kill target cells, CD8$^+$ T cells produce pro-inflammatory cytokines e.g. IFN-γ and TNF, but also a variety of chemokines, thereby shaping the immune response against IAV infections[73].

Together with CD4$^+$ T cells, memory CD8$^+$ T cells persist in the body after the acute infection. They can be rapidly activated and expand upon a repeated encounter[126]. Hence, pro-inflammatory cytokines IFN-γ and TNF are provided early on supporting an improved viral control [120,126,127]. Indeed, transfer of CD8$^+$ memory T cells led to reduced viral titers[127]. Importantly, they not only provide protection to the same but also cross-protection to heterologous virus strains which makes the T cell memory response an interesting target for influenza vaccine development[128–130].

1.4 T cell activation inhibitor, mitochondrial (TCAIM)

TCAIM, formerly known as tolerance-associated gene 1 (TOAG-1), was first described during a screening for gene markers predicting allogenic graft rejection. Here, high TCAIM expression was associated with graft acceptance[131]. TCAIM is expressed in naïve T cells and downregulated upon T cell activation. Intrigued by that, TCAIM knock-in (KI) *Cd4-Cre* and TCAIM knock-out (KO) *Cd4-Cre* mice were generated that allow to study the conditional and T-cell-specific overexpression and deficiency of TCAIM. During their maturation, all T cell express CD4 as well as CD8 before they commit to either subtype. Hence, at this point CD8$^+$ T cell are affected by the *Cd4-Cre* mediated recombinase function that leads to TCAIM overexpression or deficiency respectively. Utilizing those mouse strains, it was shown, that TCAIM overexpression interferes with effector T cell differentiation and proliferation *in vitro*[132,133]. Importantly, TCAIM KI T cells were not able to reject allogenic skin grafts in an *in vivo* mouse model[132]. However, TCAIM overexpression did not completely inhibit T cell activation as T cells were able to enter the proliferation cycle, although majority remained in the first division, and low cytokine

expression was detected *in vitro*[133]. In contrast, TCAIM KO CD8$^+$ T cell were found to have an advantage in T cell activation under suboptimal stimulation conditions *in vitro* (unpublished data from Christina Iwert, Translational Immunology group at the Berlin Institute of Health at Charité).

TCAIM is a mitochondrial protein, that is encoded in the genome, but contains a mitochondrial target sequence that drives its localization in the mitochondria[134]. The overexpression of TCAIM in T cells but also dendritic cells impacts mitochondrial functions as mitochondrial reactive oxygen species (mROS) production is abolished[132,135]. Mechanistic *in vitro* studies in TCAIM KI CD8$^+$ T cells revealed TCAIM interaction with proteins e.g. Voltage-dependent anion channel (VDAC2), that are associated with mitochondrial-endoplasmic reticulum contact sides (MERC) and cristae organization (unpublished data from C. Iwert). VDAC opening and conductance was shown to link TCR signalling and metabolic reprogramming e.g. upregulation of anabolic pathways, as it impacts mechanistic target of rapamycin complex 1 (mTORC1) signalling[136–138]. The change of the cellular metabolism towards the upregulation anabolic pathway is a prerequisite for proper T cell activation as it provides building blocks needed for the higher metabolic demands that come with cell division and effector function. Here, mTOR is an important regulator of cell growth, sensing nutrient availability and integrating environmental cues to regulate the metabolism[139]. Amongst others mTOR regulates the transcription of hypoxia inducible factor 1 alpha (HIF1a) and MYC which mediate the shift in glucose metabolism[140]. In line, TCAIM interacting with VDAC2 interferes with its conductance, which leads to reduced mTORC1 and subsequent HIF1a signalling in TCAIM KI CD8$^+$ T cells *in vitro*. Consequently, upregulation of anabolic pathways especially cholesterol biosynthesis, needed for proper T cell activation, were abrogated (unpublished data from C. Iwert).

1.5 Scope of this work

TCAIM is a mitochondrial protein that has been shown to interfere with effector T cell differentiation *in vitro* and to prevent T-cell induced graft rejection in an *in vivo* mouse model. Here, a reduced T cell differentiation and graft infiltration is beneficial as it allows graft acceptance without the application of immunosuppressive agents. Importantly, TCAIM KI T cells were able to respond to activating signals enabling them to enter the first proliferation cycle. So far, the impact of TCAIM on T cells in an infection context, at which a T cell response is needed for sufficient disease control and recovery has not been addressed. In addition, *in vivo* generation of memory T cells under TCAIM overexpression or deficiency and thereby protective capacity remains elusive.

Therefore, the following questions are addressed within the scope of this work:

I. Is the reduced extend of T cell activation and differentiation sufficient to support a protective anti-viral immune responses in TCAIM KI mice?

II. Does the overexpression of TCAIM not only interfere with effector T cell differentiation but also impact the formation of IAV-specific memory T cells?

III. Does TCAIM deficiency facilitate an improved T cell activation and effector differentiation *in vivo*, that promotes viral control and long-term memory T cell generation?

2. Materials and Methods

2.1 Materials

2.1.1 Antibodies

Table 2-1: Panel I – Marker expression

Antigen	Fluorochrome	Clone	Company	Dilution
CD4	PerCP	RM4-5	Biolegend	1:100
CD8	Pacific Blue	KT15	Bio-Rad	1:100
CD44	AF700	IM7	Biolegend	1:100
CD62L	BV605	MEL-14	Biolegend	1:100
CD103	BV785	2E7	Biolegend	1:50
TCRb	FITC	H57-597	Biolegend	1:200

Table 2-2: Panel 2 – Cytokine expression

Antigen	Fluorochrome	Clone	Company	Dilution
CD4	PerCP	RM4-5	Biolegend	1:100
CD8	Pacific Blue	KT15	Bio-Rad	1:100
CD44	APCCy7	IM7	Biolegend	1:100
CD62L	BV605	MEL-14	Biolegend	1:100
GranB	AF700	QA16A02	Biolegend	1:50
IFN-g	BV785	XMG1.2	Biolegend	1:100
IL-2	BV711	JES6-5H4	Biolegend	1:100
TCRb	FITC	H57-597	Biolegend	1:200

Table 2-3: Other antibodies

Antigen	Fluorochrome	Clone	Company	Dilution
FCR Block	-	93	Biolegend, San Diego, USA	1:1000
CD45	PE	30-F11	Biolegend, San Diego, USA	1:500
H-2 MHC class I	PE	M1/42	Biolegend, San Diego, USA	1:500

Table 2-4: Hash-tag antibodies

Name	Barcode sequence	Clone	Company	Dilution
TotalSeq™-B0301 anti-mouse Hashtag 1 Antibody	ACCCACCAGTAAGAC	M1/42 30-F11	Biolegend, San Diego, USA	1:500
TotalSeq™-B0302 anti-mouse Hashtag 2 Antibody	GGTCGAGAGCATTCA	M1/42 30-F11	Biolegend, San Diego, USA	1:500
TotalSeq™-B0303 anti-mouse Hashtag 3 Antibody	CTTGCCGCATGTCAT	M1/42 30-F11	Biolegend, San Diego, USA	1:500
TotalSeq™-B0304 anti-mouse Hashtag 4 Antibody	AAAGCATTCTTCACG	M1/42 30-F11	Biolegend, San Diego, USA	1:500

2.1.2 Influenza-specific tetramers

Table 2-5: Influenza-specific MHC-I tetramers

Tetramer	Peptide sequence	Fluorochrome	Company	Dilution
H-2Db NP	ASNENMETM	PE	MBL	1:100
H-2kb PB1	SSYRRPVGI	APC	MBL	1:100

2.1.3 Buffer and media

Table 2-6: Buffer and media

Name	Ingredients
Avicel-overlay medium	MEM + 2 % BSA + 0.05 % $NaHCO_3$ + 0.01 % dextran + 1 µg/ ml TPCK-trypsin + 1.25 % Avicel
FACS buffer	PBS + 10 % FCS (heat inactivated) + 0.1 % sodium azide
MDCK medium	MEM + 10 % FCS (heat inactivated) + 1 % Glutamine
Multiplex buffer	PBS (heat inactivated) + 0.5% BSA + 2 mM EDTA
PBS / FCS	PBS + 2 % FCS (heat inactivated)

2.1.4 Chemicals and reagents

Table 2-7: Chemicals and reagents

Name	Company
10% Tween 20	Bio-Rad, Hercules, USA
Actinomycin D	Sigma-Aldrich, St. Louis, USA
Aqua ad injectabilia	B. Braun Melsungen AG, Melsungen, Germany
Avicel	FMC BioPolymer, Philadelphia, USA
Brefeldin A	Sigma-Aldrich, St. Louis, USA
Bovine serum albumin (BSA)	Sigma-Aldrich, St. Louis, USA
Collagenase CLS II (single cell RNA seq)	Sigma-Aldrich, St. Louis, USA
Collagenase Type I (flow cytometry)	Sigma-Aldrich, St. Louis, USA
Complete Mini, Protease inihibitor cocktail	Roche Diagnostics GmbH, Mannheim, Germany
Crystal violet	Carl Roth GmbH + Co KG, Karlsruhe, Germany
Dextran	Sigma-Aldrich, St. Louis, USA
Dimethyl sulfoxide (DMSO)	Sigma-Aldrich, St. Louis, USA
Dispase	Corning, New York, USA
DNAse I (single cell RNA sequencing)	Panreac AppliChem, Darmstadt, Germany
Dynabeads MyOne Silan	Thermo Fisher Scientific, Waltham, USA
EM buffer	Qiagen, Venlo, Netherlands
EDTA	Carl Roth GmbH + Co KG, Karlsruhe, Germany
Ethanol	J. T. Baker, Schwerte, Germany
FCS	Capricorn Scientific, Ebsdorfergrund, Germany
Fixation and Permeabilization Solution	BD Biosciences, New Jersey, USA
Formaldehyd 4%	Neolab, Heidelberg, Germany
Glycerol	Sigma-Aldrich, St. Louis, USA
Intracellular Staining Permeabilization Wash Buffer	Biolegend, San Diego, USA
Ionomycin	Biotrend Chemikalien, Köln, Germany
L-Glutamine 200mM	Gibco by life technologies, Carlsbad, USA
MEM	Gibco by life technologies, Carlsbad, USA
Microvette EDTA 200	Sarstedt, Nümbrecht, Germany
NaHCO3	Sigma-Aldrich, St. Louis, USA
Nuclease-free water	Thermo Fisher Scientific, Waltham, USA
Penicillin Streptomycin	Gibco by life technologies, Carlsbad, USA

PBS	Gibco by life technologies, Carlsbad, USA
PBS^{++} (with magnesium and calcium)	Gibco by life technologies, Carlsbad, USA
PMA	Sigma-Aldrich, St. Louis, USA
RBC Lysis Buffer 10x (single cell RNA sequencing)	Santa Cruz Biotechnology, Dallas, USA
RBC Lysis Solution 10x (flow cytometry)	Miltenyi, Bergisch Gladbach, Germany
RPMI 1640	PAN-Biotech, Aidenbach, Germany
Sodium azide	SERVA, Heidelberg, Germany
SPRIselect Reagent	Beckman Coulter, Brea, USA
TE Buffer	Thermo Fisher Scientific, Waltham, USA
TPCK-trypsin	Sigma-Aldrich, St. Louis, USA
Trypan Blue solution (0.4%)	Sigma-Aldrich, St. Louis, USA
Trypsin-EDTA (0,05%)	PAN-Biotech, Aidenbach, Germany
Zombie UV Fixable Viability (LD)	Biolegend, San Diego, USA

2.1.5 Instruments

Table 2-8: Instruments

Name	Company
4200 TapeStation	Agilent Technologies, Santa Clara, USA
AccuSpin Micro 17R	Fisher Scientific, Waltham, USA
Axioskope Microscope	Zeiss, Oberkochen, Germany
Aspiration system: Vacusafe	Integra, Biebertal, Germany
Biofuge pico	Heraeus, Hanau, Germany
Bio-Plex Pro™ wash station	Bio-Rad, Hercules, USA
Bio-Plex® 200 system with HTF (high throughput fluidics)	Bio-Rad, Hercules, USA
Chromium Controller	10x Genomics, Pleasanton, USA
Heraeus Incubator	Heraeus, Hanau, Germany
HeraSafe - Biosafety cabinet	Thermo Scientific, Waltham, USA
HeraSafe KS 9 - Biosafety cabinet	Thermo Scientific, Waltham, USA
Isoflurane Vaporizer Model 100	SurgiVet, ICU medical, San Clemente, USA
LSRFortessa flow cytometer	Becton Dicinson (BD), New Jersey, USA
Mega Star 4.0R	VWR, Radnor, USA
Midi 40 CO2 Incubator	Thermo Scientific, Waltham, USA
Pipetboy	Integra, Biebertal, Germany

Qubit 4.0 Flourometer	Invitrogen, Waltham, USA
Red light lamp	Beurer, Ulm, Germany
ED2201-0CE Scale	Sartorius, Göttingen, Germany
Ultra Turrax	IKA-Werke GmbH & CO. KG, Staufen, Germany
Vortex genie 2	Scientific Industries, New York, USA
WBT6, waterbath	Carl Roth GmbH + Co KG, Karlsruhe, Germany
BAT-12 microprobe thermometer	Physitemp Instruments

2.1.6 General consumables

Table 2-9: General consumables

Name	Company
Cell strainers (40 µm, 70 µ, 100 µm), nylon	Greiner Bio-one GmbH, Kremsmünster, Austria
Centrifuge tubes (15 ml, 50 ml)	Corning, New York, USA
C-CHIP Disposable Hemocytometer - Neubauer	NanoEntek, Seoul, Korea
DNA LoBind Tubes (1.5 ml, 2 ml)	Eppendorf, Hamburg, Germany
Embedding cassette	Carl Roth GmbH + Co KG, Karlsruhe, Germany
Flowmi Cell Strainer, 40 µm	Sigma-Aldrich, St. Louis, USA
High Sensitivity D5000 ScreenTape	Agilent Technologies, Santa Clara, USA
High Sensitivity D5000 Reagents	Agilent Technologies, Santa Clara, USA
High Sensitivity D5000 Ladder	Agilent Technologies, Santa Clara, USA
Microcentrifuge tubes (0.5 ml, 1.5 ml, 2ml)	Eppendorf, Hamburg, Germany
Needles (19G, 26G)	B.Braun, Melsungen, Germany
Optical Tube 8x Strip	Agilent Technologies, Santa Clara, USA
Optical Cap 8x Strip caps	Agilent Technologies, Santa Clara, USA
PCR Tubes 0.2 ml 8-tube strips	Eppendorf, Hamburg, Germany
Petri dishes (3,5 cm, 6 cm)	Sarstedt, Nümbrecht, Germany
Pipette tips	Sarstedt, Nümbrecht, Germany
Qubit Flex Assay Tube Strips	Invitrogen, Waltham, USA
SafeSeal SurPhob Spitzen, sterile (10 µl, 100 µl, 300 µl, 1000 µl)	Biozym Scientific GmbH, Hessisch Oldendorf, Germany
Serological pipet (5 ml, 10 ml, 25 ml)	Corning, New York, USA
Syringe 1ml	B.Braun, Melsungen, Germany
Syringe (2 ml, 5 ml, 10 ml)	Becton Dicinson (BD), New Jersey, USA
T75 cell culture flask	Sarstedt, Nümbrecht, Germany

Tissue culture plate, 6 well, flat bottom	Corning, New York, USA
Tissue culture plate, 96 well, flat bottom	Corning, New York, USA
Tissue culture plate, 96 well, round bottom	Sarstedt, Nümbrecht, Germany

2.1.7 Kits

Table 2-10: Kits

Name	Company
3’ Feature Barcode Kit	10x Genomics, Pleasanton, USA
Chromium Next GEM Chip G Single Cell Kit	10x Genomics, Pleasanton, USA
Chromium Next GEM Single Cell 3’ Kit v3.1	10x Genomics, Pleasanton, USA
Dual Index Kit NT Set A	10x Genomics, Pleasanton, USA
Dual Index Kit TT Set A	10x Genomics, Pleasanton, USA
FoxP3 Staining Buffer Set	Miltenyi, Bergisch Gladbach, Germany
Library Construction Kit	10x Genomics, Pleasanton, USA
MILLIPLEX Map Mouse Cytokine/Chemokine Magnetic Bead Panel 25-plex Immunology Multiplex Assay	Merck, Kenilworth, USA
Qubit 1X dsDNA Assay Kits, high sensitivity (HS)	Invitrogen, Waltham, USA

2.1.8 Mouse strains

Table 2-11: Mouse strains

Name	Origin
Tcaim KI *Cd4Cre*	In-house facilities of the Charité Universitaetsmedizin Berlin (AG Sawitzki)
Tcaim KO *Cd4Cre*	In-house facilities of the Charité Universitaetsmedizin Berlin (AG Sawitzki)

2.1.9 Pharmaceuticals

Table 2-12: Pharmaceuticals for mouse anesthesia

Name	Company
Isoflurane	Cp Pharma, Burgdorf, Germany
Ketamine	Cp Pharma, Burgdorf, Germany
Xylazine	Cp Pharma, Burgdorf, Germany

2.1.10 Software

Table 2-13: Software

Name	Company
BD FACSDiva software v8.0.2	BD Biosciences, New Jersey, USA
Bio-Plex Manager software version 6.2	Bio-Rad, Hercules, USA
BioRender	BioRender, Toronto, Canada
Citavi 6	Swiss Academic Software GmbH, Wädenswill, Swiss
FlowJo v10	FlowJo LLC, Ashland, USA
GraphPad Prism v8	GraphPad Software, Inc., La Jolla, USA
Microsoft 365	Microsoft, Washington, USA
R Studio, R v4.0.2	R foundation for statistical computing (https://cran.r-project.org)
TapeStation Software	Agilent Technologies, Santa Clara, USA

2.1.11 R packages

Table 2-14: R packages

Name	Version	Source
Complex heatmap	2.18.0	Gu, 2022[141]
Cowplot	1.1.3	Wilke, 2024
DESeq2	1.42.0	Love et al, 2014[142]
EnrichR	3.2	Kuleshov et al, 2016[143]
Fgsea	1.28.0	Korotkevich et al, 2019[144]
Ggplot2	3.4.4	Wickham and Sievert, 2016[145]
Openxlsx	4.2.5.2	Schauberger et al, 2022
Seurat	5.0.1	Satija et al, 2015[146]; Hao et al, 2023

2.2 Methods

2.2.1 Sublethal Influenza A virus (IAV) mouse model

2.2.1.1 Experimental design

Homozygous and wildtype littermates of the TCAIM KI *Cd4Cre* and TCAIM KO *Cd4Cre* mouse strains were used. For infection experiments, male mice between 12 and 16 weeks old were infected intra-nasally with an IAV (→ 2.2.1.2). Throughout the experiment, mice were housed at 20 - 22 °C and 40 – 55 % humidity under a 12 h light/ 12 h dark cycle and specific pathogen-free conditions.
To study the performance during the acute infection phase, the following time points were chosen: d3, d5 and d8 post infection (p.i.). For long term outcome and memory T cell formation, analyses were carried out at d45 p.i.. In addition, uninfected animals were used as controls.

2.2.1.2 Intra-nasal infection

The IAV virus strain H1N1/Puerto Rico/8/1934 (PR8) was used for infection experiments. The PR8 virus stock was kindly provided by the lab of Prof. Dr. Martin Witzenrath from the Department of Infectious Diseases and Respiratory Medicine at Charité Universitätsmedizin Berlin and viral titer of the IAV stock was determined using Plaque Assay analysis (→ 2.2.2.2) and aliquots were stored at –80 °C. Aliquots were thawed only once. Infection dose was prepared by multiple dilution steps of stock solution in sterile PBS^{++} on ice. The final virus solution was stored on ice until infection.
For the IAV infection, mice were anaesthetized with isoflurane. Infection dose was applied intra-nasally via the left nostril only, which guaranteed sufficient breathing through the right nostril during infection. The application of 50 µl of the virus solution was performed slowly in a drop-wise manner to ensure proper inhalation by the mice.

2.2.1.3 Infection dose testing

To establish a sublethal IAV in vivo mouse model, an appropriate infection dose had to be found that is strong enough to elicit disease symptoms and generate a T cell response but also allows the animals to recover from the infection. Therefore, different infection doses (7 PFU (plaque forming units), 15 PFU and 40 PFU) were tested on wildtype animals of TCAIM KI *Cd4Cre* and TCAIM KO *Cd4Cre* strains. The 7 PFU dosis allowed most animals to recover and thus was used for all following experiments.

2.2.1.4 Monitoring of infected mice

The initial body weight of the mice was measured on the infection day. During the acute infection phase, mice were monitored daily based on clinical parameters. The following parameters were used to determine the infection severeness and condition of the animals: body weight, body condition score[147], body temperature, social behavior, grooming and breathing rate and quality. Once a symptom was observed, the monitoring interval was increased to twice a day with a minimum of 10 h in between for all animals of the respective infection group. Red light was applied for 30 min twice a day if the body temperature was under 35 °C for more than 24 h. Mice were euthanized when an end point criterion was reached e.g. the weight loss reached or exceeded 20 % of the initial bodyweight. Once the animals showed no symptoms, the monitoring interval was reduced to weekly measurement of body weight and temperature and daily visual control of all other parameters.

2.2.1.5 Tissue collection and sample processing

a) *for Plaque Assay*

Mice were anesthetized with ketamine (160 mg/ kg) and xylazine (16 mg/ kg). Once pedal withdrawal reflex was absent, abdomen was opened. For exsanguination, blood was drawn from vena cava caudalis and stored in an ethylenediaminetetraacetic acid (EDTA) coated tube. Then, thorax was opened. To obtain broncho alveolar lavage (BAL), lungs were flushed twice using 800 µl PBS^{++} (phosphate buffered saline with $CaCl_2$ and $MgCl_2$) via the trachea and stored on ice. To remove blood from lung vasculature, perfusion was carried out using 10 ml PBS via the heart. Lungs were collected and stored in 2 ml PBS^{++} on ice.

Blood was centrifuged for 10 min at 855 g at room temperature. Serum was transferred to a 0.5 ml tube, snap frozen in liquid nitrogen and stored at -80 °C. Collected BAL was aliquoted, snap frozen and stored at -80 °C. Whole lungs were homogenized using an Ultra-Turrax and centrifuged for 10 min at 3300 g at 4 °C. Supernatant was collected, aliquoted, snap frozen and stored at -80 °C until viral plaque assay was performed (→ 2.2.2).

b) *for flow cytometry and protein multiplex analysis*

Mice were anesthetized with ketamine (160 mg/ kg) and xylazine (16 mg/ kg). Once pedal withdrawal reflex was absent, abdomen was opened. For exsanguination, blood was drawn from vena cava caudalis and stored in an EDTA coated tube. Then, thorax was opened. To obtain broncho alveolar lavage (BAL), lungs were flushed twice using 800 µl PBS containing 1 mM protease inhibitor via the

trachea and stored on ice. To remove blood from lung vasculature, perfusion was carried out using 10 ml PBS via the heart. Lungs, drLN and femur were collected and stored in PBS on ice.

Lungs were cut into small pieces and digested with 1 mg/ ml Collagenase II and 0.3 mg/ ml DNase I in VLE RPMI 1640 with glutamine supplemented with 10 % (vol/ vol) fetal calf serum (FCS), 100 U/ mL penicillin and 100 mg/ mL streptomycin for 30 min at 37 °C. Afterwards, digestion was stopped by adding 10 ml cold PBS. Blood was centrifuged for 10 min at 855 g at room temperature. Plasma was transferred to a 0.5 ml tube, snap frozen in liquid nitrogen and stored at -80 °C. The pellet was treated with red blood cell (RBC) lysis (Miltenyi Biotec) according to manufacturer's protocol. Femur was cut at both ends and flushed with PBS. Obtained bone marrow cells were stored on ice until further processing. Collected BAL was centrifuged at 4 C and 300 g for 5 min. Supernatant was aliquoted, snap frozen and stored at -80 °C for protein multiplex analysis (→ 2.2.4).

Digested lung, RBC lysed blood, bone marrow cells and drLN were forced through 100 µm cell strainers with cold PBS and centrifuged at 4 °C and 300 g for 8 min. Then, erythrocytes of lung, bone marrow and blood cell suspensions were lysed using hypotonic PBS diluted in a 1:3 ratio with sterile deionized water for 12 seconds. Lysis was stopped by adding of PBS / FCS (see Table 2-6). Afterwards, single cell suspensions of lung, bone marrow, drLN and blood were forced through a 40 µm cell strainers with cold PBS / FCS and stored on ice until staining for flow cytometry analysis (→ 2.2.3).

c) *for Histology*

Mice were anesthetized with ketamine (160 mg/ kg) and xylazine (16 mg/ kg). Once pedal withdrawal reflex was absent, abdomen was opened. For exsanguination, blood was drawn from vena cava caudalis and stored in an EDTA coated tube. Then, only the region above the trachea was opened to get access. A suture was placed around the trachea and tied loosely. After a last inhale, suture was tied to obtain air-filled lung. Lung was excised and placed into an embedding cassette. Cassettes were stored in 4% formalin at room temperature for 1-3 hours and afterwards transferred to 4 °C over night. The next day, lungs rinsed with water for 1 h at room temperature. Water was exchanged every 10 min. For long-term storage, lungs were transferred into 70 % ethanol and stored at 4 °C until paraffin embedding (→ 2.2.5).

d) *for single cell RNA sequencing*

Mice were anesthetized with ketamine (160 mg/ kg) and xylazine (16 mg/ kg). Once pedal withdrawal reflex was absent, abdomen was opened. For exsanguination, blood was drawn from vena cava caudalis and stored in an EDTA coated tube. Then, thorax was opened. To obtain BAL, lungs were flushed twice using 800 µl PBS containing via the trachea and stored on ice. To remove blood from lung vasculature, perfusion was carried out using 5 ml Dispase containing 2mg/ml Actinomycin D via

the heart. Lungs were collected and stored in PBS on ice. Then, lungs were placed into 2 ml digest media composed of Dispase containing 2mg/ml Actinomycin D, 1 mg/ml DNAse and 1500 U Collagenase CLS II in 6 well plate and dissociated with scissors and tweezers. Digestion was performed at 37 °C for 30 min with regular shaking every 10 min. Cold PBS containing 1 % bovine serum albumin (BSA) and 2 mg/ml Actinomycin D was added to stop the reaction. For further tissue disruption and homogenization, digested lungs and medium were pipetted up and down five times Rand transferred into a 50 ml tube by forcing through a 70 µm cell strainer. Cells were centrifuged at 300 g for 8 min at 4 °C, supernatant was discarded and RBC lysis was performed using for 2 min. Lysis was stopped by adding cold PBS containing 4 % BSA. Cells were centrifuged at 300 g for 8 min at 4 °C, supernatant discarded and pellet resuspended in PBS containing 4 % BSA. Then, cells were filtered using 40 µ Flowmi cell strainers. Viability and cell concentration was checked by counting with trypan blue in a Neubauer counting chamber. Cells were stored on ice until further processing for single cell RNA sequencing (→ 2.2.6).

2.2.2 Quantification of viral concentration

The virus plaque assay is used for quantifying the titer of an IAV virus stock or the viral concentration in the lung or BAL. Therefore, Madin-Darby canine kidney (MDCK) cells are infected with serial dilutions of the virus stock or either lung or BAL samples from infected mice. The infection of a single cell spreads to its neighboring cells, generating a plaque which can subsequently be quantified. Hence, the virus plaque assay is a measure of infectious virus particles.

2.2.2.1 MDCK cell culture

MDCK cells were grown in T75 cell culture flasks in MDCK medium (see Table 2-6) at 37 °C and 5 % CO_2. Every two to three days, cells were splitted into a new flask. First, old medium was discarded and cells washed once with PBS. Then, PBS was removed and 2 ml 0,05% Trypsin-EDTA was added for 15 minutes at 37 °C and 5 % CO_2. Finally, cells were resuspended using fresh MDCK medium, transferred to a new flask in a 1:10 split and supplemented with fresh MDCK medium.

2.2.2.2 Plaque Assay

MDCK cells were grown in 12-well flat-bottom cell culture plates until approximately 95 % confluent. Then, plaque assay was performed. Lung and BAL samples were thawed on ice. Serial dilutions were prepared in PBS^{++} supplemented with 0.2 % BSA in 96-well round bottom plates on ice. For each

sample, two dilution series were carried out to perform duplicate determinations of the viral load. MDCK cells were washed with PBS twice. Afterwards, 150 µl of sample dilutions were added and incubated for 45 min with regular shaking every 10 min. Sample dilutions were discarded and 1 ml Avicel-overlay medium (see Table 2-6) was added to each well. After 48 h incubation at 37 °C and 5 % CO_2, cells were washed with PBS twice and 0.1 % crystal violet staining solution was used to visualize and count plaques.

2.2.2.3 Calculation of viral titer

To determine the viral load of lung and BAL samples, the number of PFU per millilitre was calculated using the following formula:

$$\text{PFU/ml} = \frac{\text{number of plaques}}{0.15 \times \text{dilution factor } (10^{x}))}$$

2.2.3 Flow cytometry

Single cell suspensions obtained from different organs (2.2.1.5 *b)*) were split into two fractions of $1x10^6$ cells each. If the suspension was less than $2x10^6$ it was distributed equally. One fraction was used for staining Panel I, the second fraction for Panel II (listed in 2.1.1). For detection of cytokines within Panel II, cells were incubated *in vitro* with 1 µg/ ml Ionomycin and 10 ng/ ml PMA in VLE RPMI 1640 with glutamine supplemented with 10 % (vol/ vol) fetal calf serum (FCS), 100 U/ mL penicillin and 100 mg/ mL streptomycin for 4 h at 37 °C. To block cytokine secretion, 2 µg/ ml Brefeldin A was added after 2 h to the medium.

2.2.3.1 Live-Dead and tetramer staining

Cells were washed once with 700 µl cold PBS and centrifuged at 300 g for 4 min at 4 °C. Then, FCR block (1:1000) and live dead staining (1:100) was carried out in 100 µl PBS for 15 min at 4 °C. Afterwards, cells were washed in 700 µl FACS buffer and centrifuged at 300 g for 4 min at 4 °C. The supernatant was discarded. For staining IAV-specific $CD8^+$ T cells, cells were incubated with MHC I Tetramers (listed in Table 2-5) in 100 µl FACS buffer for 30 min at room temperature in the dark. Cells were washed once as described above.

2.2.3.2 Surface and intracellular staining

Surface staining was prepared in 100 µl FACS buffer and added to the cells for 10 min at 4 °C in the dark. Cells were washed once in 700 µl to remove unbound antibodies and centrifuged at 300 g for 4 min at 4 °C. The supernatant was discarded. For intracellular staining of Panel I (CD4) and Panel II (CD4 and cytokines), cells had to be fixated.

Cells of Panel I were fixed and stained using the FoxP3 Staining Buffer Set (Miltenyi) according to manufacturer's protocol. In brief, cells were fixed with 500 µl Fix/perm solution for 30 min at 4 °C in the dark. Then, cells were washed once with 700 µl FACS buffer and afterwards once with 500 µl 1x Perm solution. Cells were centrifuged at 500g for 4 min at 4 °C and supernatant was discarded. Intracellular staining mix was prepared in 100 µl 1x Perm solution and added to the cells for 30 min at 4 °C in the dark. Incubation was stopped with 500 µl 1x Perm solution. Cells were centrifuged and stored in FACS buffer at 4 °C until measurement.

Cells of Panel II were fixed and permeabilized using Fixation and Permeabilization Solution (BD Biosciences) and Intracellular Staining Permeabilization Wash Buffer (Biolegend) according to manufacturer's protocol. In brief, cells were incubated in 250 µl Fixation and Permeabilization Solution for 30 min at 4 °C in the dark. Afterwards, cells were washed twice with 700 µl Intracellular Staining Permeabilization Wash Buffer and centrifuged at 500 g for 4 min at 4 °C. Supernatant was discarded. Staining mix was prepared in 100 µl Intracellular Staining Permeabilization Wash Buffer. Cells were stained for 30 min at 4 °C in the dark, washed as described before and stored in FACS Buffer at 4°C until measurement.

2.2.3.3 Analysis and gating strategy

Flow cytometry data were acquired using an LSRFortessa and BD FACSDiva software v8.0.2. The configuration of the machine can be found in the appendix (Table 6-1). Subsequent analysis was carried out using FlowJo v10 software. The gating strategy can be found in Fig. 2-1. Doublets and cell debris were excluded from the analysis based on size and granularity by applying gates of different forward and sideward scatter combinations. To obtain living T cells, in Panel I live-dead staining negative and TCRb positive gates were applied in a two-step process (Fig. 2-1 A) whereas in Panel II gating was carried out in one step (Fig. 2-1 B). Within living T cells, $CD4^+$ T cells and $CD8^+$ T cells were obtained by their marker respective marker expression. In addition, $CD8^+$ T cells were further divided into IAV-spec. T cells which were stained with NP and PB1 MHC Class I tetramers. Then, analysis of markers of interest (Panel I: CD44, CD62L, CD103; Panel II: IFN-γ, GranB, IL-2) was carried out on $CD4^+$ T cells, $CD8^+$ T cells and IAV-spec. $CD8^+$ T cell respectively.

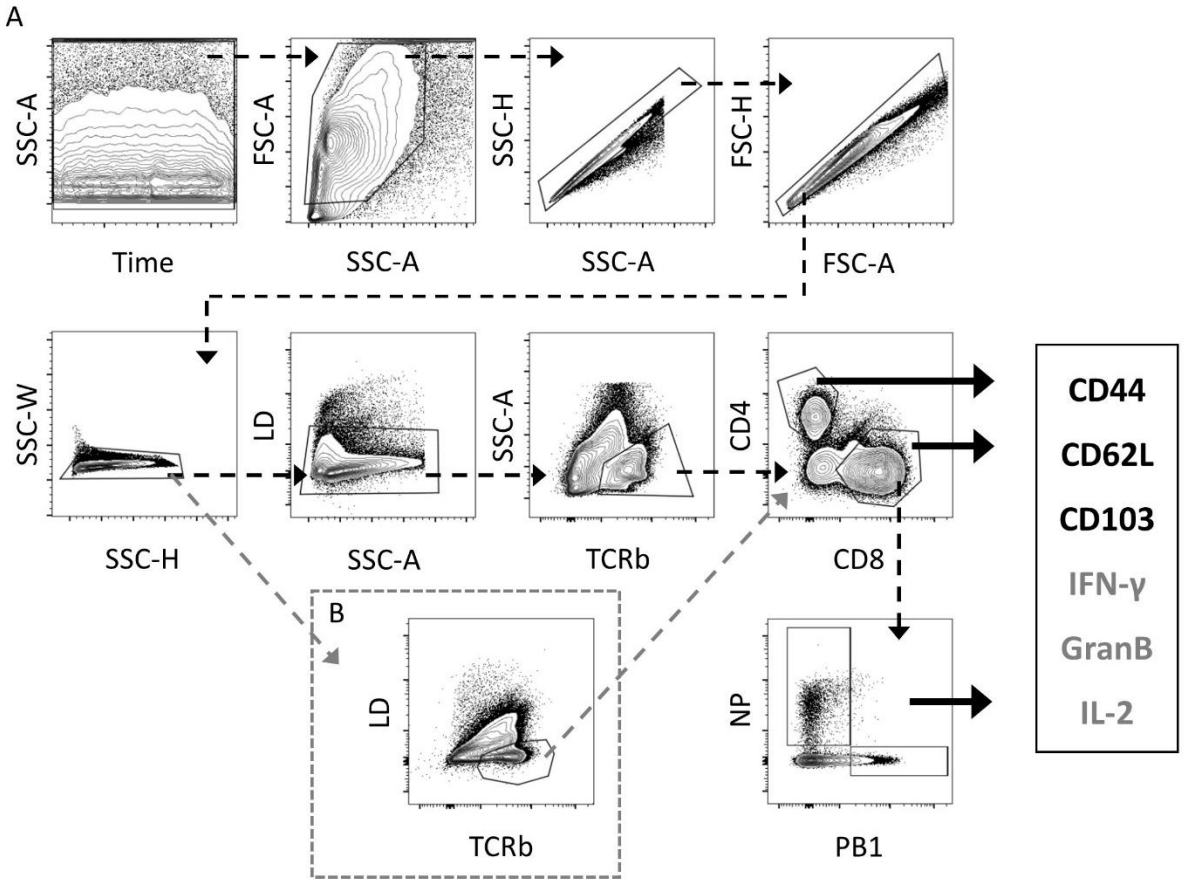

Figure 2-1 Gating strategy for flow cytometry analysis. A *First, doublets and cell debris were removed by excluding events based on their size and granularity based on gates set in forward and sideward scatters. Then living T cells were obtained by gating first on Live-dead staining (LD) negative cells and subsequently on T cell receptor beta (TCRb) positive cells. T cells were further divided into $CD4^+$ T cells, $CD8^+$ T cells and Influenza A virus (IAV)-specific $CD8^+$ T cells which are positive for nucleoprotein (NP) or polymerase basic protein 1 (PB1) tetramer staining. Based on those parental populations, subsequent analysis of marker of interest as carried out including CD44 CD62L and CD103 in Panel I and cytokines interferon γ (IFN-γ), granzyme B (GranB) and interleukin 2 (IL-2) in Panel II.* ***B*** *Gating on living T cells was performed in one gating step in Panel II.*

2.2.4 Multiplex protein analysis

Chemokine and cytokine content of BAL, obtained during preparation (2.2.1.5 *b*), was quantified using MILLIPLEX Map Mouse Cytokine/Chemokine Magnetic Bead Panel 25-plex Immunology Multiplex Assay according to the manufacturer's protocol. BAL samples were diluted 1:2. Washing was carried out using the magnetic bead-based assay wash program of the Bio-Plex Pro wash station according to the manufacturer's protocol. Samples were measured on the Bio-Plex 200 system with HTF (high throughput fluidics) and analysed with Bio-Plex Manager software version 6.2.

2.2.5 Imaging mass cytometry (IMC)

IMC is technique that allows spatial detection and analysis of up to 40 markers with metal-labelled antibodies on tissue sections. It therefore combines mass cytometry with histology and allows to study local cell accumulation and interaction in the tissue microenvironment.

IMC procedure and analysis was carried out and kindly provided by Juliette Johnson from the Translational Immunology group at the Berlin Institute of Health at Charité. The here presented IMC data are also included in her master thesis *APPLYING SPATIAL ANALYSIS TO UNRAVEL THE ROLE OF TCAIM AS A MODULATOR OF THE LOCAL IMMUNE RESPONSE DURING INFLUENZA A VIRUS INFECTION*, submitted to Freie Universität Berlin in July 2024.

a) Staining and measuring of samples

In brief, tissue micro arrays (TMAs), each containing samples from all experimental groups and time points, were generated from formalin fixed and paraffin embedded lungs (2.2.1.5 *c*). In addition, each TMA contained a control tissue from the same lung sample to correct for batch effects. As the IAV infects only single lobes and not the whole lung, haematoxylin & eosin (H&E) staining was applied to ensure that only infected regions were selected for TMA generation. H&E staining was performed at the iPATH Core Facility at Charité Benjamin Franklin. Regions were examined for morphological criteria including leukocyte infiltration, alveolar edema and haemorrhages by Dr. Sandra Kunder from the Veterinary Pathology department of the Freie Universität Berlin. Per Mouse two regions were punched to obtain 2 mm cores for TMA generation and subsequent IMC analysis.

TMAs were cut into 4 µm thick slices, mounted on slides, baked 1h at 60 °C and covered with paraffin for storage until staining by the iPATH Core Facility at Charité Benjamin Franklin. On the day of IMC staining, slides were de-paraffinized twice with xylene and rehydrated with an ethanol series: 100%, 100%, 95%, 80% and 70%. After two washes with distilled water, slides were incubated in Antigen Retrieval Buffer (10 mM Sodium citrate, 0.05% Tween 20, pH 6.0) for 30 min at 95 °C. The slides were cooled down in ice water and subsequently rinsed once with distilled water and once with PBS-T (0.1% Tween). Next, blocking was carried out for 1 h using PBS supplemented with 5% BSA. Metal-labelled antibody mix was prepared in 1% BSA/PBS-T buffer and slides were incubated over night at 4 °C. A list of used antibodies can be found in the appendix (Table 6-2). All antibodies were tested in immunohistochemistry beforehand. To obtain metal-conjugated antibodies, Maxpar Antibody Labeling Kits (Fluidigm) were used. Metal-labelled antibodies were titrated on murine lung and spleen tissue before staining of primary samples. The next day, slides were washed twice with PBS-T and twice with PBS. To stain DNA, slides were incubated with Intercalator-Iridium in PBS for 30 min at room

temperature. Then, slides were washed in PBS, dipped into distilled water and air-dried for storage until ablation.

Ablation of regions of interest (ROI) was performed at the BIH Cytometry Core Facility using a Hyperion Imgaing System (Standard BioTools) with a resolution of approximately 1 µm per pixel. Generated raw MCD files were exported for downstream processing and analysis.

b) Data processing and analysis

In brief, visual analysis of marker expression was carried out using the MCD Viewer. Brightness and contrast were subsequently changed in Microsoft Power Point. In all images brightness and contrast were increased by 40% each.

For quantitative analysis, the pre-processing and cell segmentation was done using the Steinbock pipeline and the Mesmer algorithm[148]. Data was imported into R for further analysis. Here, clustering, dimensionality reduction and visualisation were performed using the SPECTRE package. The data presented within this study were gated on T cells characterized as $CD45^+$ and $CD3^+$ cells. Then, marker signals was arcsinh-transformed with a co-factor of 2. Before clustering and dimensionality reduction, data were z-score normalized. Clustering was performed using Phenopgraph. Subsequently, clusters were presented in a uniform manifold approximation and projection (UMAPs) and marker expression of clusters were visualized in a heatmap (Appendix, Fig. 6-1) for cluster annotations.

To study different sites of the lung tissue separately, masks were generated that allow to define the areas around the vessel and bronchioles. Therefore, pixel-based training was applied on previously CellProfiler cropped images in Ilastik based on CD31 and EpCAM markers. Calculated probabilities based on the training were exported for the whole ROIs. Postprocessing and calculation of Euclidean distances was carried out in ImageJ. Due to high background in CD31 staining, artefacts were identified by checking raw signal images and removed manually.

2.2.6 Single cell RNA sequencing (scRNAseq)

2.2.6.1 Sample multiplexing

For sample multiplexing, cells were hash-tagged with unique barcode-antibodies that bind to the ubiquitously expressed surface markers CD45 and H-2 MHC Class I on cells. To determine the optimal labeling dilutions on lung derived single cell suspensions, CD45 and MHC Class I hashtag antibody clones were previously tested in flow cytometry following the surface staining protocol described earlier (2.2.3.2).

$1x10^6$ lung derived single cell suspension obtained in 2.2.1.5 *d)* were transferred to DNA LoBind tubes and centrifuged at 400 g for 5 min at 4 °C. The supernatant was discarded and cells respuspended in

49.5 µl multiplex buffer (see Table 2-6). Then, 0.5 µl FcR block was added, gently mixed and incubated for 10 min at 4 °C. TotalSeq Hashtag antibodies (listed in Table 2-4) were diluted 1:250 in multiplex buffer and centrifuged at 14000 g for 10 min at 4 °C. 50 µl of the supernatant were added to the blocked cells which led to a final antibody dilution of 1:500. After a 30 min incubation at 4 °C, cells were washed once in 3.5 ml PBS supplemented with 0.04 % BSA and three times in 3.5 ml PBS supplemented with 1 % BSA. Centrifugation steps were carried out at 400 g for 5 min and 4 °C. Cells were counted using Neubauer chambers and equal amounts of cells from two samples were mixed. Multiplexed cell suspension was counted again, cell concentration was adjusted to $1x10^3$ cells / µl with PBS containing 1 % BSA and cells were stored on ice until further processing for single cell RNA sequencing.

2.2.6.2 Library preparation and sequencing

Multiplexed samples were then loaded with target cell recovery of 5000 to 15000 cells per lane on the 10x Genomics Chromium Controller. Subsequent reverse transcription, complementary DNA (cDNA) amplification and library preparation were performed using the Chromium Next GEM Single Cell 3'Reagent Kits v.3.1 following the manufacturer's protocol.

Quantification was performed using Qubit system and Agilent 4200 TapeStation was used for quality control of generated cDNA and libraries. Sequencing of generated libraries was performed at the Genomics Facility of Berlin Institute for Medical Systems Biology in Berlin.

2.2.6.3 Data processing and analysis

Raw sequencing data processing using Cell Ranger software (10x Genomics) and de-multiplexing was carried out by Dr. Olufemi Bolaji from the Translational Immunology group at the Berlin Institute of Health at Charité. Quality control, clustering and further analysis were performed using the Seurat R package. Low-quality cells were removed by applying following criteria:

number of features >200
number of features <5000
percentage of mitochondrial genes >9%
number of counts per cell >20000

Then, data were normalized (*NormalizeData* function), feature selection of highly variable genes for downstream analysis (*FindVariableFeatures* Seurat function) and scaling (*ScaleData* function) was carried out. Subsequently, principal component analysis (PCA; *runPCA* function) was performed and based on the Elbowplot, manifold approximation and projection (UMAP) was generated for first 20

principal components (PCs). To correct for batch effects occurring between different libraries and time points (d5 and d45 p.i.), data were integrated using the *FindIntegrationAnchors* and *IntegrateData* functions of Seurat. Clustering was performed on integrated and scaled data by applying *FindNeighbors (reduction = "pca", dims = 1:20)* and *FindClusters (resolution = 0.25)* functions of Seurat. Briefly, the functions calculate a K-nearest neighbor (KNN) graph based on the Euclidean distance in PCA space considering the first 20 PCs and cluster cells based on Louvain algorithm.

As T cells are the main focus of this study, the T cell clusters (expressing CD3) were subsetted for further analysis. T cells subset (approx. 31000 cells) was rescaled and identification of variable genes, PCA and UMAP based on the first 20 PCs were carried out. Then, clustering was performed with a resolution of 1.5. Clusters were merged based on similar gene expression seen in dotplot analysis and heatmap based on top 10 differentially expressed genes (DEG; *FindMarkers* function). In addition, clusters that were contaminations from other cell types were excluded from downstream analysis.

From final 15 T cell clusters, top10 DEG were calculated (Appendix Table 6-3). Cluster were annotated based gene expression of top5 DEG and IMC markers presented in Fig. 3-7.

For DEG and gene set enrichment analysis (GSEA), $CD4^+$ and $CD8^+$ T cells were subsetted based on their expression *Cd8a* and *Cd4* expression and pseudo-bulk samples were generated based all cells of on the respective experimental group. Then, pseudo-bulk samples were normalized and modelled according to DESeq2 pipeline[142]. In addition, GO enrichment analysis was carried out with enrichR package using "GO_Biological_Process_2018" database and selected genes from DEG analysis (p-value <0.05 and baseMean >20). Tested gene lists for GSEA are listed in the appendix (Table 6-4). Fgsea package was used to perform GSEA.

All above mentioned R packages are listed in Table 2-14.

2.2.7 Hemagglutination inhibition (HAI) assay

The HAI assay was used to quantify neutralizing antibodies (AB) in the blood plasma of infected mice. IAV is binding to sialic acid receptors on red blood cells thereby inducing agglutination. The presence of HA-specific AB in the plasma prevents the agglutination of red blood cell and thus serves as a quantification of neutralizing AB.

HAI assay was performed by Dr. Jakob Trimpert at the virology department of the Freie Universität Berlin.

In brief, plasma was treated with periodate solution to inactivate non-specific binding. Then, serial dilutions of pre-treated plasma are incubated with IAV (PR8) for 30-40 min to allow binding of neutralizing AB to virus particles. Finally, a 0.5 % solution of red blood cells derived from chicken were

added and incubated for 30 min. The reciprocal of the last dilution which prevented agglutination was determined as the AB titer.

2.2.8 Statistics and data visualization

Illustrations were created in BioRender or Microsoft PowerPoint. Statistical testing and data visualization were performed either in GraphPad Prism 8 or R using functions implemented in the gglot2 or ComplexHeatmap packages. Data are represented as boxplots with whiskers from min to max, scatter dot plots with mean and standard deviation (SD) and truncated violin lots from min to max. Weight curves were depicted as scatter dot plots with mean and standard error (SEM). Graph data points symbolize biological replicates with the exception of IMC data which symbolize ROI with a maximum of two per mouse.

Statistical significance, used statistical tests and experimental samples sizes are indicated in the respective figure legend. Datasets were tested for normal distribution using ShapiroWilk test and accordingly parametric or non-parametric test were applied. Multiple t-test were corrected by Benjamini-Hochberg. A p-value or adjusted p-value of < 0.05 was considered as significant.

3. Results

3.1 Lung infiltration and intra-tissue migration is hampered in TCAIM overexpressing T cells

3.1.1 Expanded TCAIM overexpressing T cells fail to infiltrate the lung

Previous *in vitro* experiments revealed that TCAIM overexpressing T cells were able to respond to activating signals but failed to acquire full effector T cell phenotype[132,133]. In addition, TCAIM was shown to interfere *in vivo* with effector T cell differentiation and accumulation in allogenic skin grafts that ultimately prevented rejection[132]. However, it is unclear to which extend diminished effector T cell differentiation will impact a disease outcome in TCAIM overexpressing mice, where a T cell response is needed for recovery. On the other hand, TCAIM KO was shown to support T cell activation under suboptimal stimulation conditions *in vitro* by lowering the activation threshold. Hence, TCAIM deficiency might also be advantageous in an *in vivo* setting by promoting early T cell activation and differentiation. Moreover, we lack knowledge if *in vivo* memory T cell generation is altered in TCAIM overexpressing and deficient mice.

To address those open questions, the T cell-specific overexpression or deficiency of TCAIM was tested in an *in vivo* IAV mouse model. Here, T cell responses play an important role as the absence of effector T cells during the acute infection phase impairs viral clearance[149]. Furthermore, IAV infections allow IAV-spec. memory T cell generation. For the experiments, 12 to 16 weeks old mice of the TCAIM KI *Cd4Cre* and TCAIM KO *Cd4Cre* mouse strains were used (Fig. 3-1 A). Homozygous (TCAIM KI or TCAIM KO) and respective wildtype littermates (wt) were intranasally infected with an IAV dose, that induces a T cell response but allows viral clearance and recovery. Organs and blood were collected for different analyses during the acute infection (d3, d5 and d8 p.i.) or after the recovery phase (d45 p.i.). In addition, uninfected control animals (d0) were used.

First, the question was asked if TCAIM overexpression or deficiency affects T cell infiltration at the side of infection. Therefore, whole lungs of TCAIM KI *Cd4Cre*, TCAIM KO *Cd4Cre* and respective wt littermates were perfused and collected on d0 and d8 p.i., which is the peak of the T cell response. Flow cytometry analysis was applied to determine frequencies of total $CD4^+$ T cell, $CD8^+$ T cells or IAV-spec. $CD8^+$ T cells. Latter were defined by MHC class I tetramer antibodies, which are specific for a peptide sequences of the viral proteins NP or PB1 respectively (Fig. 3-1 B).
Wildtype littermates of TCAIM KI *Cd4Cre* strain (light grey) showed a significant expansion and T cell infiltration of $CD4^+$ T cells during the acute infection phase indicated by higher $CD4^+$ T cell numbers in the lungs at d8 p.i. compared to the uninfected control animals at d0 (Fig. 3-1 C, *left*). In contrast, in TCAIM KI mice (blue) no increase in $CD4^+$ T cell numbers in the lung at d8 p.i. was found. A similar but

even stronger pattern was observed for CD8⁺ T cells (Fig. 3-1 C, *middle*). Whereas CD8⁺ T cell number in the lungs of TCAIM KI mice at d8 p.i. remained at a comparable level to d0, wildtype mice showed a profound rise in CD8⁺ T cell numbers compared to uninfected control animals. Not only total CD8⁺ T cell numbers, but also IAV-spec. CD8⁺ T cells numbers increased strongly in lungs of wildtype littermates (Fig. 3-1 C, *right*). There was the tendency of a slightly enhanced lung infiltration of IAV-

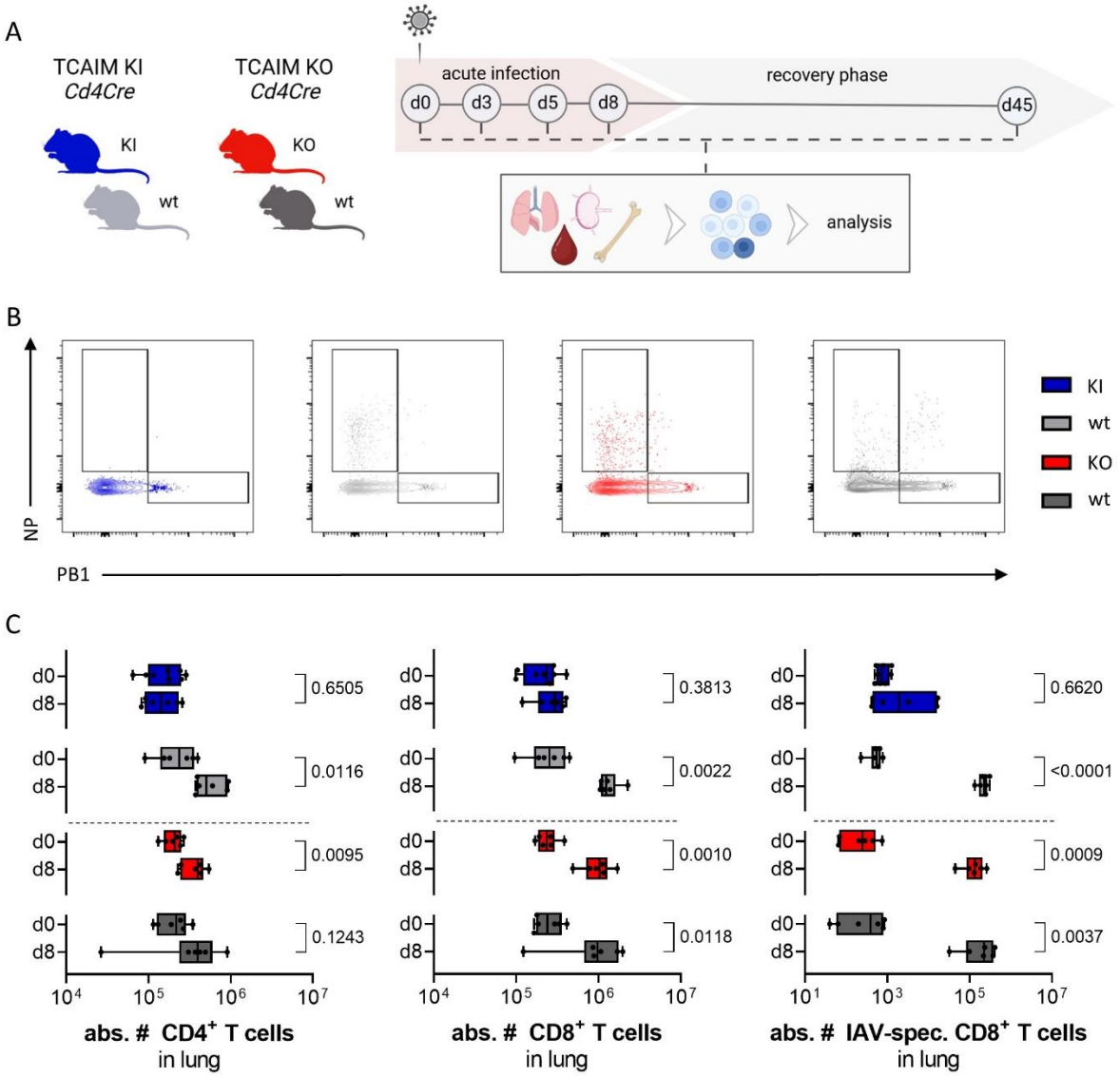

Figure 3-1 T cell expansion and infiltration in the lung is compromised in TCAIM KI Cd4Cre mice. A *Schematic overview of the experimental setup. TCAIM KI Cd4Cre (blue), TCAIM KO Cd4Cre (red) and respective wildtype littermates (light and dark grey) were infected intranasally with 7PFU (plaque forming units) of IAV/PR8. At d3, d5 and d8 during the acute infection phase and d45 in the recovery phase mice were sacrificed and organs collected for analyses.* ***B*** *Representative contour plots of NP and PB1 tetramer staining in CD8⁺ T cells isolated from lungs on d8 p.i. in the different experimental groups.* ***C*** *Boxplots of cell numbers of CD4⁺ (left), CD8⁺ (middle) and IAV-spec. CD8⁺ T cells (right) at d8 p.i. in the lungs of TCAIM KI Cd4Cre, TCAIM KO Cd4Cre and respective wild type littermates. n = 6-8. For statistical analyses data were tested for normal distribution and accordingly, unpaired t-Test or Mann-Whitney test was used to compare d0 and d8 time points of respective experimental groups.*

spec. $CD8^+$ T cells observed in 50 % of TCAIM KI mice, although numbers were around one log-fold lower than in samples of wildtype littermates.
TCAIM KO mice (red) and their respective wildtype littermates (dark grey) both showed a similar and significant increase of total $CD4^+$ T cell, total $CD8^+$ T cell and IAV-spec. $CD8^+$ T cell numbers at d8 p.i. compared to uninfected control animals on d0 (Fig. 3-1 C, *left, middle, right*).

The lack of $CD4^+$ and $CD8^+$ T cell accumulation at the side of infection in TCAIM overexpressing mice raised the question whether the initial T cell activation and expansion in the drLN or the migration and extravasation into the lung tissue was impaired. During IAV infections, MHC mediated presentation of antigens to naïve T cells by APCs in the lung drLN initiates T cell activation and subsequent clonal expansion of antigen-specific T cells. Thus, lung-draining lymph nodes of all experimental groups were collected on d0 and d8 p.i. and T cell frequencies determined using flow cytometry analysis.
Interestingly, TCAIM KI mice showed an expansion of $CD4^+$ T cells (Fig. 3-2 A, *left*), total $CD8^+$ T cells (Fig. 3-2 A, *middle*) and IAV-spec. $CD8^+$ T cells (Fig. 3-2 A, *right*) in drLN on d8 p.i. compared to uninfected control animals. A similar, but slightly stronger expansion of T cell numbers was observed in wildtype littermates. This indicated that TCAIM overexpressing T cells are able to respond to activation signals in drLN, which drive T cell expansion. TCAIM KO and wildtype littermates showed a similar increase in $CD4^+$ T cell, total $CD8^+$ T cell and IAV-spec. $CD8^+$ T cell numbers upon IAV infection (Fig. 3-2A, *left, middle, right).*

After activation and expansion, T cells need to migrate to target tissues to carry out effector functions at the side of infection. Hence, T cells exit the SLO into the blood circulation for transport throughout the body. To see if in drLN expanded TCAIM overexpressing T cells were able to enter the blood circulation for migration to the lung, blood was collected from TCAIM KI *Cd4Cre* and wt littermates at d0 and d8 p.i. T cell frequencies were determined using flow cytometry analysis. TCAIM KI mice showed the tendency of increased $CD4^+$ T cell numbers (Fig. 3-2 B, *left*) and $CD8^+$ T cells (Fig. 3-2 B, *right*) were significantly enriched in the blood at d8 p.i. compared to uninfected controls. In contrast, $CD4^+$ T cells of wildtype littermates tended to be reduced at d8. For $CD8^+$ T cell, no differences in cell numbers were observed. In summary, TCAIM overexpressing $CD4^+$ T cells, $CD8^+$ T cells and IAV-spec. T cells were able to expand in the drLN upon IAV infection similar to wildtype littermates. However, TCAIM KI T cells accumulated in the blood at d8 p.i., but failed to migrate to the side of infection indicated by lower T cell numbers in the lung. A comparable T cell expansion and lung migration was observed in TCAIM KO and wt littermates.

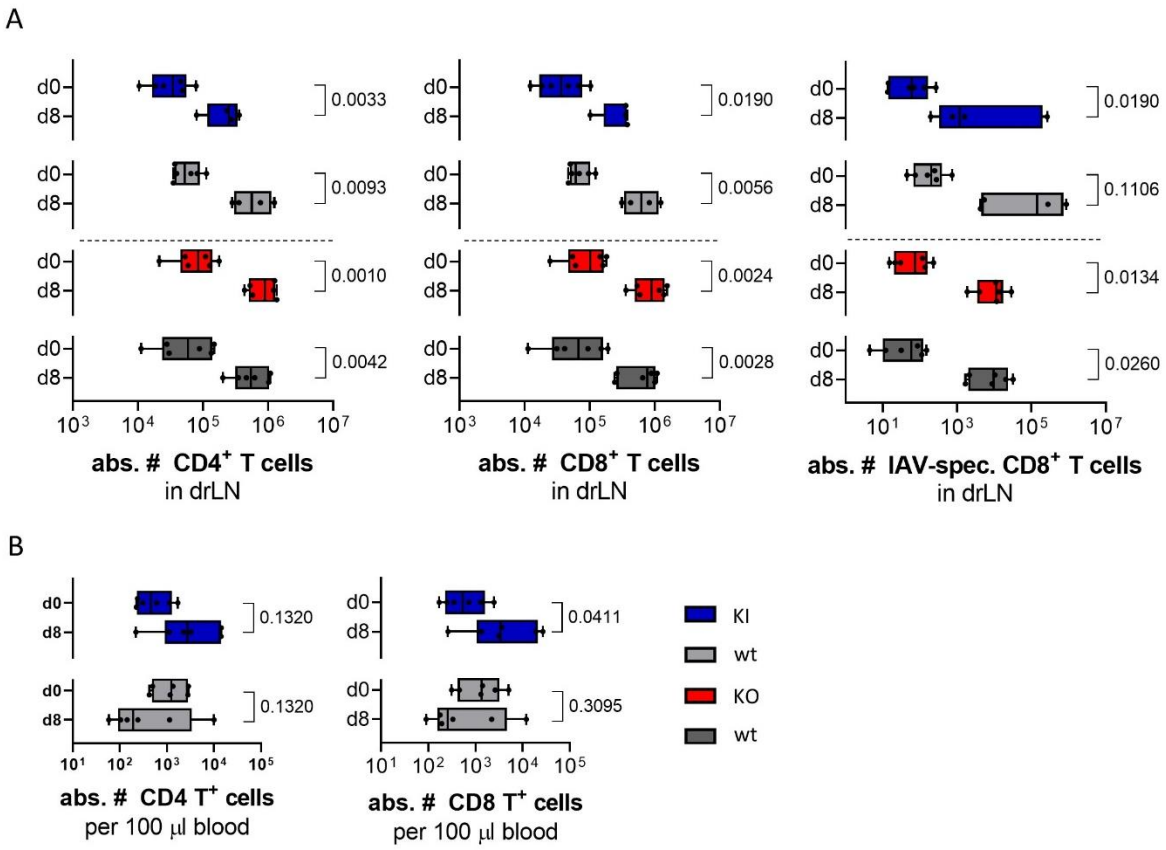

Figure 3-2 TCAIM is not interfering with T cells expansion in drLN and egress into the blood. *TCAIM KI Cd4Cre, TCAIM KO Cd4Cre and respective wildtype littermates were infected intranasally with 7PFU of IAV/PR8. At d8 p.i. drLN and blood were collected and cells analysed using flow cytometry.* ***A*** *Boxplots showing cell numbers of CD4+ (left), CD8+ (middle) and IAV-spec. CD8+ T cells (right) at d8 p.i. in the drLN. n = 4-6.* ***B*** *Boxplots showing cell numbers of CD4+ (left) and CD8+ (right) at d8 p.i. per 100 µl blood. n = 6. For statistical analyses data were tested for normal distribution and accordingly, unpaired t-Test or Mann-Whitney test was used to compare d0 and d8 time points of respective experimental groups.*

3.1.2 Reduced lung accumulation of TCAIM overexpressing T cells is linked to failure in modulating CD44 and CD62L expression

The previous findings demonstrated that TCAIM inhibits the accumulation of T cells in the lung upon IAV infection and was therefore intervening with the migratory potential of T cells. Hence, the question arose if TCAIM influenced the expression of molecules that drive tissue migration. In the drLN, recently activated T cells need to shed the lymph node homing receptor CD62L from the cell surface to allow egress into the blood circulation and migration towards peripheral tissues[83]. As TCAIM overexpressing T cells were able to enter the blood stream, it was hypothesized that TCAIM does not interfere with CD62L shedding. Therefore, at d8 p.i. the CD62L expression of $CD4^+$ T cells and $CD8^+$ T cell in drLN, blood and lung of TCAIM KI, TCAIM KO and respective wild type littermates was determined by flow cytometry.

Wild type littermates of the TCAIM KI *Cd4Cre* mice strain showed high frequencies of CD62L expressing $CD4^+$ T cells (Fig. 3-3 A and B, *upper row*) in the drLN. As expected, CD62L was shed from the cell surface upon egress into the blood circulation and stayed at low levels in $CD4^+$ T cells isolated from whole lungs. In TCAIM KI mice, frequencies of $CD62L^+$ $CD4^+$ T cells in drLN were comparable to wild type littermates and indeed, shedding was observed in T cells in the blood. Surprisingly and in contrast to wt animals,

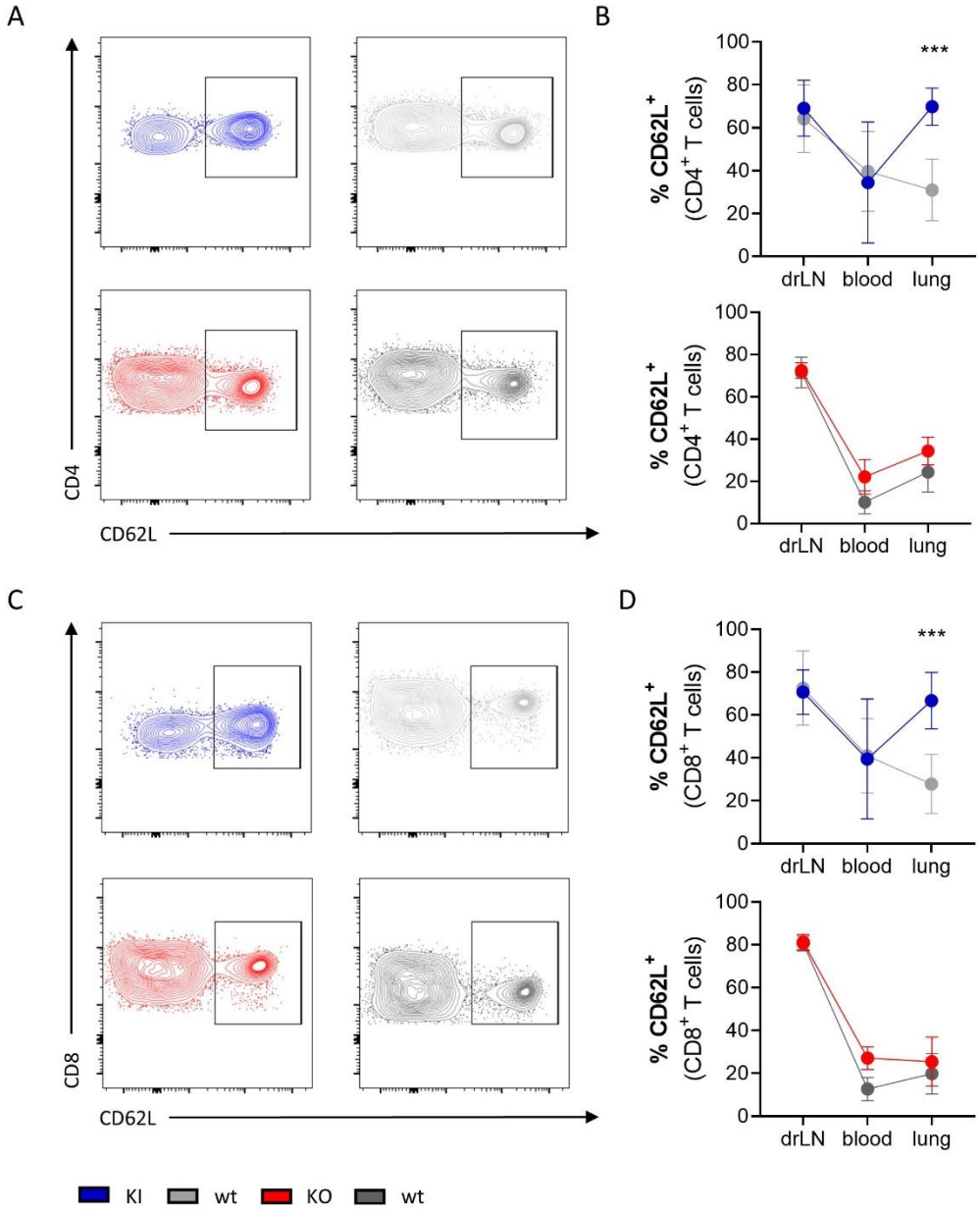

Figure 3-3 CD62L expression is enhanced in T cells in the lungs of TCAIM KI mice. *TCAIM KI Cd4Cre, TCAIM KO Cd4Cre and respective wildtype littermates were infected intranasally with 7PFU of IAV/PR8. At d8 p.i. drLN, blood and lung were collected and cells analysed using flow cytometry.* ***A*** *Representative contour plots of CD62L staining in $CD4^+$ T cells in the different experimental groups.* ***B*** *Frequencies of $CD62L^+$ of $CD4^+$ T cells in the drLN, blood and lung of TCAIM KI and wild type littermates (upper row, n = 6-7) or TCAIM KO and wild type littermates (lower row, n = 6).* ***C*** *Representative contour plots of CD62L staining in $CD8^+$ T cells in the different experimental groups.* ***D*** ***F****requencies of $CD62L^+$ of $CD8^+$ T cells in the drLN, blood and lung of TCAIM KI and wild type littermates (upper row, n = 6-7) or TCAIM KO and wild type littermates (lower row, n = 6). Mean with SD is shown. For statistical analyses multiple T-test adjusted with Benjamini-Hochberg were utilized to compare experimental groups for each collected organ respectively.*

T cells isolated from whole lungs of TCAIM KI *Cd4Cre* mice showed a rise in CD62L expressing T cells to levels as high as in drLN. The same observation was made for $CD8^+$ T cells (Fig. 3-3 C and D, *upper row*). TCAIM KI $CD8^+$ T cells showed similar frequencies of $CD62L^+$ T cells in drLN and shedding was seen in blood located T cells but TCAIM overexpressing $CD8^+$ T cells in the lung re-induced CD62L surface expression.
TCAIM KO did not influence the frequencies of CD62L expressing $CD4^+$ T cells (Fig. 3-3 A and B, *lower row*) nor $CD8^+$ T cell (Fig. 3-3 C and D, *lower row*) in either organ in comparison to wild type littermates.

To enter peripheral tissues, T cells follow tissue specific cues by binding of integrins and selectins that mediate adhesion and extravasation into the target tissue. The glycoprotein CD44 is expressed on activated T cells and was found to play a role in cell adhesion as it binds to hyaluronic acid and E-selectins on the endothelium[89–91]. To check if the expression of the adhesion molecule CD44 was influenced by either TCAIM overexpression or deficiency, CD44 expression of $CD4^+$ T cells and $CD8^+$ T cell in drLN, blood and lung of TCAIM KI, TCAIM KO and respective wild type littermates was determined at d8 p.i. by flow cytometry.

$CD4^+$ T cells of wild type littermates showed low frequencies of $CD44^+$ expressing cells in drLN and blood, but strongly upregulated CD44 surface expression in the lung (Fig. 3-4 A and B, *upper row*). TCAIM overexpressing $CD4^+$ T cells had a tendency of already reduced CD44 expression in drLN, blood and failed to increase the frequency of $CD44^+$ $CD4^+$ T cells in the lung. A similar pattern was observed for TCAIM KI $CD8^+$ T cells (Fig. 3-4 C and D, *upper row*). Here, frequencies of TCAIM overexpressing $CD44^+$ $CD8^+$ T cells in the lung were significantly reduced compared to wild type littermates. TCAIM KO mice and respective wild types were found to have no differences in $CD44^+$ T cell frequencies in $CD4^+$ T cells (Fig. 3-4 A and B, *lower row*) nor $CD8^+$ T cells (Fig. 3-4 C and D, *lower row*) in all organs.

Taken together, TCAIM overexpression was shown to interfere with the expression of proteins involved in T cell migration. Although the lymph node homing receptor CD62L was shed from the surface for exit into the blood circulation, high expression in the lung might drive circulation of TCAIM KI T cells back to SLO.
Already in drLN and blood the trend towards a lower CD44 expression of $CD4^+$ and $CD8^+$ TCAIM KI T cells was observed. Surprisingly, as some cells were able to extravasate, the majority of T cells analyzed in the lung failed to upregulate CD44 surface expression as well. CD44 expression is also well known as an activation marker indicating effector T cell differentiation. In previous in vitro studies, TCAIM KI was shown to impair $CD44^+CD62L^-$ effector T cell differentiation. Hence, reduced CD44 surface expression in TCAIM overexpressing lung T cells shows an inhibited ability to acquire an effector phenotype. TCAIM KO did not interfere with CD62L nor CD44 expression.

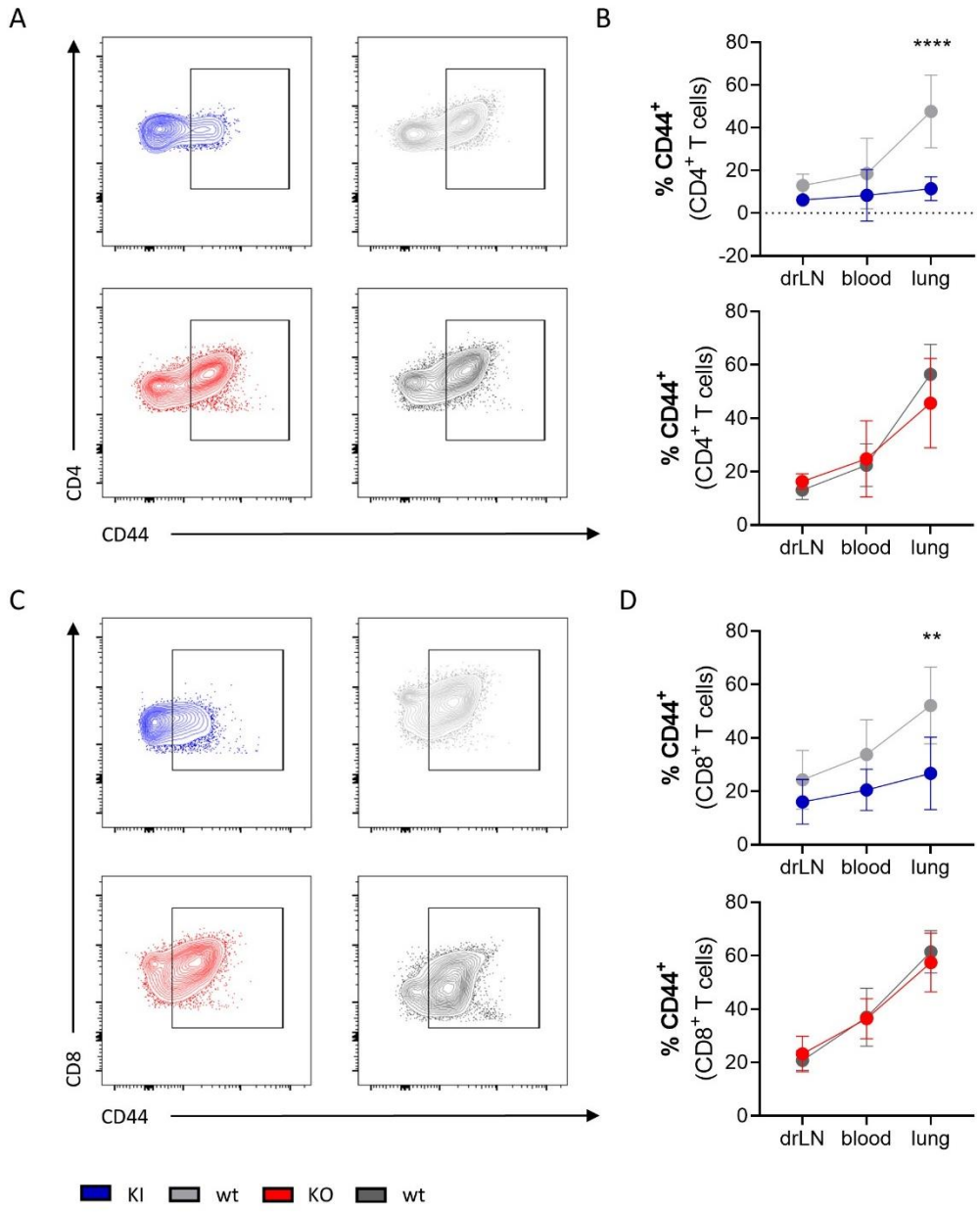

Figure 3-4 TCAIM prevents upregulation of CD44 surface expression in the lung. *TCAIM KI Cd4Cre, TCAIM KO Cd4Cre and respective wildtype littermates were infected intranasally with 7PFU of IAV/PR8. At d8 p.i. drLN, blood and lung were collected and cells analysed using flow cytometry.* ***A*** *Representative contour plots of CD44 staining in CD4⁺ T cells in the different experimental groups.* ***B*** *Frequencies of CD44⁺ of CD4⁺ T cells in the drLN, blood and lung of TCAIM KI and wild type littermates (upper row, n = 6-7) or TCAIM KO and wild type littermates (lower row, n = 6).* ***C*** *Representative contour plots of CD44 staining in CD8⁺ T cells in the different experimental groups.* ***D*** ***F****requencies of CD44⁺ of CD8⁺ T cells in the drLN, blood and lung of TCAIM KI and wild type littermates (upper row, n = 6-7) or TCAIM KO and wild type littermates (lower row, n = 6-). Mean with SD is shown. For statistical analyses multiple T-test adjusted with Benjamini-Hochberg were utilized to compare experimental groups for each collected organ respectively.*

3.1.3 TCAIM deficiency enhances accumulation of T cells across the whole lung tissue

To carry out their effector function at the side of infection, T cells need to exit the vasculature, migrate through the lung tissue and locate at the bronchioles. Here, IAV replicates and spreads further, mainly within epithelial cells of the airways. T cell mediated killing of infected epithelial cells is limiting viral spread, but effector function itself can also cause collateral tissue damage[150,151]. Thus, intra-tissue location and migration of T cells is important to ensure immune response takes place at the correct tissue site.

Although TCAIM KO mice did not show a higher infiltration of the whole lung tissue in flow cytometry analysis, it could be that they especially infiltrate the sides of local inflammation and virus replication. While TCAIM overexpression diminished T cell accumulation in the lung, a small fraction of T cells was found to extravasate and infiltrate the tissue. Here, it is of interest, where TCAIM KI T cells reside within the lung and if they are able to migrate throughout the tissue to reach the side of active viral replication.

To study infiltration at the side of infection and local distribution of infiltrating T cells, imaging mass cytometry (IMC) was applied. Here, metal-labeled antibodies stain proteins on sectioned tissue samples and allow multiplex imaging. TCAIM KI, TCAIM KO and respective wild type animals were infected with IAV and lungs were collected at d3 and d8 p.i. and formalin fixed and paraffin embedded. The IAV infection does not spread into all lung lobes. Instead single lobes are affected[152]. To guarantee that analyzed areas are from infected tissue, H&E staining was utilized to localize areas of ongoing infection and two areas of those regions of interest (ROIs) per mouse were analyzed by IMC. IMC staining and analysis was carried out by Juliette Johnson (Translational Immunology group at the Berlin Institute of Health at Charité).

First, the overall degree of T cell infiltration into the lung tissues was determined by calculating the number of $CD3^+$ cells per 100sqare-pixel (sqpx) to account for different sizes of accessible tissue for the IMC measurement. As previously seen in flow cytometry analysis, TCAIM KI mice did not increase T cell numbers from d3 to d8 p.i., whereas wt littermates showed a significant infiltration of T cells on d8 p.i. (Fig. 3-5 A). Importantly, TCAIM deficient T cells showed a pronounced accumulation of T cells on d8 p.i. (Fig. 3-5 A).

Next, it was of interest to study where lung infiltrating T cells are located within the lung tissue at d8 p.i.. In Fig. 3-5-B exemplary pictures are shown. The vessels are marked by CD31 expression of endothelial cells (yellow), the bronchioles by EpCAM expression of epithelial cells (cyan) and T cells are depicted by the CD3 signal (red). It appears that fewer TCAIM overexpressing T cells are located within the lung and seemingly prefer to accumulate around the vessels. This pattern reminded of the perivascular niche, which is characterized by the accumulation of immune cells upon infection and in

tumor context[153]. In contrast, wt T cells were found to accumulate around the vessels and bronchioles, whereas T cells of TCAIM KO mice seemed to be distributed throughout the whole tissue. To obtain statistical evidence, masks were generated that allow to analyze specific areas of the lung tissue (Fig. 3-5 C). Therefore, CD31 and EpCAM signals were used to mark the endothelial cells of the vessel (red) and epithelial cells of the bronchioles (blue) respectively. The perivascular and peribronchi niches are region of accelerated immune cell accumulation. Hence, the median distance of T cells to the nearest twelve non-immune cells was utilized to determine the size of the niches. At 30 pixel distance from the vessel, the median distance to non-immune cells plateaued and marked the end of the niches.

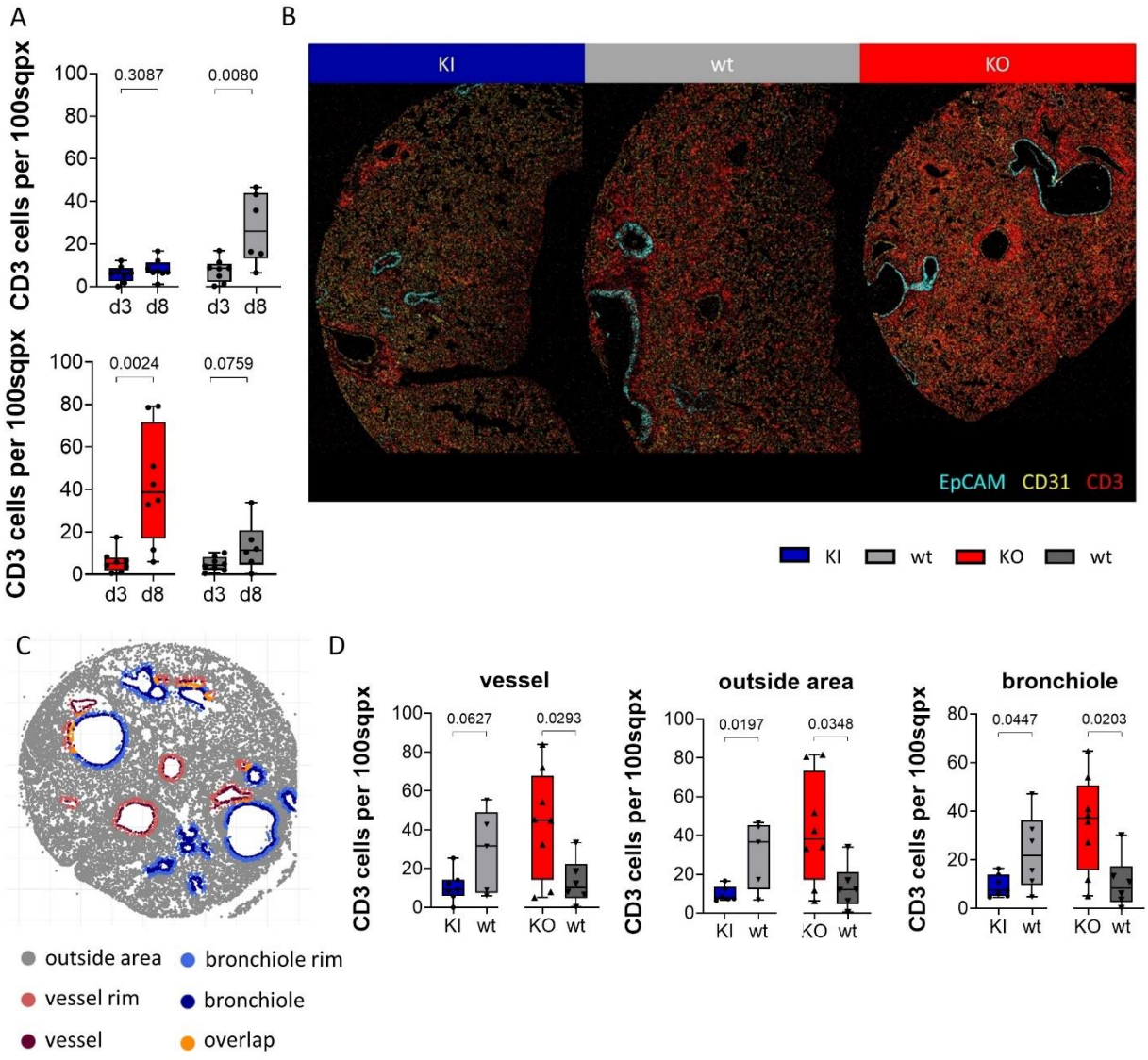

Figure 3-5 Accumulation of TCAIM deficient T cells is increased throughout the lung tissue. *TCAIM KI Cd4Cre, TCAIM KO Cd4Cre and respective wildtype littermates were infected intranasally with 7PFU of IAV/PR8. At d3 and d8 p.i. lungs were collected, formalin fixed paraffin embedded and analysed using imaging mass cytometry.* ***A*** *Boxplots showing T cell numbers per 100 square pixel (sqpx), n = 6-8.* ***B*** *Exemplary lung tissue pictures of d8 p.i. samples representing T cell accumulation patterns (CD3, red) in the tissue, around the vessels (CD31, yellow) or bronchioles (EpCAM, cyan).* ***C*** *Exemplary mask depicting rim areas around vessels or bronchioles.* ***D*** *T cell accumulation per 100 sqpx in the vessel rim (left), the outside area (middle) and bronchiole rim (right) on d8 p.i., n = 5-8. N numbers are representing regions of interest (ROIs) with a maximum of two per mouse. For statistical analyses data were tested for normal distribution and accordingly, unpaired t-Test or Mann-Whitney test was used to compare d3 and d8 time points or respective experimental groups.*

Consequently, a 30 pixel large rim was generated around the vessels and bronchioles. The area outside of the rims is composed of interstitium and alveolar spaces. Finally, T cell numbers per 100 sqpx were calculated for each distinct lung area.

Analyzing the T cell numbers of the determined tissue region revealed that TCAIM overexpressing T cell accumulation did not differ around the vessel compared to wild type littermates (Fig. 3-5 D, *left*), but were significantly reduced in the outside area (Fig. 3-5 D, *middle*) and at the bronchioles (Fig 3-5 D, *right*). This indicates a disadvantage of T cells to leave the perivascular niche and further migrate throughout the lung tissue in TCAIM KI mice. As already proposed based on the representative image, TCAIM KO T cells show enhanced accumulation in all areas (Fig. 3-5 D).

3.2. Reduced intra-tissue accumulation and function of effector T cells in lungs of TCAIM KI mice

So far the data revealed a reduced lung infiltration of TCAIM overexpressing T cells and a decreased ability to leave the perivascular niche. Now, the question arises what causes this disadvantage in TCAIM KI mice and what drives the broad tissue accumulation in TCAIM KO mice. E.g. which phenotypical and molecular differences enable the T cells for migration throughout the tissue. The reduced expression of CD44 and impaired effector T cell differentiation in previous *in vitro* studies already suggests that only differentiated $CD44^+$ T cell might be able to leave the perivascular space. Therefore, first IMC analysis was utilized to study phenotype of T cell populations in the lung and their spatial distribution. Then, scRNAseq analysis was carried out to study molecular differences that cause the alterations in migratory potential of TCAIM overexpressing and deficient T cells.

3.2.1 Expansion of effector T cells and intra-tissue accumulation is abrogated in TCAIM KI mice

For studying the phenotype and spatial distribution of T cell population, T cells measured in IMC were clustered and annotated based on their specific marker expression (Fig. 3-6 A and Fig. 6-1). Then, cell numbers per 100 sqpx were calculated for individual clusters.

To check, whether an effector phenotype including CD44 expression is associated with tissue accumulation and migration during IAV infection, the clusters $CD8^+$ $CD25^+$ $CD44^+$ $CD137^+$ (Fig. 3-6 B and C) and $CD8^+$ $CD127^+$ $CD44^+$ $CD137^+$ (Fig. 3-6 D and E) were analyzed. CD25 is the alpha chain of the IL-2 receptor, thus important for receiving survival and proliferation signals[154,155]. CD127 and CD137 are molecules only expressed on activated T cells[154]. Therefore, the chosen clusters represent activated effector T cell populations. T cells from both clusters were expanding on d8 compared to d3 in TCAIM

KO mice and wild type littermates, whereas accumulation was abrogated in TCAIM KI mice (Fig. 3-6 B, C, D, E, *left panels*). In addition, TCAIM overexpressing T cells of the $CD8^+$ $CD25^+$ $CD44^+$ $CD137^+$ cluster were significantly reduced in all tissue areas (Fig. 3-6 B, *right panel*).

Although predominantly $CD8^+$ T cells are infiltrating the lung during IAV infections, also $CD4^+$ T cells are accumulating at the side of infection. For instance, Tregs are shaping the immune response locally and therefore migrate to the lung. Indeed, activated Treg numbers per 100 sqpx are increased in wild type littermates but not TCAIM KI mice and accumulation was reduced in all tissue areas (cluster $CD4^+$ $FoxP3^+$ $CD25^+$ $CD137^+$ Fig 3-6 F). In contrast, TCAIM deficient Tregs showed a strong expansion on d8 p.i. (Fig 3-6 G). Interestingly, $CD4^+$ $CD16^+$ T cells were enriched only in TCAIM KO mice (Fig. 3-6 H and I, *left panel*) and they tended to accumulate in the outside area (Fig. 3-6 I, *right panel*). $CD16^+$ T cells have been described recently in severe patients of Covid-19[156], highlighting their contribution to tissue damage and disease severity in viral infections.

Those findings showed that TCAIM KI mice did not expand effector T cell populations in the lung which consequently were found to a lesser extend in the different lung areas. This suggests that the acquisition of a proper effector phenotype might be necessary to further migrate throughout the lung tissue.

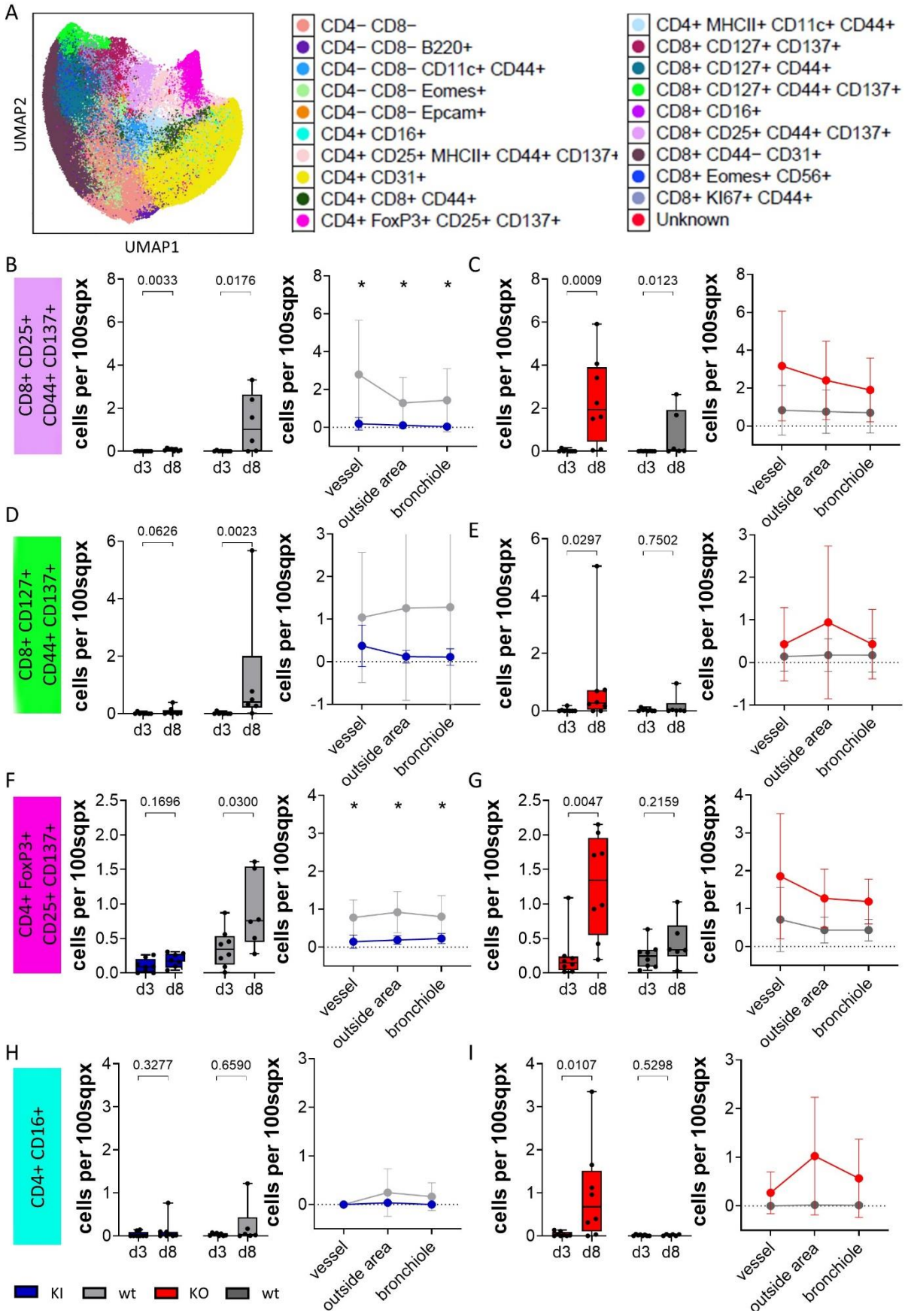
A
UMAP2
UMAP1
CD4− CD8−
CD4− CD8− B220+
CD4− CD8− CD11c+ CD44+
CD4− CD8− Eomes+
CD4− CD8− Epcam+
CD4+ CD16+
CD4+ CD25+ MHCII+ CD44+ CD137+
CD4+ CD31+
CD4+ CD8+ CD44+
CD4+ FoxP3+ CD25+ CD137+
CD4+ MHCII+ CD11c+ CD44+
CD8+ CD127+ CD137+
CD8+ CD127+ CD44+
CD8+ CD127+ CD44+ CD137+
CD8+ CD16+
CD8+ CD25+ CD44+ CD137+
CD8+ CD44− CD31+
CD8+ Eomes+ CD56+
CD8+ KI67+ CD44+
Unknown
B
CD8+ CD25+ CD44+ CD137+
cells per 100sqpx
0.0033
0.0176
d3
d8
vessel
outside area
bronchiole
C
0.0009
0.0123
D
CD8+ CD127+ CD44+ CD137+
0.0626
0.0023
E
0.0297
0.7502
F
CD4+ FoxP3+ CD25+ CD137+
0.1696
0.0300
G
0.0047
0.2159
H
CD4+ CD16+
0.3277
0.6590
I
0.0107
0.5298
KI
wt
KO
wt

Figure 3-6 Impaired expansion and intra-tissue accumulation of CD44⁺ effector T cells in TCAIM KI mice. *TCAIM KI Cd4Cre, TCAIM KO Cd4Cre and respective wildtype littermates were infected intranasally with 7PFU of IAV/PR8. At d3 and d8 p.i. lungs were collected, formalin fixed paraffin embedded and analysed using imaging mass cytometry.* ***A*** *UMAP and cluster-overview of T cell space measured in IMC analysis. Cells per 100 square pixel (sqpx) on d3 and d8 p.i. and in the different lung tissue areas (vessel rim, outside area and bronchiole rim) on d8 p.i. are shown for clusters* ***B+C*** *CD8+ CD25+ CD44+ CD137+,* ***D+E*** *CD8+ CD127+ CD44+ CD137+,* ***F+G*** *CD4+ FoxP3+ CD25+ CD137+ and CD4+ CD16+. n = 5-8. N numbers are representing regions of interest (ROIs) with a maximum of two per mouse. For statistical analyses data were tested for normal distribution and accordingly, unpaired t-Test or Mann-Whitney test was used to compare d3 and d8 time points or respective experimental groups. Scatter dot plots are showing mean with SD. For statistical analyses multiple T-test adjusted with Benjamini-Hochberg were utilized to compare experimental groups for each tissue area respectively.*

3.2.2 Failed acquisition of effector and migration gene signature in TCAIM overexpressing T cells

To unravel the molecular differences that might drive the observed reduced infiltration and intra-tissue migration in TCAIM KI mice and a higher and broader tissue distribution of TCAIM deficient T cells, scNAseq was applied. TCAIM KI, KO and respective wild type littermates were infected with IAV intra-nasally. On d5 p.i, BAL was performed. After perfusion lungs were collected, processed to obtain single cell suspensions and total amount of cells per lung was determined by cell counting. Then, single cells were used for single cell RNA sequencing. Infection success was verified by plaque assay analysis of BAL samples. Four wild type animals neither showed any virus in the BAL nor clinical symptoms and therefore are referred to as uninfected d0 samples. First, cluster analysis was performed to compare changes in T cell populations to IMC analysis.

Unsupervised clustering of T cells led to 15 distinct T cell clusters here visualized in a uniform manifold approximation and projection (UMAP, Fig. 3-7 A). To confirm that $CD4^+$, $CD8^+$ and γδ T cells subpopulations cluster separately, gene expressions of the marker genes *Cd3e*, *Trdc*, Cd4 and *Cd8a* were plotted on the UMAP (Fig. 3-7 B). For cluster annotation, the top 5 differentially expressed genes per cluster were used (Fig. 3-7, A and C). Knowing the total amount of cells per lung and the frequency of the T cell clusters allowed the calculation of total T cell counts for the individual clusters. Those total T cell numbers were then z-score normalized and presented in a heatmap ordered by the clusters (Fig. 3-7 D). Statistical analysis found only one significantly increase when comparing the experimental groups to the uninfected wild type group. This might be due to few replicates and high variation within the groups. Nevertheless, some tendencies were observed and will be introduced hereafter. T cell numbers of clusters 7, 8 and 11 tended to be higher at d5 p.i. in comparison to d0 uninfected animals indicating those clusters might be induced by the viral infection (Fig. 3-7 D and E).

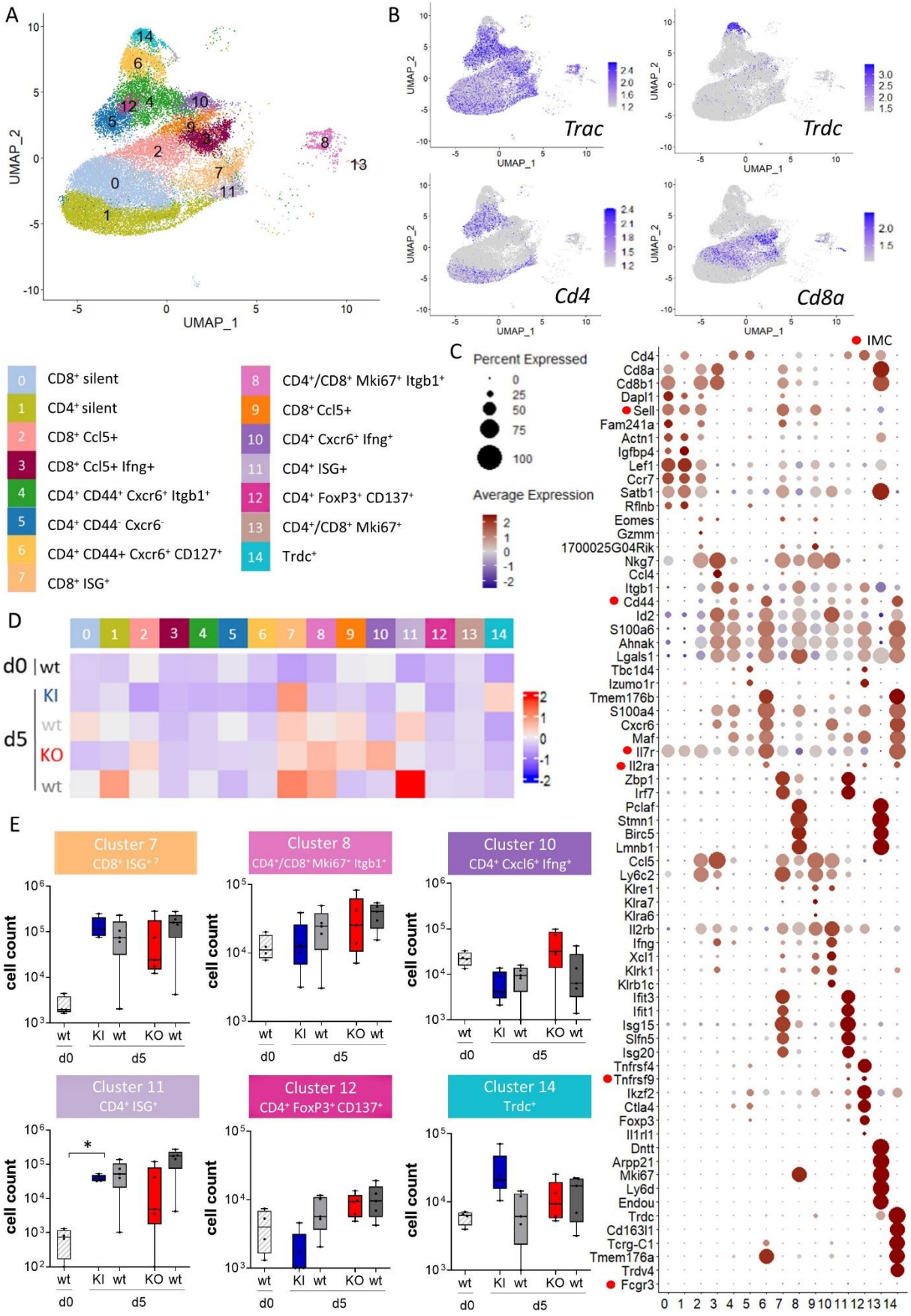
A
B
C
D
E
UMAP_1
UMAP_2
Trac
Trdc
Cd4
Cd8a
0 CD8+ silent
1 CD4+ silent
2 CD8+ Ccl5+
3 CD8+ Ccl5+ Ifng+
4 CD4+ CD44+ Cxcr6+ Itgb1+
5 CD4+ CD44- Cxcr6-
6 CD4+ CD44+ Cxcr6+ CD127+
7 CD8+ ISG+
8 CD4+/CD8+ Mki67+ Itgb1+
9 CD8+ Ccl5+
10 CD4+ Cxcr6+ Ifng+
11 CD4+ ISG+
12 CD4+ FoxP3+ CD137+
13 CD4+/CD8+ Mki67+
14 Trdc+
Percent Expressed
Average Expression
IMC
d0 | wt
d5 KI wt KO wt
Cluster 7
CD8+ ISG+ 7
Cluster 8
CD4+/CD8+ Mki67+ Itgb1+
Cluster 10
CD4+ Cxcl6+ Ifng+
Cluster 11
CD4+ ISG+
Cluster 12
CD4+ FoxP3+ CD137+
Cluster 14
Trdc+
cell count
wt KI wt KO wt
d0 d5

Figure 3-7 TCAIM promotes γδ-T cells but dampens regulatory T cell infiltration. *TCAIM KI Cd4Cre, TCAIM KO Cd4Cre and respective wildtype littermates were infected intranasally with 7PFU of IAV/PR8. At d5 p.i. lungs were collected for scRNAseq analysis.* ***A*** *UMAP of T cell clusters and* ***B*** *highlighted expression of Trac Trdc, Cd4 and Cd8a.* ***C*** *Dotplot showing average gene expression, sclaed per gene, of top5 differntial expressed genes of clusters and markers included in previous IMC analysis indicated with red dot.* ***D*** *Heatmap of z-score normalized cell numbers per cluster and respective experimental group and* ***E*** *cell numvers of selected lusters shown as boxplots. For statistical analyses multiple T-test adjusted with Benjamini-Hochberg were utilized to compare experimental groups (n = 5) to the d0 wild type control group (n = 4).*

T cells from cluster 7 are $CD8^+$ whereas cluster 11 is composed of $CD4^+$ T cells. Both clusters show a strong upregulation of ISG like *Isg15*, *Ifit1* and *Ifit3* (Fig.3-7 C)[157]. This finding reveals that TCAIM overexpressing T cells are able to respond to type I interferon signaling. Surprisingly, T cell numbers of cluster 8 were lower in Tcaim KO mice indicating a reduced expansion of $CD4^+$ ISG^+ T cells on d5 p.i. Cluster 8 cluster is a mix of $CD4^+$ and $CD8^+$ T cells expressing the genes *Stmn1* and *Mki67* known for their role in cell proliferation. Here, TCAIM KI mice showed no expansion of T cell numbers whereas there was a slight increase in wild type littermates. The expansion of cells within ISG^+ clusters indicates that TCAIM overexpressing T cells might be able to respond to IFN signaling in the lung but fail to acquire the effector phenotype for intra-tissue migration seen in IMC analysis.

TCAIM KO showed a tendency of higher T cell numbers in cluster 12, which is a $CD4^+$ T cell cluster expressing *Cxcr6* and *Ifng*. CXCR6 is a chemokine receptor described for tissue resident memory T cells (Trm) cells and positioning of T cells within peripheral tissues hinting towards persistency within the tissue and might also explain the broad tissue distribution seen in IMC analysis[158]. Importantly, scRNAseq data revealed reduced T cell numbers in cluster 14 in TCAIM KI mice compared to wild type littermates on d 5 p.i. Cluster 14 is a $CD4^+$ T cell cluster with a Treg gene signature indicated by *FoxP3* expression. Hence, TCAIM overexpression not only impairs infiltration of conventional T cells seen in flow cytometry analysis, but also inhibits Treg accumulation and local lung expansion, which was also seen in the IMC analysis. In contrast, TCAIM overexpression enhanced the cell count per lung of cluster 16, which is composed of γδ T cells. This was not seen in IMC analysis, as no γδ T cells marker was included. One could speculate that the increase in γδ T cells acts as a compensatory mechanism counterbalancing the missing αβ T cell infiltration in the lungs of IAV infected TCAIM KI animals.

So far, the scRNAseq analysis revealed tendencies in T cell population that were in line with IMC analysis. To find genes or a gene signature that might explain the altered migration potential, differentially expressed gene analysis (DEG), gene ontology (GO) term and gene set enrichment analysis (GSEA) for $CD4^+$ and $CD8^+$ T cell respectively.

DEG analysis of TCAIM KI and wild type littermates revealed three differentially expressed genes in $CD4^+$ T cells (Fig. 3-8 A). TCAIM overexpressing $CD4^+$ T cells showed a higher gene expression of *Bcl2 (B-cell lymphoma 2)*, described for playing a role in cell survival[159], and *Ppp1r21 (Protein Phosphatase 1 Regulatory Subunit 21)*, a regulator of protein phosphatase 1, which is involved in cell division and glycogen metabolism[160,161]. Interestingly, BCL2 is a mitochondria localized protein that has been shown

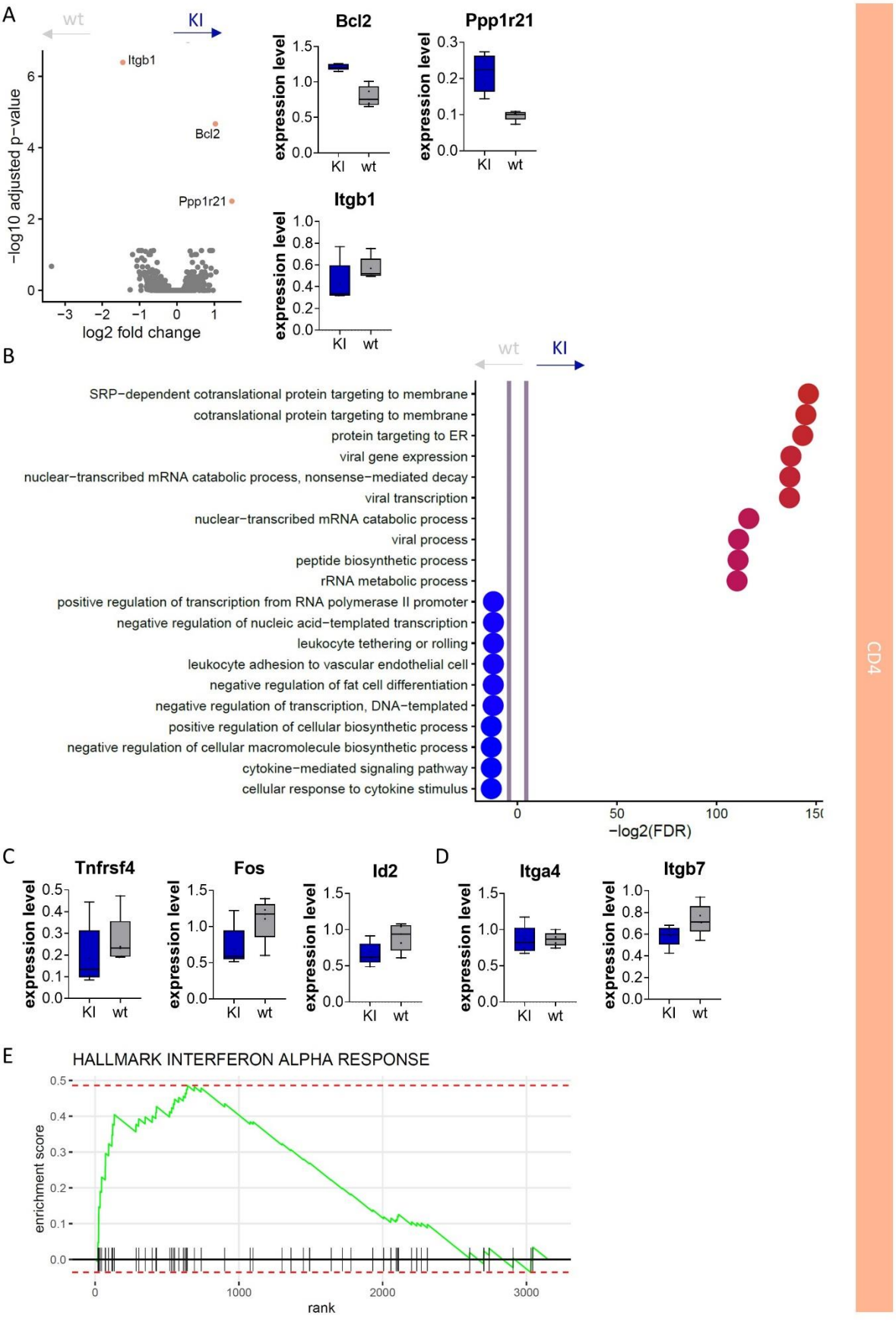
A
wt
KI
Itgb1
Bcl2
Ppp1r21
−log10 adjusted p−value
log2 fold change
Bcl2
Ppp1r21
Itgb1
expression level
KI
wt
B
wt
KI
SRP−dependent cotranslational protein targeting to membrane
cotranslational protein targeting to membrane
protein targeting to ER
viral gene expression
nuclear−transcribed mRNA catabolic process, nonsense−mediated decay
viral transcription
nuclear−transcribed mRNA catabolic process
viral process
peptide biosynthetic process
rRNA metabolic process
positive regulation of transcription from RNA polymerase II promoter
negative regulation of nucleic acid−templated transcription
leukocyte tethering or rolling
leukocyte adhesion to vascular endothelial cell
negative regulation of fat cell differentiation
negative regulation of transcription, DNA−templated
positive regulation of cellular biosynthetic process
negative regulation of cellular macromolecule biosynthetic process
cytokine−mediated signaling pathway
cellular response to cytokine stimulus
−log2(FDR)
C
Tnfrsf4
Fos
Id2
D
Itga4
Itgb7
E
HALLMARK INTERFERON ALPHA RESPONSE
enrichment score
rank
CD4

Figure 3-8 Decreased expression of genes playing a role in T cell differentiation and migration in CD4⁺ TCAIM overexpressing T cells. *ScRNAseq data of CD4⁺ T cells of TCAIM KI and wild type littermates on d5 p.i.. **A** Volcano plot showing the differential expressed genes (DEGs) for TCAIM KI vs. wild type littermates on d5 (DE parameters: log2FC = 0.25, min.pct =0.1, left) and boxplots of selected genes from DEG analysis (right). **B** GO enrichment analysis and selected genes playing a role in **C** T cell activation and differentiation and **D** cell migration. E Gene set enrichment analysis (GSEA) using DEG genes. Ticks represent genes ranked by log2 fold change. Trend in enrichment score is symbolized as green line. Positive trend indicates enrichment in TCAIM KI. n = 5.*

to also interact with VDAC proteins[162,163]. In addition, *Bcl2* is expressed in naïve and memory T cells, but downregulated in effector T cells[164,165]. Here, *Bcl2* expression is high in TCAIM KI CD4⁺ T cells indicating TCAIM preventing acquisition of an effector cell gene signature that matches the previously seen inability to upregulate CD44 and inhibited effector T cell differentiation seen in *in vitro* experiments. The only significantly lower expressed gene in CD4⁺ T cells of TCAIM KI mice was *Itgb1*, also known as CD29 or integrin β1. CD29 is a subunit of VLA-4, a receptor facilitating cell adhesion and firm arrest at the endothelium[92]. This finding shows that the expression of not only CD44 but other receptors needed for cell migration are reduced in TCAIM KI mice, explaining the reduced T cell infiltration in the lung.

GO term analysis showed an enrichment of GO terms describing pathways of protein translation and involvement in viral processes in TCAIM overexpressing CD4⁺ T cells including multiple genes encoding ribosomal proteins e.g. *Rpl3, Rps26* (not shown). In contrast, GO terms describing transcriptional and biosynthetic processes are negatively impacted by the TCAIM KI (Fig. 3-8 B). Genes repeatedly contributing are for example *Tnfrsf4 (Tumor necrosis factor receptor superfamily, member 4), Id2 (Inhibitor of DNA binding 2)* and *Fos*. Tnfrsf4, also known as CD134 or OX40, is a co-stimulatory molecule that is upregulated within the first days upon TCR engagement and supports T cells activation and differentiation[166,167]. Another target of downstream TCR signaling is *Fos*, a subunit of the transcription factor Activator protein 1 (AP-1), which regulates the expression of several activation and cytokine related genes e.g. *Il-2, Cd25* and *Ifng*[168]. Furthermore, *Id2* was shown to be essential for Th1 effector T cell differentiation[169]. Thus, TCAIM overexpression is interfering with the acquisition of an activated effector T cell gene signature. That goes alongside the reduced effector T cell infiltration and expansion seen in IMC, which might be needed to exit the perivascular niche as proposed earlier. In addition, GO term analysis revealed a reduction of genes involved in leukocyte adhesion and tethering. Besides *Itgb1,* the integrins *Itga4* (integrin α4 or CD49d, subunit of VLA-4) and *Itgb7* (integrin β7) were contributing to the GO terms *leukocyte tethering and rolling* and *leukocyte adhesion to vascular endothelial cells.* The lower expression of several adhesion and migration molecules further strengthens the hypothesis of TCAIM dampening the migratory potential of T cells.

In GSEA, interferon alpha response genes were enriched in TCAIM overexpressing CD4⁺ T cells (Fig. 3-8 C) indicating that TCAIM not only allows to respond towards a virus induced stimulus but enhances the signaling activity.

Next, molecular differences within the CD8⁺ T cell of TCAIM KI and wildtype littermates on d5 p.i. were analyzed. In line with CD4⁺ T cells, TCAIM overexpressing CD8⁺ T cells showed a higher expression of *Bcl2* in DEG analysis (Fig. 3-9 A). Another gene that is usually downregulated during T cell activation but is highly expressed in TCAIM KI mice is *Slfn1* (*Schlafen 1*)[170]. *Ikzf2* is encoding for the transcription factor HELIOS, which is well known for its expression in Tregs leading to a lower *IL-2* expression by binding to *Foxp3*[171]. However, HELIOS expression was also described in exhausted CD8⁺ T cells that show impaired cytokine production and effector function[172]. Those findings further support the idea of TCAIM affecting the acquisition of a proper effector phenotype. The high expression of *Irf7* is matching the enhanced type I interferon signaling gene signature seen in CD4⁺ T cells.

TCAIM overexpressing CD8⁺ T cells showed a significantly lower expression of the integrin *Itgb1* that was also observed in CD4⁺ T cells. In addition, gene expression of the chemokine receptor Ccr2 was reduced in TCAIM KI. CCR2 is contributing to T cell migration by its chemotactic properties and is expressed in activated and memory T cells, but not naïve T cells during viral infections[173]. Notably, CCR2 deficient T cells were found to have abolished effector function as IFN-γ and IL-17 cytokine production is impaired[174]. Another gene upregulated during T cell activation and involved in effector phenotype is ICOS. Upon TCR engagement, ICOS is induced in T cells and serves alongside of CD28 as a co-stimulatory molecule during T cell activation[175]. Although best described for its role in Tfh cells and the GC reaction, ICOS is also important for CD8⁺ T cell function. Studies found ICOS deficiency is impairing effector T cell function and memory T cell generation and also reduction of cytokine expressing CD8⁺ T cells in IAV infection[176,177]. Furthermore, the histone encoding genes *Hist1h1c* (H1.2) and *Hist1h1e* (H1.4) were lower expressed in TCAIM KI. In general, histone expression is associated with various cellular processes like cell cycle progression and control of gene expression[178].

In line with CD4⁺ T cells, GO terms describing translation and viral processes (e.g. *Rpl3*, *Rps26; not shown*) and type I IFN signaling (e.g. *Stat2*, *Ifit3*, *Isg20*) were enriched in TCAIM KI CD8⁺ T cells (Fig. 3-9 B). In addition, GSEA showed enriched interferon alpha response. On the other hand, GO term analysis revealed a lower expression of genes contributing to transcriptional processes e.g. *Id2 and Jun,* a subunit of AP-1. Although GO terms describing adhesion and migration were not amongst the most reduced GO terms, GSEA showed GOBP LEUKOCYTE ADHESION TO VASCULAR ENDOTHELIAL CELLS to be reduced in TCAIM KI CD8⁺ T cells (Fig. 3-9 C). Overall, TCAIM overexpressing CD8⁺ T cells were not able to acquire a proper effector T cell and migratory gene signature.

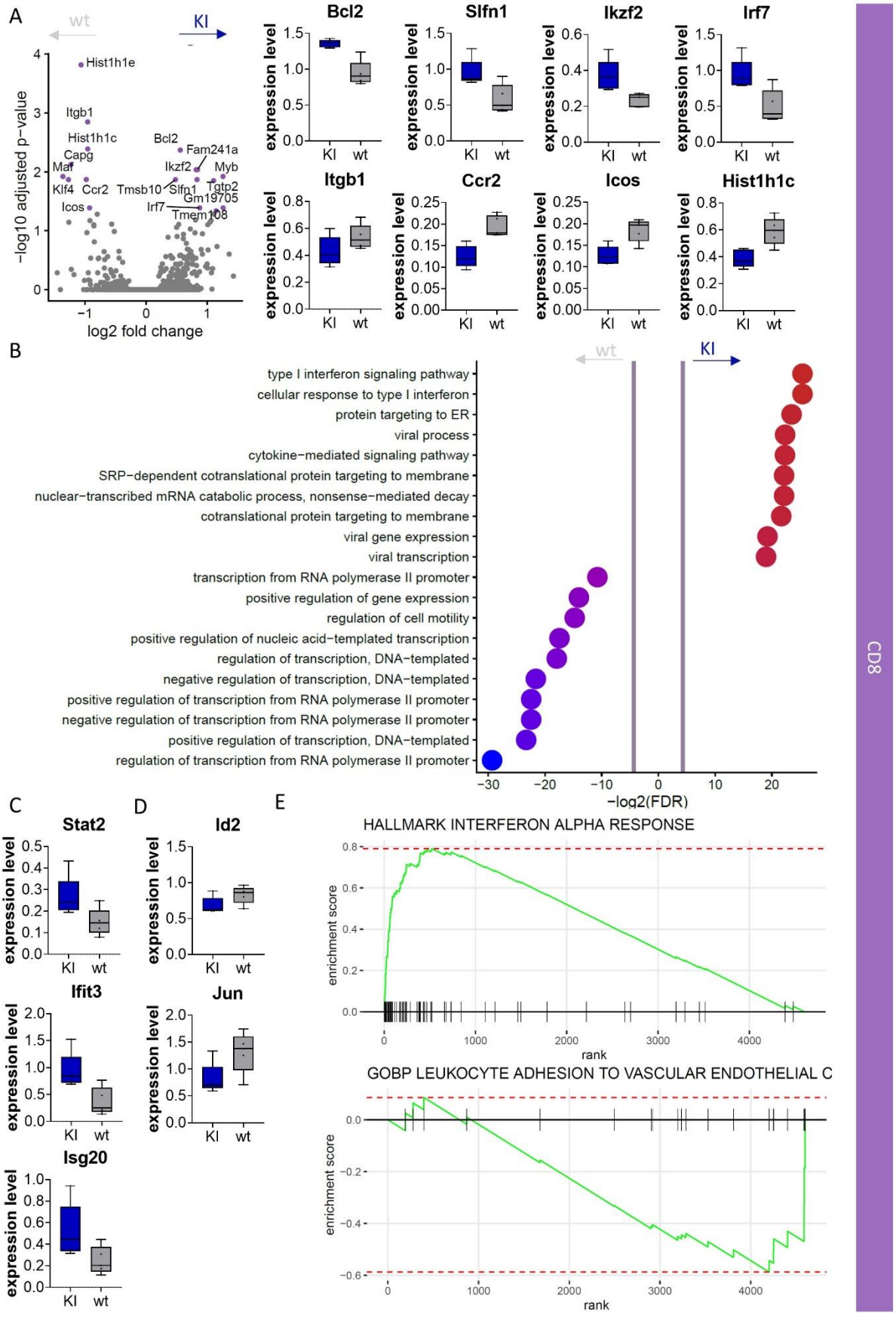
A
wt
KI
Hist1h1e
Itgb1
Hist1h1c
Capg
Maf
Klf4
Ccr2
Icos
Bcl2
Fam241a
Ikzf2
Myb
Tmsb10
Slfn1
Tgtp2
Gm19705
Irf7
Tmem108
−log10 adjusted p−value
log2 fold change
Bcl2
Slfn1
Ikzf2
Irf7
Itgb1
Ccr2
Icos
Hist1h1c
expression level
KI
wt
B
type I interferon signaling pathway
cellular response to type I interferon
protein targeting to ER
viral process
cytokine−mediated signaling pathway
SRP−dependent cotranslational protein targeting to membrane
nuclear−transcribed mRNA catabolic process, nonsense−mediated decay
cotranslational protein targeting to membrane
viral gene expression
viral transcription
transcription from RNA polymerase II promoter
positive regulation of gene expression
regulation of cell motility
positive regulation of nucleic acid−templated transcription
regulation of transcription, DNA−templated
negative regulation of transcription, DNA−templated
positive regulation of transcription from RNA polymerase II promoter
negative regulation of transcription from RNA polymerase II promoter
positive regulation of transcription, DNA−templated
regulation of transcription from RNA polymerase II promoter
−log2(FDR)
C
Stat2
Ifit3
Isg20
D
Id2
Jun
E
HALLMARK INTERFERON ALPHA RESPONSE
GOBP LEUKOCYTE ADHESION TO VASCULAR ENDOTHELIAL C
enrichment score
rank
CD8

Figure 3-9 TCAIM overexpressing CD8⁺ T cells are able to respond to type I IFN signaling but do not show migrationa nd effector T cell gene signature*. ScRNAseq data of CD8⁺ T cells of TCAIM KI and wild type littermates on d5 p.i.. **A** Volcano plot showing the differential expressed genes (DEGs) for TCAIM KI vs. wild type littermates on d5 (DE parameters: log2FC = 0.25, min.pct =0.1, left) and boxplots of selected genes from DEG analysis (right). **B** GO enrichment analysis and selected genes playing a role in **C** type I interferon signaling and **D** T cell activation and differentiation. **E** Gene set enrichment analysis (GSEA) using DEG genes. Ticks represent genes ranked by log2 fold change. Trend in enrichment score is symbolized as green line. Positive trend indicates enrichment in TCAIM KI. n = 5.*

Differences in DEG, GO term and GSEA analysis in T cell from TCAIM KO mice compared to wild type littermates were found within CD4⁺ T cells but not for CD8⁺ T cells. Among the significantly higher expressed genes in CD4⁺ T cells in DEG analysis was *Cxcr6* (Fig. 3-10 A) that was already been shown to be expressed in cluster 10, which was enriched in TCAIM KO. The transcription factors *Fosl2*, a subunit of AP-1, and *Bhlhe40* as well as *Rgs2* are upregulated during T cell activation. Higher expression in TCAIM deficient CD4⁺ T cells at d5 p.i. indicates a faster activation and supports the idea of TCAIM KO may providing an advantage during T cell activation. Deficiency of those genes was shown to interfere with T cell activation and cytokine production which strengthens their importance for T cell activation and differentiation. In addition, *Ifng* gene expression was increased in TCAIM KO CD4⁺ T cells. Reduced gene expression was observed for *Chil3* (*chitinase-like protein 3*), normally downregulated during T cell activation[179], and *GM42418*, a long non-coding RNA.

In GO term analysis, heat shock proteins (e.g. *Hspa5*, *Hspa1a*; not shown) contributing to stress induced GO term e.g. response to unfolded proteins were enriched in TCAIM KO CD4⁺ T cells. Importantly, also transcription and activation associated GO terms were enriched. Here, amongst others, *Id2*, *Cd28* and *Egr1*, a transcription factor downstream of TCR signaling[180], are contributing (Fig. 3 B). In contrast, reduced expression of genes partaking in the type I interferon signaling was observed (Fig. 3-10 C).

In summary, TCAIM overexpression allows type I interferon signaling but prevents transcription of genes involved in migration as well as T cell differentiation, which includes expression of integrins, co-stimulatory molecules and components of TCR signaling. The opposite was observed in TAIM KO CD4⁺ T cells. Here, TCAIM deficiency supports an increased expression of T cell activation associated genes.

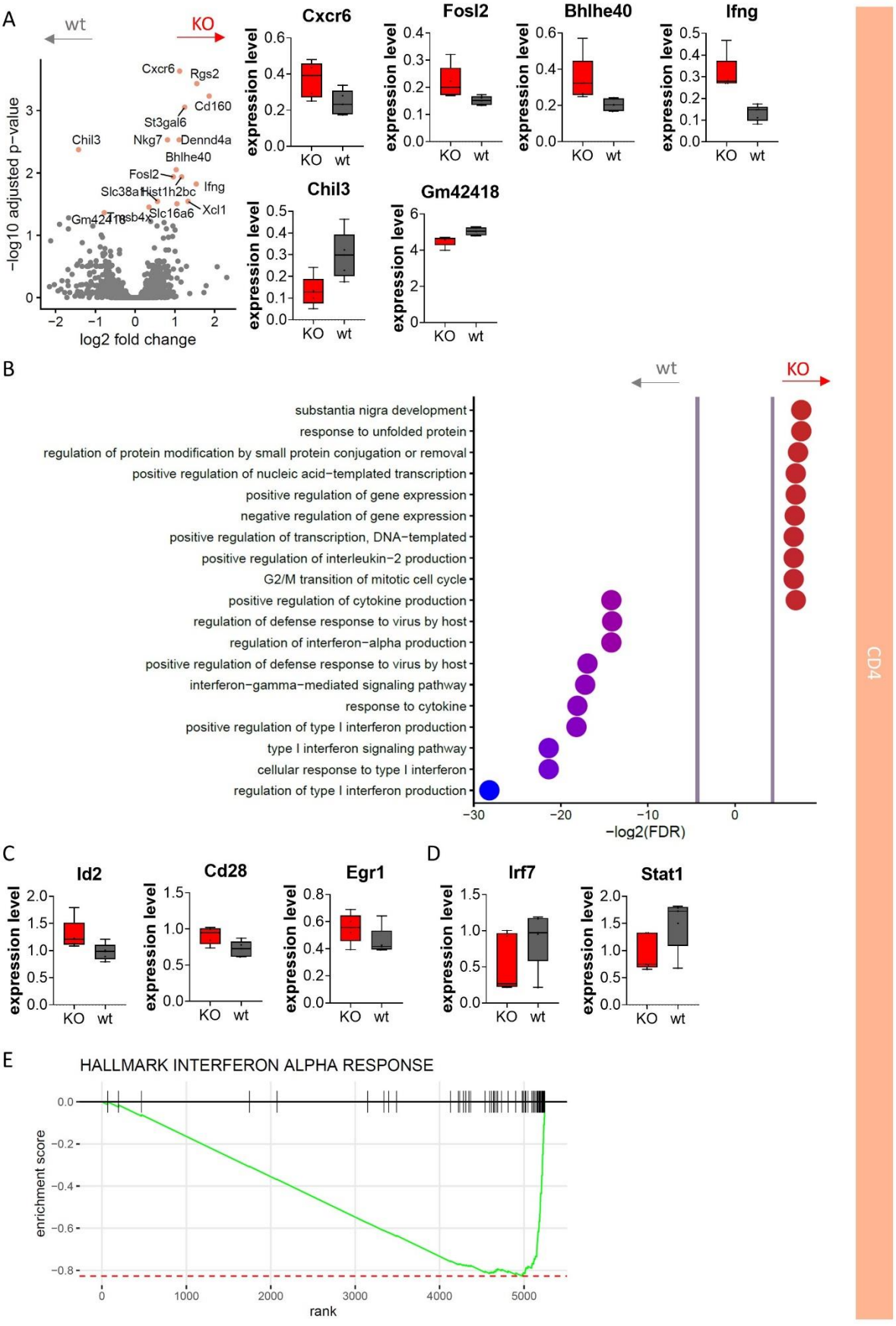
A
wt
KO
Cxcr6
Rgs2
Cd160
St3gal6
Chil3
Nkg7
Dennd4a
Bhlhe40
Fosl2
Slc38a1
Hist1h2bc
Ifng
Xcl1
Slc16a6
Gm42418
Tmsb4x
−log10 adjusted p−value
log2 fold change
Cxcr6
Fosl2
Bhlhe40
Ifng
Chil3
Gm42418
expression level
KO
wt
B
wt
KO
substantia nigra development
response to unfolded protein
regulation of protein modification by small protein conjugation or removal
positive regulation of nucleic acid−templated transcription
positive regulation of gene expression
negative regulation of gene expression
positive regulation of transcription, DNA−templated
positive regulation of interleukin−2 production
G2/M transition of mitotic cell cycle
positive regulation of cytokine production
regulation of defense response to virus by host
regulation of interferon−alpha production
positive regulation of defense response to virus by host
interferon−gamma−mediated signaling pathway
response to cytokine
positive regulation of type I interferon production
type I interferon signaling pathway
cellular response to type I interferon
regulation of type I interferon production
−log2(FDR)
C
Id2
Cd28
Egr1
D
Irf7
Stat1
E
HALLMARK INTERFERON ALPHA RESPONSE
enrichment score
rank
CD4

Figure 3-10 Increased expression of genes asscciated with T cell activation and differentiation in TCAIM deficient CD4⁺ T cells. *ScRNAseq data of CD4⁺ T cells of TCAIM KO and wild type littermates on d5 p.i.. **A** Volcano plot showing the differential expressed genes (DEGs) for TCAIM KI vs. wild type littermates on d5 (DE parameters: log2FC = 0.25, min.pct =0.1, left) and boxplots of selected genes from DEG analysis (right). **B** GO enrichment analysis and selected genes playing a role in **C** T cell activation and differentiation and **D** type I interferon signaling. E Gene set enrichment analysis (GSEA) using DEG genes. Ticks represent genes ranked by log2 fold change. Trend in enrichment score is symbolized as green line. Positive trend indicates enrichment in TCAIM KO. n = 5.*

3.2.3 Impaired effector T cell gene signature translates into decreased effector T cell function in TCAIM KI mice

One hallmark of proper effector T cell differentiation is carrying out effector functions like the production of cytokines and cytotoxic molecules that contribute to the immune response against IAV. As the scRNAseq analysis of TCAIM overexpressing T cells revealed not only an inhibition of genes playing a role in cell migration but also genes involved in downstream TCR signaling and T cell differentiation, it was consequently hypothesized that TCAIM KI T cells might have a reduced effector function. In contrast, the increased expression especially of *Ifng* in TCAIM deficient CD4⁺ T cells might lead to enhanced effector function.

To investigate the functional properties of the T cells, analyses were performed at d8 p.i., as this is the peak of the infection induced T cell response. First, the IFN-γ protein concentration in BAL samples of TCAIM KI, TCAIM KO and wild type littermate mice was determined using a multiplex protein assay. Strikingly, TCAIM KI mice had not only reduced but almost absent IFN-γ protein concentration in contrast to wild type littermates (Fig. 3-11 A). TCAIM KO mice did not show higher IFN-γ concentration in the BAL (Fig. 3-11 A).

IFN-γ is not exclusively secreted by T cells but can also originate from e.g. NK cells[60]. Thus, IFN-γ concentrations in BAL cannot be solely attributed to T cells. To see if T cells of TCAIM KI, KO and wt mice were able to produce IFN-γ, cytokine production was measured specifically in CD4⁺, total CD8⁺ and IAV-spec. CD8⁺ T cells using flow cytometry. Cells were isolated from infected lungs at d8 p.i. and re-stimulated *in vitro* with PMA and ionomycin for 4 h. The addition of Brefeldin A 2 h before the end of the re-stimulation prevented the secretion of cytokines and allows the intracellular staining and detection in flow cytometry.

Indeed, TCAIM overexpressing CD4⁺ T cells showed a strong reduction in the frequencies of IFN-γ producing cells compared to wild type littermates (Fig. 3-11 B). However, no difference was observed in CD8⁺ T cells (Fig. 3-11 C). In contrast, the tendency of reduced IFN-γ producing TCAIM KI IAV-spec. CD8⁺ T cells was found (Fig. 3-11 C). Surprisingly, the higher *Ifng* gene expression observed in scRANseq on d5 p.i. did not translate to increased frequencies of IFN-γ producing CD4⁺, total CD8⁺ and IAV-spec. CD8⁺ T cells in TCAIM deficient mice on d8 p.i. (Fig. 3-11, B and C).

IFN-γ is only one example to study the effector function of lung located T cells. One signature cytokine of activated $CD4^+$ T cells is the cytokine IL-2, which supports T cell expansion and differentiation[181]. In $CD8^+$ T cells, GranB production is a hallmark of their cytotoxic function. In line with IFN-γ, lower frequencies of IL-2^+ $CD4^+$ T cells and $GranB^+$ $CD8^+$ T cell were detected in the lungs of TCAIM overexpressing mice compared to wild type littermates (Fig. 3-11 D and E) indicating an overall reduced effector function. For TCAIM KO no differences in IL-2 nor GranB producing T cells were observed.

The previously seen reduced expression of genes involved in T cell differentiation and migration in TCAIM overexpressing T cells, translated into reduced effector function seen by lower frequencies of cytokine producing T cells in the lung. Although *Ifng* was highly expressed in TCAIM deficient $CD4^+$ T cells at d5 p.i., that did not translate to higher frequencies of IFN-γ producing T cells at the peak of infection.

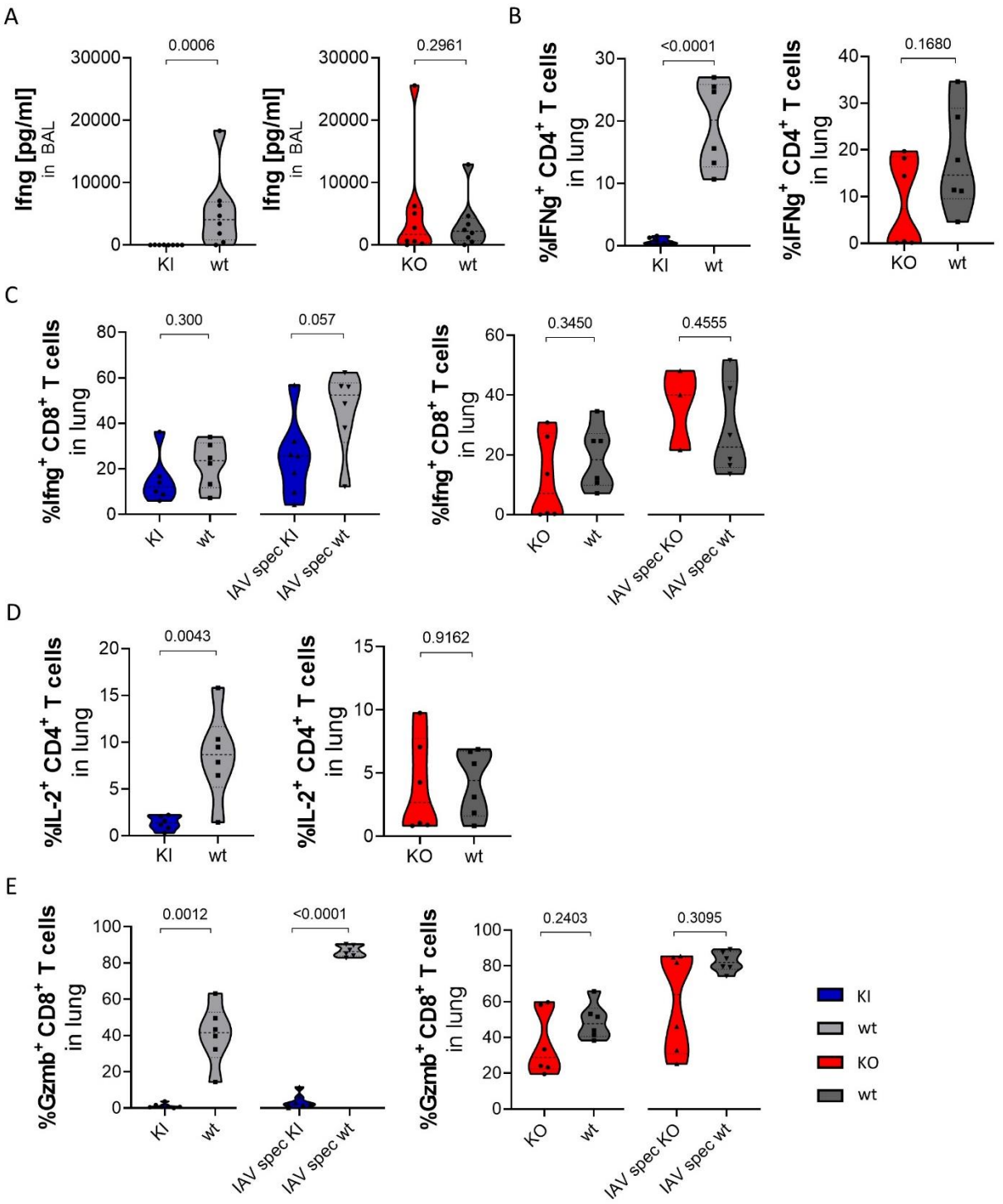

Figure 3-11 TCAIM impairs cytokine production of T cells located in the lung. *TCAIM KI Cd4Cre, TCAIM KO Cd4Cre and respective wildtype littermates were infected intranasally with 7PFU of IAV/PR8. At d8 p.i. broncho alveolar lavage (BAL) and lungs were collected.* ***A*** *Protein analysis of FN-γ concentrations in BAL n = 8. Flow cytometric analysis of* ***B*** *IFN-γ⁺ CD4⁺,* ***C*** *IFN-γ CD8⁺ (left) and IAV.spec. CD8⁺ (right),* ***D*** *IL-2⁺ CD4⁺ and* ***E*** *Gzmb⁺ CD8⁺ (left) and IAV spec. CD8⁺ T cells (right) of experimental groups, n = 3-7. For statistical analyses data were tested for normal distribution and accordingly, unpaired t-Test or Mann-Whitney test was used to compare experimental group with respective wild type littermates.*

3.3 Reduced T cell infiltration and function is linked to abolished immunopathology in TCAIM KI mice

During IAV infections, local $CD8^+$ T cell mediated cytotoxic activity is important to control and clear the viral infection in the lung. Hence, the lack of T cell infiltration and function in TCAIM KI mice led to the hypothesis, that viral clearance is comprised in TCAIM KI mice. Due to the equal cytokine production at d8 p.i. in TCAIM KO mice, no differences in viral control were expected. Lungs and BAL samples of infected TCAIM KI, KO and wild type littermates were collected at d3 p.i. during the early infection phase and at d8 p.i., the peak of the IAV infection. Viral loads of lung and BAL samples were determined in plaque assay analysis.

Indeed, although viral loads of lung and BAL samples of TCAIM KI mice were comparable to wt mice at d3 p.i., TCAIM KI mice showed higher viral loads in both tissues at d8 p.i. (Fig.3-12 A and B, *left*). Thus, viral clearance was delayed or even inhibited due to reduced performance and infiltration of TCAIM overexpressing T cells. No differences in viral loads in lung nor BAL of TCAIM KO mice in comparison to wild type mice were observed (Fig.3-12 A and B, *right*).

T cell are not only playing a role in viral clearance, but can also contribute to immunopathology. It has been described before, that weight loss during viral infection is part of the T cell induced immunopathology[149,150]. Hence, lack of T cell infiltration and function in TCAIM KI mice might have abrogated T cell induced immunopathology. Indeed, TCAIM KI mice did not lose as much weight as compared to wild type littermates (Fig.3-12 C, *left*). A similar weight loss was observed TCAIM KO mice and respective wild types (Fig.3-12 C, *right*).

Taken together, TCAIM KI mice showed a delayed viral clearance on d8 p.i. and prevented weight loss during the acute infection, which might be a direct consequence from the lack of T cell infiltration and function in the lung.

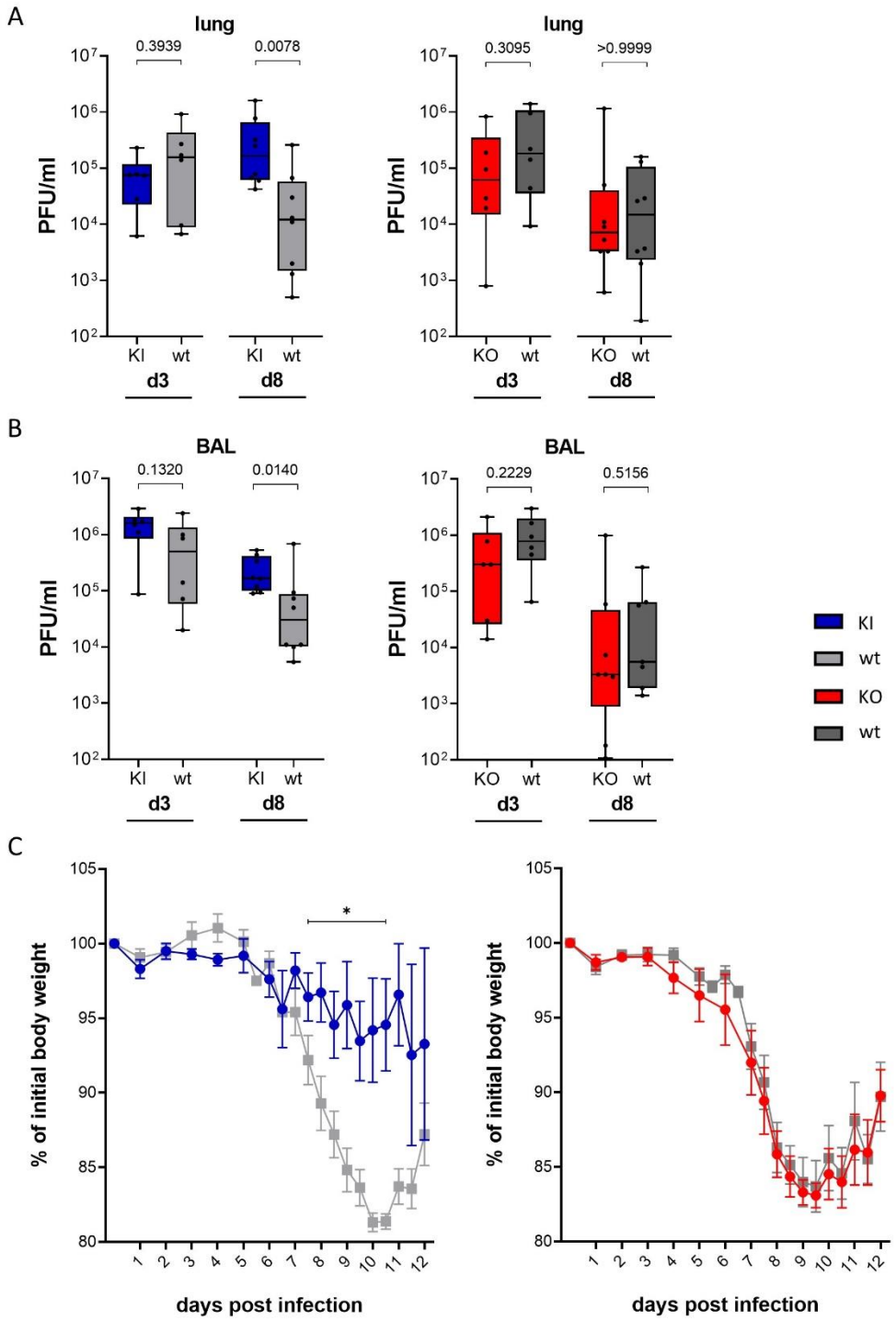

Figure 3-12 TCAIM delays viral clearance but reduces T cell induced weight loss. *TCAIM KI Cd4Cre, TCAIM KO Cd4Cre and respective wildtype littermates were infected intranasally with 7PFU of IAV/PR8. Body weight was monitored and at d3 and d8 p.i. lung and BAL were collected for plaque assay analysis. Viral load was measured in* ***A*** *lung and* ***B*** *BAL on d3 and d8 p.i. respectively, n = 6-8, PFU = plaque forming unit, BAL = broncho alveolar lavage.* ***C*** *Weight curves of IAV-infected TCAIM KI (upper row, n=8), TCAIM KO (lower row, n=6) and wild type littermates representing the mean percentage with SEM of the intial body weight. For statistical analyses of viral load data were tested for normal distribution and accordingly, unpaired t-Test or Mann-Whitney test was used to compare experimental group with respective wild type littermates. For statistical analyses of weight curves multiple T-test adjusted with Benjamini-Hochberg were utilized to compare experimental groups at each time point post infection.*

3.4 Generation of neutralizing antibodies despite failure to promote differentiation of tissue-resident memory T cells in TCAIM overexpressing mice

3.4.1 Recovery from the IAV infection is accompanied by reduced formation of tissue-resident memory T cell in TCAIM KI mice

Beside the performance during the acute infection phase, it was of interest, what long term consequences the TCAIM mediated alterations in T cell performance had for disease outcome and the ability to form a protective memory. The here chosen infection dose of 7 PFU is a mild dose that allowed recovery of the animals. Importantly, studies found that mice without $CD4^+$ and $CD8^+$ T cells are unable to clear and recover from viral infections[149]. TCAIM KI mice not only had less T cell accumulation of both at the side of infection but also their effector function was impaired, which led to the hypothesis that recovery from IAV infection is impacted.

One hallmark of successful recovery from the IAV infection is a weight gain not only returning to the initial body weight but also exceeding it as part of the normal mouse aging process. Therefore, body weight of infected TCAIM KI, KO and wild type littermates was documented until d45 p.i.
Surprisingly, weight curves of TCAIM KI mice did not drop at a later time point but instead showed a comparable, although flatter, ascent compared to wild type littermates (Fig. 3-13 A, *top*), indicating a recovery of infected animals. Weight gain of TCAIM KO animals tended to be slower compared to respective wild type animals (Fig. 3-13 A, *bottom*).
Recovery does not only come with gaining weight but it also requires clearance of the viral infection. Thus, viral loads of BAL samples on d45 p.i. were measured in plaque assay analysis. 75 % of TCAIM KI mice were able to completely clear the viral infection and overall viral loads were not significantly different from wild type mice (Fig. 3-13 B).. Two mice of TCAIM KI strain remain slightly positive with 6.7 PFU/ml in plaque assay analysis. Compared to viral titer at d3 or d8 p.i. this is a very low viral load indicating that viral load is almost cleared and presumably will be.

Now, knowing that TCAIM KI mice could survive and clear the IAV infection, it was of interest whether a memory T cell pool was generated that could potentially offer protection upon a re-challenge. Therefore, TCAIM KI, TCAIM KO and wild type littermates were infected, organs collected at d45 p.i. and resulting single cells analyzed using flow cytometry. To ensure that the effector T cell response of the acute infections phase was concluded and only memory T cell, a late time point was chosen for the analysis.
One important memory T cell subtype are Trm which reside in the lungs long term. Cell numbers of total $CD4^+$ and $CD8^+$ T cells showed the tendency to be reduced in TCAIM KI mice compared to

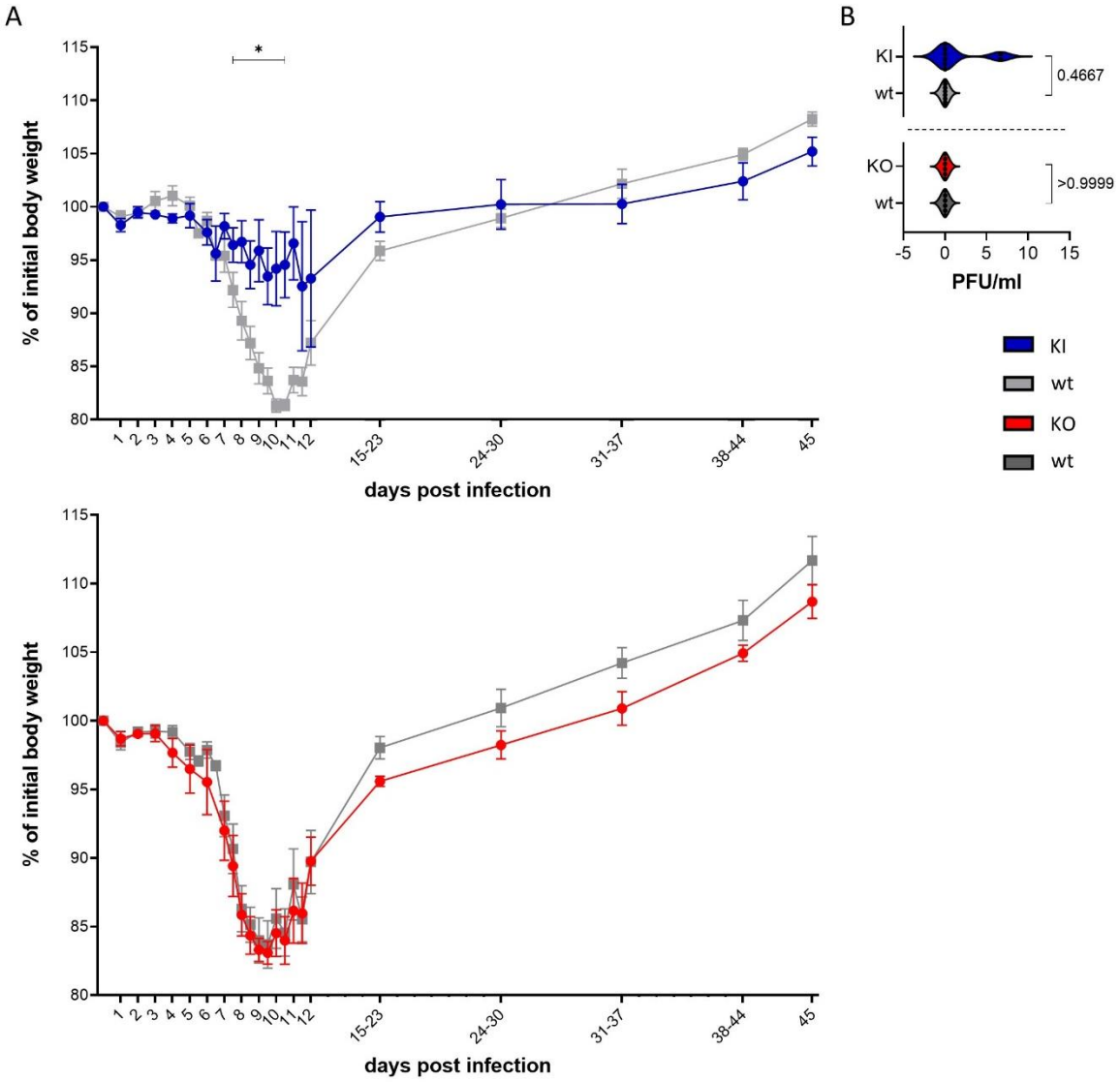

Figure 3-13 Recovery from IAV infection is supported in TCAIM KI mice.. *TCAIM KI Cd4Cre, TCAIM KO Cd4Cre and respective wildtype littermates were infected intranasally with 7PFU of IAV/PR8. Body weight was monitored and at d45 p.i. BAL was collected for plaque assay analysis.* ***A*** *Weight curves of IAV-infected TCAIM KI (upper row, n=8), TCAIM KO (lower row, n=6) and wild type littermates representing the mean percentage with SEM of the intial body weight.* ***B*** *Viral load in BAL on d45 p.i. measured in plaque assay analysis. PFU = plaque forming unit, BAL = broncho alveolar lavage, n = 6-8. For statistical analyses of weight curves multiple T-test adjusted with Benjamini-Hochberg were utilized to compare experimental groups at each time point post infection. For statistical analyses of viral load data were tested for normal distribution and accordingly, unpaired t-Test or Mann-Whitney test was used to compare experimental group with respective wild type littermates.*

respective wild types (Fig. 3-14 A, *left and middle*). Of note, total $CD4^+$ and $CD8^+$ T cell count includes non-IAV-specific T cells which are not necessarily memory T cells. When looking into the cell numbers of IAV-spec. T cells on d45 p.i., one can be confident that those T cells are memory T cells. Here, a striking inhibition of lung accumulation of TCAIM overexpressing IAV-spec. $CD8^+$ T cells was found (Fig. 3-14 A, *right*). In lungs of TCAIM KO mice, no differences in cell numbers of $CD4^+$, $CD8^+$ nor IAV-spec. $CD8^+$ T cells compared to wild type littermates on d45 p.i. was observed, indicating no beneficial effect on memory T cell generation (Fig. 3-14 A, *left, middle and right*). Lung Trm are known to downregulate

CD62L, but express CD44 and CD103 on their surface. CD103, also integrin αE, is an integrin binding to E-cadherin thereby facilitating adhesion and tissue retention[182,183]. To check if TCAIM overexpressing IAV-spec. $CD8^+$ memory T cells showed phenotypical differences in the lung, expression of CD44, CD62L and the Trm marker CD103 were investigated. In line with T cell during the acute infection phase, higher frequencies of IAV-spec. $CD8^+$ memory T cells of TCAIM KI mice did express CD62L on their surface (Fig. 3-14 B, *left*), whereas frequencies of $CD44^+$ and $CD103^+$ cells were reduced (Fig. 3-14 B, *middle and right*). In addition, effector function was impaired seen in lower frequencies of IFN-γ (Fig. 3-14 C, *left*) and GranB (Fig. 3-14 C, *right*) producing *in vitro* re-stimulated IAV-spec. $CD8^+$ T cells. Trm cells are especially important as their lung location positions them right at the side of infection and provides local and rapid recall responses. In addition to Trm, other memory T cell subpopulations can be found in the SLO e.g. drLN, the blood circulation and the bone marrow[120]. Here, it was speculated that CD62L expression in TCAIM overexpressing cells may support the localization in drLN. As memory T cell in the bone marrow express the adhesion receptor CD44, an impairment of accumulation in TCAIM KI was assumed. Indeed, cell numbers of TCAIM overexpressing IAV-spec. $CD8^+$ T cells in drLN were comparable to respective wild types on d45 p.i. (Fig. 3-14 D) whereas cell numbers were lower in the bone marrow (Fig. 3-14 E).

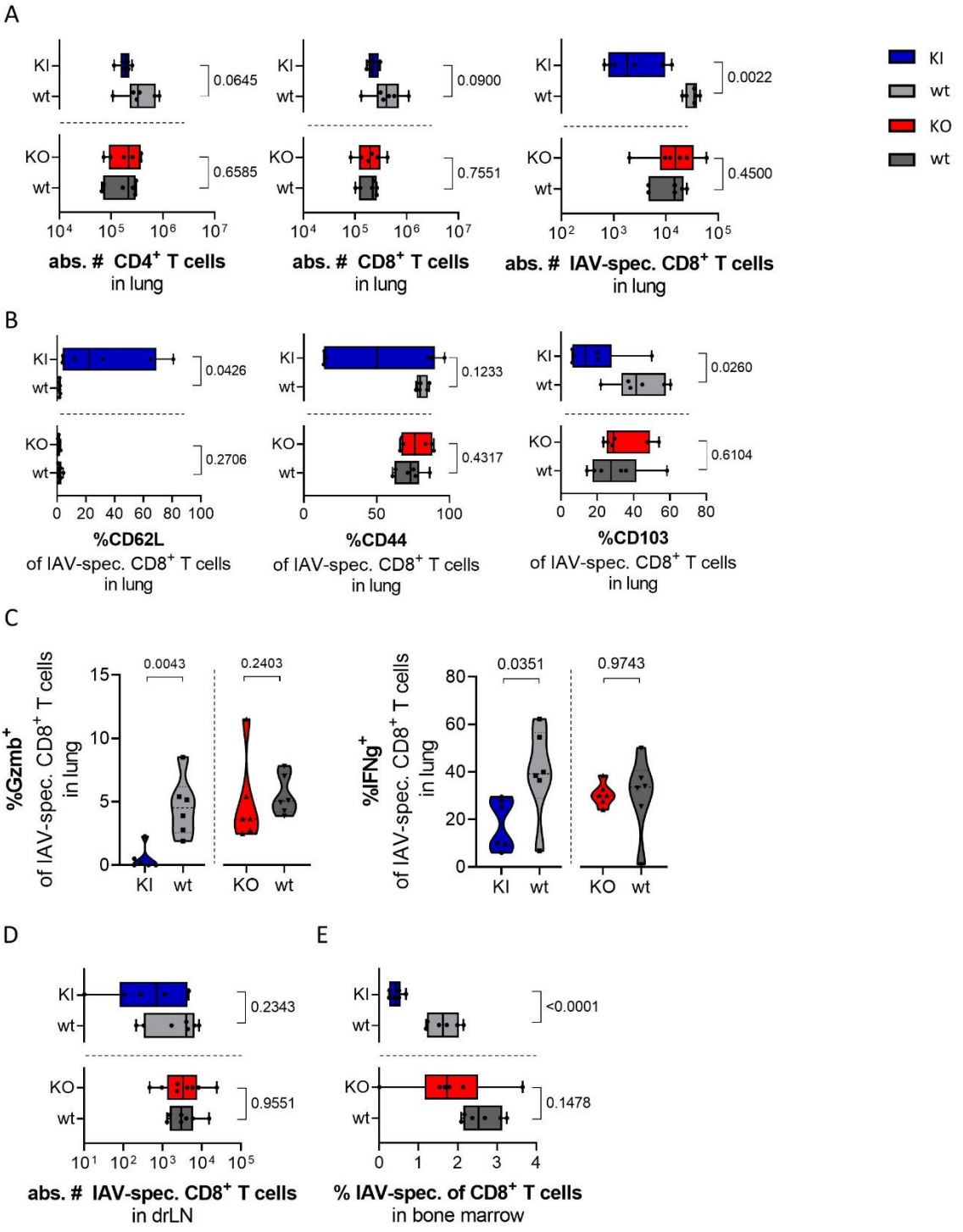

Figure 3-14 TCAIM interferes with local memory T cell accumulation and phenotype in the lung. *TCAIM KI Cd4Cre, TCAIM KO Cd4Cre and respective wildtype littermates were infected intranasally with 7PFU of IAV/PR8. At d45 p.i. lung, drLN and bone marrow were collected and cells analysed using flow cytometry.* ***A*** *Boxplots showing cell numbers of CD4⁺ (left), CD8⁺ (middle) and IAV-spec. CD8⁺ T cells (right) at d45 p.i. in the lung. n = 6.* ***B*** *Frequencies of CD62L⁺ (right), CD44⁺ (middle) and CD103⁺ (left) IAV spec. CD8⁺ T cells at d45 in the lung.* ***C*** *Frequencies of Gzmb⁺ and IFN-γ⁺ in vitro re-stimulated IAV spec. CD8⁺ T cells at d45 in the lung. Cell numbers of IAV-spec. CD8⁺ T cells at d45 p.i. in the* ***D*** *drLN (n = 6-8) and* ***E*** *bone marrow (n = 6). For statistical analyses data were tested for normal distribution and accordingly, unpaired t-Test or Mann-Whitney test was used to compare experimental group with respective wild type littermates.*

3.4.2 TCAIM overexpression allows generation of neutralizing antibodies

While T cell numbers, activation and migration marker expression and effector function of TCAIM overexpressing T cells were strongly impaired in the lung, T cell expansion and marker expression in drLN did not differ to respective wild type animals indicating a regular T cell performance. One important attribute of $CD4^+$ T cell in drLN is providing B cell help during the GC reaction that promote generation of antibody (AB) secreting plasma cells[99,107]. This raised the question whether AB are produced in TCAIM KI mice.

To study AB production, neutralizing activity of blood plasma was used as an indicator. Therefore, TCAIM KI, TCAIM KO and wild type littermates were infected and blood was collected at d8 and d45 p.i. Then, plasma from obtained blood was tested in an HAI assay, where red blood cells are infected with IAV *in vitro*. A serum dilution series is utilized to determine the highest dilution in which haemagglutination of red blood cells is prevented by the blood plasma AB binding to IAV. HAI assay was performed at at the virology department of the Freie Universität Berlin by Dr. Jakob Trimpert.

On d8 p.i. as well as d45 p.i. IAV-spec. AB were detected in all experimental groups (Fig. 3-15 A). TCAIM KI mice did not show significant differences compared to respective wild type animals, but there was the tendency of a higher neutralizing activity at d45 p.i. in plasma of TCAIM KI mice. No differences between TCAIM KO mice and wild type littermates were observed (Fig. 3-15 A).

To better understand, if $CD4^+$ T cell in drLN were not only able to expand upon infection but are also functional and therefore able to support B cells, cytokine production of T cells obtained from drLN at d8 p.i. was measured upon *in vitro* re-stimulation using flow cytometry. IL-2 is not expressed by Tfh cell, but gives general information about the capacity to carry out effector functions. Besides Th1 cells, also Tfh cell are producers of IFN-γ. TCAIM overexpressing $CD4^+$ T cells did not differ in the frequency of IL-2 (Fig. 3-15 B, *left*) and IFN-γ producing cells (Fig. 3-15 B, *right*) compared to wild type littermates, indicating a regular effector function.

Taken together, TCAIM KI mice were found to generate neutralizing AB that might serve as a protective memory. Expansion and functionality of TCAIM overexpressing T cells in drLN might support T cell mediated generation of those AB.

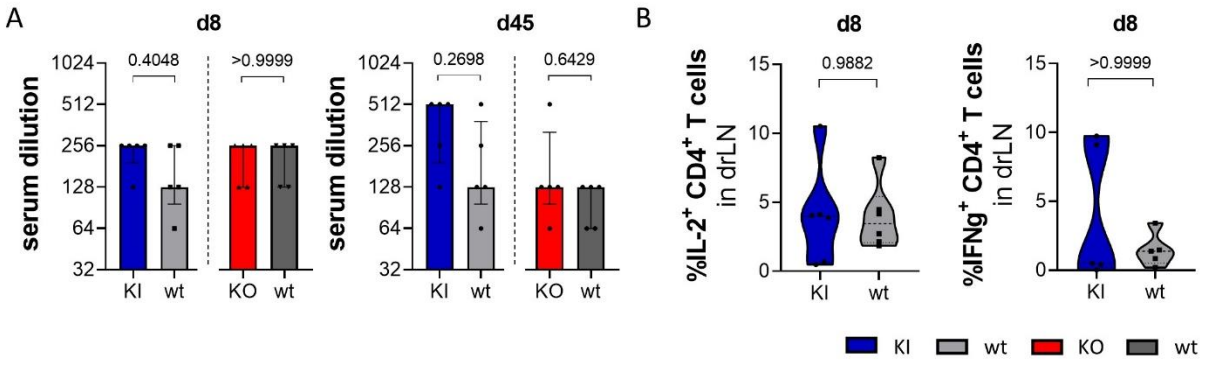

Figure 3-15 Generation of neutralizing antibodies (AB) might be supported by functional TCAIM overexpressing T cells in drLN*. TCAIM KI Cd4Cre, TCAIM KO Cd4Cre and respective wildtype littermates were infected intranasally with 7PFU of IAV/PR8.* ***A*** *At d8 (left) and d45 p.i. (right) neutralizing antibodies were measured in blood plasma using haemaglutinin inhibition assay, n = 5* ***B*** *Violin plots showing frequencies of IL-2⁺ (left) and IFN-γ⁺ (right) of CD4⁺ T cells in the drLN at d8 p.i., n = 5-6* ***.*** *For statistical analyses data were tested for normal distribution and accordingly, unpaired t-Test or Mann-Whitney test was used to compare experimental group with respective wild type littermates.*

4. Discussion

Within the scope of this work, TCAIM overexpressing T cells were found to be able to respond to infection induced activation stimuli as expansion and generation of IAV-spec. T cells was observed. However, lung infiltration and intra-tissue accumulation was disturbed. This observation was linked to an altered expression of CD62L/CD44 and genes involved in differentiation and migration. Consequently, effector function was inhibited. In contrast, TCAIM deficient T cells showed early expression of *Ifng* and genes involved in differentiation and a strong accumulation across the lung tissue, but that did not translate into an improved cytotoxic function and virus clearance at the peak of infection. Importantly, the absence of a full effector T cell response in the lung prevented weight loss in TCAIM KI mice and thus immunopathology. Nevertheless, mice were able to recover from the IAV infection. Surprisingly, although Trm formation was abrogated, generation of neutralizing AB might serve as a protective memory function during a re-infection.

4.1 Mitochondrial proteins as modulators of T cell migration

4.1.1 Role of TCAIM in T cell migration and effector function

Previous data showed that TCAIM overexpressing T cells are able to respond to activating stimuli *in vitro as* they are able to enter the cell cycle. However, cell proliferation analysis revealed an accumulation mainly in the first cell cycle whereas wild type cells progressed. Furthermore, expression of activation markers differ at 48 h but not 24 h, indicating TCAIM KI T cells are able to carry out an early response upon stimulation. Instead, TCAIM KI was found to interfere with $CD4^+$ and $CD8^+$ effector T cell differentiation *in vitro* and prevent allogenic skin graft infiltration *in vivo*. Unpublished *in vitro* work of Christina Iwert suggested that TCAIM interacts with the mitochondrial outer membrane located protein VDAC which impaires mTOR mediated HIF1a expression. As a consequence, upregulation of anabolic pathways including cholesterol biosynthesis was abrogated, thereby preventing effector T cell differentiation. Importantly, forced VDAC opening or cholesterol substitution in TCAIM KI $CD8^+$ T cells rescued the effect of inhibited effector T cell differentiation in TCAIM KI $CD8^+$ T cells.

The results of this study further strengthen and deepen the previously described findings. In line with *in vitro* experiments, TCAIM overexpressing T cells did show a general ability to respond to the IAV infection and enter the cell cycle *in vivo* as T cell expansion in the drLN, most likely upon antigen presentation by migrating APCs, was observed. In addition, scRNAseq data revealed lung located T cells were able to respond to local IFN signaling by upregulation of ISG. However, lung infiltration, intra-tissue accumulation and the acquisition of a full effector phenotype of lung located T cells was impaired

in TCAIM KI mice. Importantly, IAV-spec. T cell generation was not completely inhibited. Therefore, the here presented results indicate that TCAIM mediated reduction of anabolic metabolism and cholesterol biosynthesis is not preventing T cell activation per se but rather interfering with tissue homing potential and acquisition of full effector function of lung located T cells.

This might be due to the TCAIM mediated interference of mTOR signaling leading to abrogated upregulation of anabolic pathways and thereby missing building blocks and expression of molecules needed for effector function and lung migration. In line, the deprivation of e.g. glucose diminishes effector T cell function[184]. Moreover, studies found that mTOR signaling and cellular metabolism are impacting T cell migration and effector function. Finlay et al found that the mTOR-Hif1a pathway sustains glucose metabolism and is linked to transcriptional programs of effector T cells[185]. They show, for instance, that deletion of Hif1a in $CD8^+$ T cells impaired expression of effector molecules like perforin and granzymes. Furthermore, expression of chemokines and chemokine receptors was altered. In line, Palazon et al observed reduced expression of effector molecules IFN-γ and GranB as well as co-stimulatory molecules CD137 and OX40 due to HIF1a deletion[186]. Importantly, tumour infiltration of $CD8^+$ T cells was impaired. MTOR-deficiency in Tregs was found to induce accumulation in SLO whereas migration to peripheral non-lymphoid tissues like lung, colon and skin was reduced[187]. Similar to the here described results in TCAIM overexpressing T cells, CD62L expression was upregulated and CD44 expression reduced in mTOR-deficient Tregs. This was also associated with metabolic alteration.

In previous *in vitro* studies, TCAIM deficiency resulted in the tendency of an advantage for T cell activation under sub-optimal but not optimal stimulation conditions (unpublished data, C. Iwert). The infection with IAV elicits a proper T cell response that could be considered as an optimal stimulus. Nevertheless, the question was asked if TCAIM KO mice have an advantage in T cell activation and viral control. Expansion magnitude and timing in drLN was similar to wild type littermates. Yet, TCAIM KO mice showed an enhanced accumulation in the inflamed tissue and differences in scRNAseq analysis on d5. A $Cxcr6^+$ T cell cluster was enriched and expression of genes that are upregulated during T cell activation and the *Ifng* gene were higher compared to wild type littermates. This indicates a potential advantage in T cell activation and differentiation at an early time point. However, this did not translate to higher frequencies of IFN-γ producing T cells at the peak of infection (d8 p.i.) nor a faster viral clearance. One explanation could be, that the faster upregulation is qualitatively not sufficient to improve the viral control by TCAIM deficient T cells. Another explanation is that the earlier upregulation might be lasting only for a short time before wild type cells reach similar gene expression and thus is not enough to facilitate an advantage in viral control. This is supported by the fact that wild type cells had the same frequencies of cytokine producing cells on d8.

4.1.2 CD62L and CD44 as a potential cause of impaired lung infiltration

To partake in viral clearance at the side of infection, effector T cells must be able to act locally in the lung and therefore have to leave the drLN, travel through the blood, extravasate and migrate into the lung. Several migration and adhesion molecules play a role in that process.

In this study TCAIM overexpression was found to influence the migratory potential of T cells. Accumulation in the lung was drastically reduced as detected by flow cytometry as well as IMC analysis. Those findings go along with TCAIM KI T cells not being able to upregulate the expression of CD44, which facilitates adhesion and extravasation by binding to hyaluronic acid of the extracellular matrix, but also e-selectins[89,90]. Consequently, the reduced T cell accumulation and therefore effector function at the side of infection led to delayed viral clearance. Those findings are supported by the work of other groups that found interference with CD44 expression results in reduced T cell extravasation. For instance, block of CD44 results in reduced skin infiltration[188] and enzymatic cleavage of CD44 on islet-antigen specific T cells prevented pancreas migration[189]. CD44 was also found to be associated with the integrin VLA-4[93]. Nandi et al showed that CD44 lacking its cytoplasmic tail resolves this association and leads to impaired extravasation at the side of imflammation[190]. VLA-4 is a dimer composed of CD49a and CD29, which are both lower expressed in TCAIM overexpressing T cells. Thus, CD44, VLA-4 and thereby their association is reduced in TCAIM KI, contributing to reduced ability of T cells to extravasate and accumulate in the lung.
In addition to its role for extravasation, CD44 deficiency was described to impair IFN-γ production of $CD4^+$ T cells in response to *Toxoplasma gondii* infection[191] and overall pro-inflammatory cytokine production in an respiratory virus model[192]. This matches the reduced cytokine production seen in TCAIM overexpressing T cells.

So far, involvement of molecules for extravasation and tissue migration have been discussed. However, also expression molecules that drive the T cell migration away from the lung might explain the reduced lung accumulation in TCAIM KI mice. CD62L is a selectin that mediates entry into drLN. In line, Arbonés et al showed that the lack of CD62L reduced lymphocyte homing of peripheral LN[193]. In the here presented study, CD62L surface expression in TCAIM overexpressing T cell was reduced in blood, but surprisingly high expression was found in the lung. This could be explained by the two mechanisms in which CD62L can be regulated: First, endoproteolytic cleavage by ADAM17 proteins and second, by transcriptional regulation. The proteolysis was described by Mohammed et al to promote early clonal expansion[194]. Expansion of T cells in drLN of TCAIM KI mice and reduced surface expression in blood are suggesting that cleavage of CD62L was not inhibited. Instead, transcriptional control of *Sell* and thereby long-term downregulation of gene expression could have been impaired leading to the high

expression in the lung. Importantly, CD62L is regulated by KLF2 transcription factor that in turn is regulated by the mTOR pathway[82] and thus is directly linked to the proposed TCAIM mechanism that is acting through the TCAIM-VDAC-mTOR axis. Indeed, inhibition of mTOR prevents CD62L downregulation and favours migration to SLO[82]. The observed high expression of CD62L might draw T cells back into the blood circulation and shuttle them back to drLN. Indeed, higher frequencies of T cells were observed in blood on d8 p.i. in TCAIM KI mice. However, no higher accumulation in drLN was found. Richards et al described that the block of proteolytic cleavage of CD62L did not affect T cell distribution in non-lymphoid tissues upon infection[195], which makes it most likely that inhibition of CD44 and integrin expression seen in scRNAseq could drive the reduced accumulation of TAIM overexpressing T cells. Notably, interference with CD62L expression was found to impact T cell function[196] and viral control[195], which matches the here presented findings of reduced effector function and delayed viral clearance in TCAIM KI mice and suggests a role for CD62L in the overall phenotype and function of T cells.

4.1.3 The perivascular niche as a checkpoint for further tissue migration

Importantly, TCAIM overexpressing T cells that reached the lung were located around the vessels in the perivascular niche and showed a reduced migration further throughout the tissue to the bronchioles, the side of virus replication. This might be explained by the lack of CD44 expression that also plays a role in cell motility and migration within the tissue. Mrass et al found that CD44 stabilizes the shape of polarized cells during interstitial migration in the tumor environment and CD44 deficiency hinders migration and tumor-shrinkage[197,198].

Another explanation would be the perivascular niche itself as a checkpoint for further tissue migration. The location within a peripheral tissue has to be tightly regulated to prevent uncontrolled migration of effector cells which can cause tissue damage. Besides T cells, also other immune cells including APCs are residing within the perivascular niche and have been described to provide a peripheral, additional activation signal thereby licensing further migration of appropriate cells[153,199]. In a skin inflammation model, co-localization of Th1 effector cells and MHC class II expressing DCs in distinct immune cell clusters was found to be chemokine driven and serves as preferred entry sides for migrating Th1 cells[200]. However, antigen presentation was also mediating the localisation, as well as retention, cell motility and APC-T cell contact length. Absence of chemokine and antigen stimulus led to reduced frequency of IFN-γ producing Th1 cells. Hence, contact to APC and peripheral activation signals determine effector response magnitude. Further, IFN-γ production of infiltrating Th1 cells served as an amplifying positive feed-back loop. Along the line, Goddery et al showed in brain infections that

perivascular macrophages upregulate the expression of MHC class I for antigen presentation to $CD8^+$ T cells which promotes T cell infiltration into the brain[199]. In IAV infections, depletion of DCs and macrophages in the lung impaired local $CD8^+$ T cell response and interaction of pulmonary DCs and $CD8^+$ T cells were necessary for peripheral antigen driven establishment of an effective T cell response[201]. However, the impact of the perivascular niche in the context of IAV infections, local antigen presentation and re-activation of T cells as a checkpoint for further tissue migration has not been addressed in detail so far.

The majority of TCAIM overexpressing T cells are not entering the lung tissue, thus they are not able to receive the peripheral activation signal provided by local APCs. Importantly, a small amount of TCAIM overexpressing T cells did enter the tissue, but to a lesser extend in lung tissue areas as wt T cells. Therefore, although local contact to APCs was possible, peripheral activation signal did not induce the acquisition of a full effector phenotype. This might be explained by the reduced expression of the co-stimulatory molecules CD44, ICOS and OX40 that are supporting the signal transduction initiated by antigen binding. In addition, impaired IFN-γ production might hinder the described positive feedback loop that would drive further T cell infiltration and could also play a role in the context of respiratory infections.

In contrast, TCAIM KO mice were found to have a higher and broader T cell distribution over the whole lung tissue at d8 p.i. Besides the above-described antigen driven licensing in the perivascular niche, chemokine mediated localization cues play a role in intra-tissue migration. Wein et al described CXCR6 as a critical regulator of Trm cell migration and localization in the lung tissue[158]. Importantly, highest CXCR6 expression was found in T cells located in the interstitium of the lung. CXCR6 is a marker associated with later stages of the T cell response around d8 p.i.[202,203] Notably, $CXCR6^+$ T cells were enriched and *Cxcr6* gene expression upregulated already at d5 p.i. in TCAIM KO mice, which proposes an early CXCR6 driven localization of TCAIM deficient T cells in the lung tissue. Importantly, the accumulation of TCAIM KO T cells in the outside area, containing the interstitium, was highest which correlates to the finding of highest CXCR6 expression.

4.2 T cell response against IAV is shaped by mitochondrial proteins

4.2.1 T cell contribution during acute and memory IAV phases under the impact of TCAIM

When challenged with a viral infection, the immune system is in charge of recognizing and clearing the invading pathogens. This process is orchestrated by various cell types of the innate and adaptive immune system. In the context of IAV infections, a functional T cell response is crucial for viral control and subsequent recovery. Already in 1981 Wells et al provided evidence that nude mice, which are athymic and therefore lack T cells, had a poorer disease outcome and survival[149]. Similarly, deficiency of *Rag* expression that is needed for development of T and B cells is causing accelerated succumbing in IAV infections[204,205]. The T cell response against IAV consists of cytotoxic $CD8^+$ T cells and different $CD4^+$ T cell populations that have cytotoxic, regulatory and helping properties. Notably, mice only able to generate a $CD8^+$ T cell response are able to clear the viral infection[206], whereas $CD4^+$ T cell response alone is not sufficient[207]. But, $CD4^+$ T cell mediated help is important for the generation and function of $CD8^+$ memory T cells[104].

In TCAIM overexpressing mice, $CD4^+$, total $CD8^+$ and IAV spec. $CD8^+$ T cell were found to expand in drLN but lung infiltration was diminished leading to a reduced local accumulation and T cell response at the side of infection. As described above, complete absence of T cells during IAV infections cause decreased survival. However, survival was not diminished and majority of TCAIM KI mice were able to completely clear the viral infection, although delayed. Those findings suggest that the performance in drLN and the remaining, reduced T cell response in the lung are sufficient to support, control and clear the acute IAV Infection.

Moreover, T cells are also important for offering protection against a secondary infection or even heterosubtypic infections by formation of memory T cell pools that can reside at the side of infection (Trm), circulate (effector memory T cell; Tem) or reside within SLO (central memory T cell; Tcm)[76]. Notably, only IAV-spec. memory T cells in drLN but no Trm cells in lung were generated in TCAIM KI mice upon IAV challenge. Several contributions have been described in this context that can explain the prevented Trm formation under the TCAIM overexpression. Of course, the inability to enhance expression of migration receptors and integrins that are necessary for proper tissue migration prevent the cell to reach the location to reside. Here, CD103 expression is commonly known as a marker for Trm cells, which facilitates tissue retention by binding to its ligand E-cadherin on epithelial cells[76,182]. Reduced CD103 expression in IAV-spec. TCAIM KI $CD8^+$ T cells might explain abrogated accumulation in the lung. Laidlaw et al found that generation of $CD103^+$ $CD8^+$ Trm cells requires $CD4^+$ T cell help[208]. However, they used a complete CD4 T cell depletion and did not distinguish between help provided in the SLO and in the peripheral lung tissue. The here presented results indicate that $CD4^+$ T cell help in

drLN and absence in the lung was able to induce IAV-spec. Tcm, but not Trm residing in the lung indicating that location of $CD4^+$ T cell help impacts different memory T cell populations. Additionally, as described beforehand, antigen presentation is thought to license effector T cell for further migration throughout the lung tissue. Thus it suggest itself that local antigen encounter might be important for Trm generation and residing within the lung as well. Indeed, McMaster et al found local, pulmonary antigen encounter to prolong e.g. CD103 expression and be a prerequisite of $CD8^+$ Trm in the lung[209]. Furthermore, it has been shown that antibody and co-stimulatory mediated Trm formation is abrogated under mTOR inhibition, highlighting the importance of cellular metabolism[210].

Apart from helping $CD8^+$ T cell, $CD4^+$ T cell help is also important for B cell maturation and generation of antibody secreting, high affinity plasma cells. In line, nude mice were found to have disturbed antibody production due to lack of T cell responses[149]. However, recent studies also found T cell-independent AB production either extra-follicular or even isotype-switched[68,211], latter only to a diminished extend compared to T cell-helped conditions[211]. In TCAIM KI mice, similar neutralizing AB in blood plasma indicate, that either extra-follicular or follicular plasma cell generation was occurring. Expansion of functional $CD4^+$ T cells in drLN is pointing towards an ability to form long lasting plasma cells in a GC and $CD4^+$ T cell-dependent manner. Either way, neutralizing AB in blood plasma provide in addition to remaining Tcm formation in drLN a promising alternative memory capacity that might offer protection although Trm generation is absent.

4.2.2 T cells as drivers of immunopathology

The optimal immune response to an infection is a tight balance between being sufficiently strong to provide viral control and clearance but not excessively strong causing collateral and extensive tissue damage and thereby worsening the disease outcome. In the context of an IAV infection, $CD8^+$ T cell have been shown to contribute to the immunopathology[150]. One common concomitant of IAV infections is accelerated weight loss during the acute phase. Notably, in studies where a T cell response was absent, mice showed later weight loss and survived longer although overall mortality was higher[149,205]. Enelow et al highlighted the ability to cause immunopathology even in the absence of viral contribution[151]. Adoptive transfer of HA specific $CD8^+$ T cells into mice where epithelial cells express HA antigen caused weight loss and lung tissue damage. One should keep in mind that in a real infection setting reduction of viral burden and subsequent clearance decreases antigen exposure whereas in this study epithelial cells constitutively express HA thereby extending the T cell response. Nevertheless, the study provides evidence that $CD8^+$ T cells induce immunopathology[150]. The tight balance and dual

role becomes even more clear in a study were $CD8^+$ T cells offered protection in the course of mild IAV infection, but when challenged with a high dose conferred enhanced pathology and mortality[212].

The reduced accumulation of T cells in the lungs of TCAIM KI mice was accompanied by diminished immunopathology seen in slighter weight loss of the animals. Whereas above described studies found a correlation between absence of T cell responses and higher mortality of infected mice, TCAIM KI mice were able to clear the viral infection, although delayed, and recovered from IAV infection. This turns the reduced T cell response at the side of infection into a beneficial effect for the overall disease outcome.

4.3 Outlook and conclusion

The mitochondrial protein TCAIM was previously found to be downregulated upon T cell activation under physiological conditions and prevent effector T cell differentiation when being constantly expressed. In contrast, TCAIM deficiency is leading to a reduced activation threshold under sub-optimal conditions. The mode of action is proposed as TCAIM facilitating closure of the ion channel VDAC which inhibits mTOR dependent upregulation of anabolic pathways especially cholesterol biosynthesis and subsequent building blocks that are needed for proliferation and effector function.

The here presented results deepen and extend our understanding of the role and importance of TCAIM in T cell responses. TCAIM overexpressing T cells are not only able to respond to activation stimuli in vitro but can also respond to infection-induced type I IFN signaling seen by upregulation of ISG in scRNAseq analysis. Moreover, expansion of cytokine producing T cells in drLN and formation of a neutralizing AB response are further supporting the ability of TCAIM KI T cells to become in principal activated. Apart from the GC mediated and T cell-dependent production of high affinity AB by a long-lasting plasma cells pool, low affinity AB can also be produced by short lived plasma cells in a T cell-independent extrafollicular pathway[64,68]. Hence, it is of interest if detected AB in TCAIM KI mice received $CD4^+$ T cell help. Therefore, one could apply spatial transcriptomics of spleen or drLN which allows to study the location, phenotype and nature of B and T cell interactions and would provide evidence if AB generation is carried out in the follicular or extrafollicular way.

In addition, the influence of TCAIM in memory T cell formation was studied. *In vivo* memory T cell formation was found to be impacted by TCAIM overexpression, as IAV-spec. memory T cell were detectable in drLN but not in the lungs of TCAIM KI mice. TCAIM deficiency did not alter memory T cell generation compared to wt. Here, it would be of interest if TCAIM mediated altered immunization state composed of the IAV-spec. memory pool in drLN and neutralizing antibodies in blood are sufficient to protect from a re-challenge with a lethal IAV infection. This could be tested either by re-

infecting primed TCAIM KI mice with a second, higher dose of IAV or AB mediated protection alone could be studied *in vivo* by transferring AB obtained from blood of primary infected TCAIM KI mice into naïve host that are then challenged with a lethal dose.

Furthermore, this study shows that not only effector T cell differentiation is abrogated in TCAIM KI mice but that also influences the migration capacity and accumulation of T cells in the lung tissue. The thereby reduced T cell induced immunopathology highlights the dual roles, beneficial and damaging, of T cells and the importance of the location for T cell mediated responses in IAV infections. Excessive T cell responses and pro-inflammatory cytokines have been attributed to severe disease cases of IAV but also SARS-CoV2 in patients[213], raising the need for a therapy that reduces T cell mediated immunopathology. Unpublished data showed a correlation of reduced TCAIM expression in SARS-CoV2 patients with severe symptoms. Thus, TCAIM might be an interesting target to control excessive T cell responses. However, here TCAIM overexpression was conditionally applied as early as in naïve T cells. In the clinical context, patients would receive an intervention at a time point where effector T cells are already formed in response to the infection. Thus, one would need to test if TCAIM overexpression in effector T cells would reduce their potential harmful effector function mediated immunopathology and thereby would contribute to a better disease outcome. Here, the Cre-ERT2 system could be applied which allows the overexpression of TCAIM upon Tamoxifen treatment in already generated effector T cells.

In summary, the here presented results position the mitochondrial protein TCAIM as a link between mitochondrial and metabolic dynamics and effector T cell function and migration potential. The data propose a beneficial role for a T cell specific TCAIM overexpression in IAV infections as it prevents T cell induced immunopathology, but allows recovery and neutralizing antibody production as a potential protective memory function.

5. References

1. The top 10 causes of death. Available at https://www.who.int/news-room/fact-sheets/detail/the-top-10-causes-of-death (2023).
2. Influenza (Seasonal). Available at https://www.who.int/news-room/fact-sheets/detail/influenza-(seasonal) (2023).
3. Killingley, B. & Nguyen-Van-Tam, J. Routes of influenza transmission. *Influenza and other respiratory viruses* **7 Suppl 2,** 42–51; 10.1111/irv.12080 (2013).
4. Monto, A. S., Gravenstein, S., Elliott, M., Colopy, M. & Schweinle, J. Clinical signs and symptoms predicting influenza infection. *Archives of internal medicine* **160,** 3243–3247; 10.1001/archinte.160.21.3243 (2000).
5. Ohmit, S. E. & Monto, A. S. Symptomatic predictors of influenza virus positivity in children during the influenza season. *Clinical infectious diseases : an official publication of the Infectious Diseases Society of America* **43,** 564–568; 10.1086/506352 (2006).
6. Thompson, W. W. *et al.* Influenza-associated hospitalizations in the United States. *JAMA* **292,** 1333–1340; 10.1001/jama.292.11.1333 (2004).
7. van Kerkhove, M. D. *et al.* Risk factors for severe outcomes following 2009 influenza A (H1N1) infection: a global pooled analysis. *PLoS medicine* **8,** e1001053; 10.1371/journal.pmed.1001053 (2011).
8. Andrew, M. K. *et al.* Age Differences in Comorbidities, Presenting Symptoms, and Outcomes of Influenza Illness Requiring Hospitalization: A Worldwide Perspective From the Global Influenza Hospital Surveillance Network. *Open forum infectious diseases* **10,** ofad244; 10.1093/ofid/ofad244 (2023).
9. Mortality, morbidity, and hospitalisations due to influenza lower respiratory tract infections, 2017: an analysis for the Global Burden of Disease Study 2017. *The Lancet. Respiratory medicine* **7,** 69–89; 10.1016/S2213-2600(18)30496-X (2019).
10. Su, S., Fu, X., Li, G., Kerlin, F. & Veit, M. Novel Influenza D virus: Epidemiology, pathology, evolution and biological characteristics. *Virulence* **8,** 1580–1591; 10.1080/21505594.2017.1365216 (2017).
11. Collin, E. A. *et al.* Cocirculation of two distinct genetic and antigenic lineages of proposed influenza D virus in cattle. *Journal of virology* **89,** 1036–1042; 10.1128/JVI.02718-14 (2015).
12. Gouarin, S. *et al.* Study of influenza C virus infection in France. *Journal of medical virology* **80,** 1441–1446; 10.1002/jmv.21218 (2008).
13. Matsuzaki, Y. *et al.* Clinical features of influenza C virus infection in children. *The Journal of infectious diseases* **193,** 1229–1235; 10.1086/502973 (2006).
14. Uyeki, T. M., Hui, D. S., Zambon, M., Wentworth, D. E. & Monto, A. S. Influenza. *Lancet (London, England)* **400,** 693–706; 10.1016/S0140-6736(22)00982-5 (2022).
15. Tong, S. *et al.* A distinct lineage of influenza A virus from bats. *Proceedings of the National Academy of Sciences of the United States of America* **109,** 4269–4274; 10.1073/pnas.1116200109 (2012).

16. Ma, W., García-Sastre, A. & Schwemmle, M. Expected and Unexpected Features of the Newly Discovered Bat Influenza A-like Viruses. *PLoS pathogens* **11,** e1004819; 10.1371/journal.ppat.1004819 (2015).

17. Boudewijns, B., Paget, J., Del Riccio, M., Coudeville, L. & Crépey, P. Preparing for the upcoming 2022/23 influenza season: A modelling study of the susceptible population in Australia, France, Germany, Italy, Spain and the United Kingdom. *Influenza and other respiratory viruses* **17,** e13091; 10.1111/irv.13091 (2023).

18. Sandbulte, M. R. *et al.* Discordant antigenic drift of neuraminidase and hemagglutinin in H1N1 and H3N2 influenza viruses. *Proceedings of the National Academy of Sciences of the United States of America* **108,** 20748–20753; 10.1073/pnas.1113801108 (2011).

19. Rambaut, A. *et al.* The genomic and epidemiological dynamics of human influenza A virus. *Nature* **453,** 615–619; 10.1038/nature06945 (2008).

20. Webster, R. G. & Govorkova, E. A. Continuing challenges in influenza. *Annals of the New York Academy of Sciences* **1323,** 115–139; 10.1111/nyas.12462 (2014).

21. Olsen, B. *et al.* Global patterns of influenza a virus in wild birds. *Science (New York, N.Y.)* **312,** 384–388; 10.1126/science.1122438 (2006).

22. Harrington, W. N., Kackos, C. M. & Webby, R. J. The evolution and future of influenza pandemic preparedness. *Experimental & molecular medicine* **53,** 737–749; 10.1038/s12276-021-00603-0 (2021).

23. Saunders-Hastings, P. R. & Krewski, D. Reviewing the History of Pandemic Influenza: Understanding Patterns of Emergence and Transmission. *Pathogens (Basel, Switzerland)* **5**; 10.3390/pathogens5040066 (2016).

24. Yamayoshi, S. & Kawaoka, Y. Current and future influenza vaccines. *Nature medicine* **25,** 212–220; 10.1038/s41591-018-0340-z (2019).

25. Krammer, F. *et al.* Influenza. *Nature reviews. Disease primers* **4,** 3; 10.1038/s41572-018-0002-y (2018).

26. Kawai, K. & Kawai, A. T. Racial/Ethnic and Socioeconomic Disparities in Adult Vaccination Coverage. *American journal of preventive medicine* **61,** 465–473; 10.1016/j.amepre.2021.03.023 (2021).

27. Lu, P.-J. *et al.* Surveillance of Vaccination Coverage Among Adult Populations -United States, 2018. *Morbidity and mortality weekly report. Surveillance summaries (Washington, D.C. : 2002)* **70,** 1–26; 10.15585/mmwr.ss7003a1 (2021).

28. CHU, C. M., DAWSON, I. M. & ELFORD, W. J. Filamentous forms associated with newly isolated influenza virus. *Lancet (London, England)* **1,** 602; 10.1016/S0140-6736(49)91699-2 (1949).

29. KILBOURNE, E. D. & MURPHY, J. S. Genetic studies of influenza viruses. I. Viral morphology and growth capacity as exchangeable genetic traits. Rapid in ovo adaptation of early passage Asian strain isolates by combination with PR8. *The Journal of experimental medicine* **111,** 387–406; 10.1084/jem.111.3.387 (1960).

30. Gamblin, S. J. & Skehel, J. J. Influenza hemagglutinin and neuraminidase membrane glycoproteins. *The Journal of biological chemistry* **285,** 28403–28409; 10.1074/jbc.R110.129809 (2010).

31. Pielak, R. M. & Chou, J. J. Influenza M2 proton channels. *Biochimica et biophysica acta* **1808,** 522–529; 10.1016/j.bbamem.2010.04.015 (2011).

32. Rossman, J. S. & Lamb, R. A. Influenza virus assembly and budding. *Virology* **411,** 229–236; 10.1016/j.virol.2010.12.003 (2011).

33. Moeller, A., Kirchdoerfer, R. N., Potter, C. S., Carragher, B. & Wilson, I. A. Organization of the influenza virus replication machinery. *Science (New York, N.Y.)* **338,** 1631–1634; 10.1126/science.1227270 (2012).

34. Pflug, A., Guilligay, D., Reich, S. & Cusack, S. Structure of influenza A polymerase bound to the viral RNA promoter. *Nature* **516,** 355–360; 10.1038/nature14008 (2014).

35. Krug, R. M. Functions of the influenza A virus NS1 protein in antiviral defense. *Current opinion in virology* **12,** 1–6; 10.1016/j.coviro.2015.01.007 (2015).

36. Hamilton, B. S., Whittaker, G. R. & Daniel, S. Influenza virus-mediated membrane fusion: determinants of hemagglutinin fusogenic activity and experimental approaches for assessing virus fusion. *Viruses* **4,** 1144–1168; 10.3390/v4071144 (2012).

37. Cohen, M. *et al.* Influenza A penetrates host mucus by cleaving sialic acids with neuraminidase. *Virology journal* **10,** 321; 10.1186/1743-422X-10-321 (2013).

38. Dou, D., Revol, R., Östbye, H., Wang, H. & Daniels, R. Influenza A Virus Cell Entry, Replication, Virion Assembly and Movement. *Frontiers in immunology* **9,** 1581; 10.3389/fimmu.2018.01581 (2018).

39. Pinto, L. H. & Lamb, R. A. The M2 proton channels of influenza A and B viruses. *The Journal of biological chemistry* **281,** 8997–9000; 10.1074/jbc.R500020200 (2006).

40. Li, H.-C., Yang, C.-H. & Lo, S.-Y. Strategies of Influenza A Virus to Ensure the Translation of Viral mRNAs. *Pathogens (Basel, Switzerland)* **11**; 10.3390/pathogens11121521 (2022).

41. Chen, X. *et al.* Host Immune Response to Influenza A Virus Infection. *Frontiers in immunology* **9,** 320; 10.3389/fimmu.2018.00320 (2018).

42. Iwasaki, A. & Pillai, P. S. Innate immunity to influenza virus infection. *Nature reviews. Immunology* **14,** 315–328; 10.1038/nri3665 (2014).

43. Biondo, C., Lentini, G., Beninati, C. & Teti, G. The dual role of innate immunity during influenza. *Biomedical journal* **42,** 8–18; 10.1016/j.bj.2018.12.009 (2019).

44. Balachandran, S. *et al.* Essential role for the dsRNA-dependent protein kinase PKR in innate immunity to viral infection. *Immunity* **13,** 129–141; 10.1016/S1074-7613(00)00014-5 (2000).

45. Brass, A. L. *et al.* The IFITM proteins mediate cellular resistance to influenza A H1N1 virus, West Nile virus, and dengue virus. *Cell* **139,** 1243–1254; 10.1016/j.cell.2009.12.017 (2009).

46. Bailey, C. C., Huang, I.-C., Kam, C. & Farzan, M. Ifitm3 limits the severity of acute influenza in mice. *PLoS pathogens* **8,** e1002909; 10.1371/journal.ppat.1002909 (2012).

47. Everitt, A. R. *et al.* IFITM3 restricts the morbidity and mortality associated with influenza. *Nature* **484,** 519–523; 10.1038/nature10921 (2012).

48. Wu, W. & Metcalf, J. P. The Role of Type I IFNs in Influenza: Antiviral Superheroes or Immunopathogenic Villains? *Journal of innate immunity* **12,** 437–447; 10.1159/000508379 (2020).

49. Ferko, B. *et al.* Immunogenicity and protection efficacy of replication-deficient influenza A viruses with altered NS1 genes. *Journal of virology* **78,** 13037–13045; 10.1128/jvi.78.23.13037-13045.2004 (2004).

50. Feng, W. *et al.* Influenza a virus NS1 protein induced A20 contributes to viral replication by suppressing interferon-induced antiviral response. *Biochemical and biophysical research communications* **482,** 1107–1113; 10.1016/j.bbrc.2016.11.166 (2017).

51. Mibayashi, M. *et al.* Inhibition of retinoic acid-inducible gene I-mediated induction of beta interferon by the NS1 protein of influenza A virus. *Journal of virology* **81,** 514–524; 10.1128/JVI.01265-06 (2007).

52. Talon, J. *et al.* Activation of interferon regulatory factor 3 is inhibited by the influenza A virus NS1 protein. *Journal of virology* **74,** 7989–7996; 10.1128/jvi.74.17.7989-7996.2000 (2000).

53. Tumpey, T. M. *et al.* Pathogenicity of influenza viruses with genes from the 1918 pandemic virus: functional roles of alveolar macrophages and neutrophils in limiting virus replication and mortality in mice. *Journal of virology* **79,** 14933–14944; 10.1128/JVI.79.23.14933-14944.2005 (2005).

54. Jenne, C. N. *et al.* Neutrophils recruited to sites of infection protect from virus challenge by releasing neutrophil extracellular traps. *Cell host & microbe* **13,** 169–180; 10.1016/j.chom.2013.01.005 (2013).

55. Cortjens, B. *et al.* Neutrophil extracellular traps cause airway obstruction during respiratory syncytial virus disease. *The Journal of pathology* **238,** 401–411; 10.1002/path.4660 (2016).

56. Brinkmann, V. *et al.* Neutrophil extracellular traps kill bacteria. *Science (New York, N.Y.)* **303,** 1532–1535; 10.1126/science.1092385 (2004).

57. Arnon, T. I. *et al.* Recognition of viral hemagglutinins by NKp44 but not by NKp30. *Eur. J. Immunol.* **31,** 2680–2689; 10.1002/1521-4141(200109)31:9<2680::AID-IMMU2680>3.0.CO;2-A (2001).

58. Frank, K. & Paust, S. Dynamic Natural Killer Cell and T Cell Responses to Influenza Infection. *Frontiers in cellular and infection microbiology* **10,** 425; 10.3389/fcimb.2020.00425 (2020).

59. Mandelboim, O. *et al.* Recognition of haemagglutinins on virus-infected cells by NKp46 activates lysis by human NK cells. *Nature* **409,** 1055–1060; 10.1038/35059110 (2001).

60. Dunn, P. L. & North, R. J. Early gamma interferon production by natural killer cells is important in defense against murine listeriosis. *Infection and immunity* **59,** 2892–2900; 10.1128/iai.59.9.2892-2900.1991 (1991).

61. Hintzen, G. *et al.* Induction of tolerance to innocuous inhaled antigen relies on a CCR7-dependent dendritic cell-mediated antigen transport to the bronchial lymph node. *Journal of immunology (Baltimore, Md. : 1950)* **177,** 7346–7354; 10.4049/jimmunol.177.10.7346 (2006).

62. Takahama, Y. Journey through the thymus: stromal guides for T-cell development and selection. *Nature reviews. Immunology* **6,** 127–135; 10.1038/nri1781 (2006).

63. Nemazee, D. Mechanisms of central tolerance for B cells. *Nature reviews. Immunology* **17,** 281–294; 10.1038/nri.2017.19 (2017).

64. Shapiro-Shelef, M. & Calame, K. Regulation of plasma-cell development. *Nature reviews. Immunology* **5,** 230–242; 10.1038/nri1572 (2005).

65. Akkaya, M., Kwak, K. & Pierce, S. K. B cell memory: building two walls of protection against pathogens. *Nature reviews. Immunology* **20,** 229–238; 10.1038/s41577-019-0244-2 (2020).

66. Huang, C. Germinal Center Reaction. *Advances in experimental medicine and biology* **1254,** 47–53; 10.1007/978-981-15-3532-1_4 (2020).

67. Crotty, S. T Follicular Helper Cell Biology: A Decade of Discovery and Diseases. *Immunity* **50,** 1132–1148; 10.1016/j.immuni.2019.04.011 (2019).

68. Lam, J. H. & Baumgarth, N. The Multifaceted B Cell Response to Influenza Virus. *Journal of immunology (Baltimore, Md. : 1950)* **202,** 351–359; 10.4049/jimmunol.1801208 (2019).

69. Lee, S. K. *et al.* B cell priming for extrafollicular antibody responses requires Bcl-6 expression by T cells. *The Journal of experimental medicine* **208,** 1377–1388; 10.1084/jem.20102065 (2011).

70. Guthmiller, J. J., Utset, H. A. & Wilson, P. C. B Cell Responses against Influenza Viruses: Short-Lived Humoral Immunity against a Life-Long Threat. *Viruses* **13**; 10.3390/v13060965 (2021).

71. Tamura, M., Webster, R. G. & Ennis, F. A. Antibodies to HA and NA augment uptake of influenza A viruses into cells via Fc receptor entry. *Virology* **182,** 211–219; 10.1016/0042-6822(91)90664-w (1991).

72. Guermonprez, P., Valladeau, J., Zitvogel, L., Théry, C. & Amigorena, S. Antigen presentation and T cell stimulation by dendritic cells. *Annual review of immunology* **20,** 621–667; 10.1146/annurev.immunol.20.100301.064828 (2002).

73. Hufford, M. M., Kim, T. S., Sun, J. & Braciale, T. J. The effector T cell response to influenza infection. *Current topics in microbiology and immunology* **386,** 423–455; 10.1007/82_2014_397 (2015).

74. Eriksson, M., Nylén, S. & Grönvik, K.-O. T cell kinetics reveal expansion of distinct lung T cell subsets in acute versus in resolved influenza virus infection. *Frontiers in immunology* **13,** 949299; 10.3389/fimmu.2022.949299 (2022).

75. Turner, D. L., Bickham, K. L., Farber, D. L. & Lefrançois, L. Splenic priming of virus-specific CD8 T cells following influenza virus infection. *Journal of virology* **87,** 4496–4506; 10.1128/JVI.03413-12 (2013).

76. Spitaels, J., Roose, K. & Saelens, X. Influenza and Memory T Cells: How to Awake the Force. *Vaccines* **4**; 10.3390/vaccines4040033 (2016).

77. Valkenburg, S. A. *et al.* Early priming minimizes the age-related immune compromise of $CD8^+$ T cell diversity and function. *PLoS pathogens* **8,** e1002544; 10.1371/journal.ppat.1002544 (2012).

78. Lustgarten, J., Waks, T. & Eshhar, Z. CD4 and CD8 accessory molecules function through interactions with major histocompatibility complex molecules which are not directly associated with the T cell receptor-antigen complex. *Eur. J. Immunol.* **21,** 2507–2515; 10.1002/eji.1830211030 (1991).

79. Chen, L. & Flies, D. B. Molecular mechanisms of T cell co-stimulation and co-inhibition. *Nature reviews. Immunology* **13,** 227–242; 10.1038/nri3405 (2013).

80. Curtsinger, J. M., Lins, D. C. & Mescher, M. F. Signal 3 determines tolerance versus full activation of naive CD8 T cells: dissociating proliferation and development of effector function. *The Journal of experimental medicine* **197,** 1141–1151; 10.1084/jem.20021910 (2003).

81. Shah, K., Al-Haidari, A., Sun, J. & Kazi, J. U. T cell receptor (TCR) signaling in health and disease. *Signal transduction and targeted therapy* **6,** 412; 10.1038/s41392-021-00823-w (2021).

82. Sinclair, L. V. *et al.* Phosphatidylinositol-3-OH kinase and nutrient-sensing mTOR pathways control T lymphocyte trafficking. *Nature immunology* **9,** 513–521; 10.1038/ni.1603 (2008).

83. Venturi, G. M. *et al.* Leukocyte migration is regulated by L-selectin endoproteolytic release. *Immunity* **19,** 713–724; 10.1016/S1074-7613(03)00295-4 (2003).

84. Jung, T. M. & Dailey, M. O. Rapid modulation of homing receptors (gp90MEL-14) induced by activators of protein kinase C. Receptor shedding due to accelerated proteolytic cleavage at the cell surface. *Journal of immunology (Baltimore, Md. : 1950)* **144,** 3130–3136 (1990).

85. Chao, C. C., Jensen, R. & Dailey, M. O. Mechanisms of L-selectin regulation by activated T cells. *Journal of immunology (Baltimore, Md. : 1950)* **159,** 1686–1694 (1997).

86. McEver, R. P. & Zhu, C. Rolling cell adhesion. *Annual review of cell and developmental biology* **26,** 363–396; 10.1146/annurev.cellbio.042308.113238 (2010).

87. Kohlmeier, J. E. *et al.* The chemokine receptor CCR5 plays a key role in the early memory CD8+ T cell response to respiratory virus infections. *Immunity* **29,** 101–113; 10.1016/j.immuni.2008.05.011 (2008).

88. Kohlmeier, J. E. *et al.* CXCR3 directs antigen-specific effector CD4+ T cell migration to the lung during parainfluenza virus infection. *Journal of immunology (Baltimore, Md. : 1950)* **183,** 4378–4384; 10.4049/jimmunol.0902022 (2009).

89. DeGrendele, H. C., Estess, P. & Siegelman, M. H. Requirement for CD44 in activated T cell extravasation into an inflammatory site. *Science (New York, N.Y.)* **278,** 672–675; 10.1126/science.278.5338.672 (1997).

90. DeGrendele, H. C., Estess, P., Picker, L. J. & Siegelman, M. H. CD44 and its ligand hyaluronate mediate rolling under physiologic flow: a novel lymphocyte-endothelial cell primary adhesion pathway. *The Journal of experimental medicine* **183,** 1119–1130; 10.1084/jem.183.3.1119 (1996).

91. Katayama, Y., Hidalgo, A., Chang, J., Peired, A. & Frenette, P. S. CD44 is a physiological E-selectin ligand on neutrophils. *The Journal of experimental medicine* **201,** 1183–1189; 10.1084/jem.20042014 (2005).

92. Nourshargh, S. & Alon, R. Leukocyte migration into inflamed tissues. *Immunity* **41,** 694–707; 10.1016/j.immuni.2014.10.008 (2014).

93. Siegelman, M. H., Stanescu, D. & Estess, P. The CD44-initiated pathway of T-cell extravasation uses VLA-4 but not LFA-1 for firm adhesion. *The Journal of clinical investigation* **105,** 683–691; 10.1172/JCI8692 (2000).

94. Muller, W. A. Getting leukocytes to the site of inflammation. *Veterinary pathology* **50,** 7–22; 10.1177/0300985812469883 (2013).

95. Harris, T. H. *et al.* Generalized Lévy walks and the role of chemokines in migration of effector CD8+ T cells. *Nature* **486,** 545–548; 10.1038/nature11098 (2012).

96. Hickman, H. D. *et al.* CXCR3 chemokine receptor enables local CD8(+) T cell migration for the destruction of virus-infected cells. *Immunity* **42,** 524–537; 10.1016/j.immuni.2015.02.009 (2015).

97. Crotty, S. T follicular helper cell differentiation, function, and roles in disease. *Immunity* **41,** 529–542; 10.1016/j.immuni.2014.10.004 (2014).

98. Wang, X. *et al.* Follicular dendritic cells help establish follicle identity and promote B cell retention in germinal centers. *The Journal of experimental medicine* **208,** 2497–2510; 10.1084/jem.20111449 (2011).

99. Swain, S. L., McKinstry, K. K. & Strutt, T. M. Expanding roles for CD4$^+$ T cells in immunity to viruses. *Nature reviews. Immunology* **12,** 136–148; 10.1038/nri3152 (2012).

100. Romani, L., Puccetti, P. & Bistoni, F. Interleukin-12 in infectious diseases. *Clinical microbiology reviews* **10,** 611–636; 10.1128/cmr.10.4.611 (1997).

101. Szabo, S. J. *et al.* A novel transcription factor, T-bet, directs Th1 lineage commitment. *Cell* **100,** 655–669; 10.1016/s0092-8674(00)80702-3 (2000).

102. Seder, R. A. & Paul, W. E. Acquisition of lymphokine-producing phenotype by CD4+ T cells. *Annual review of immunology* **12,** 635–673; 10.1146/annurev.iy.12.040194.003223 (1994).

103. Elgueta, R. *et al.* Molecular mechanism and function of CD40/CD40L engagement in the immune system. *Immunological reviews* **229,** 152–172; 10.1111/j.1600-065X.2009.00782.x (2009).

104. Belz, G. T., Wodarz, D., Diaz, G., Nowak, M. A. & Doherty, P. C. Compromised Influenza Virus-Specific CD8+-T-Cell Memory in CD4+-T-Cell-Deficient Mice. *Journal of virology* **76,** 12388–12393; 10.1128/JVI.76.23.12388-12393.2002 (2002).

105. Bourgeois, C., Rocha, B. & Tanchot, C. A role for CD40 expression on CD8+ T cells in the generation of CD8+ T cell memory. *Science (New York, N.Y.)* **297,** 2060–2063; 10.1126/science.1072615 (2002).

106. Schoenberger, S. P., Toes, R. E., van der Voort, E. I., Offringa, R. & Melief, C. J. T-cell help for cytotoxic T lymphocytes is mediated by CD40-CD40L interactions. *Nature* **393,** 480–483; 10.1038/31002 (1998).

107. Lu, Y. *et al.* CD4+ follicular regulatory T cells optimize the influenza virus-specific B cell response. *The Journal of experimental medicine* **218**; 10.1084/jem.20200547 (2021).

108. Hua, L. *et al.* Cytokine-dependent induction of CD4+ T cells with cytotoxic potential during influenza virus infection. *Journal of virology* **87,** 11884–11893; 10.1128/JVI.01461-13 (2013).

109. Takeuchi, A. & Saito, T. CD4 CTL, a Cytotoxic Subset of CD4+ T Cells, Their Differentiation and Function. *Frontiers in immunology* **8**; 10.3389/fimmu.2017.00194 (2017).

110. Brown, D. M., Lee, S., La Garcia-Hernandez, M. d. L. & Swain, S. L. Multifunctional CD4 Cells Expressing Gamma Interferon and Perforin Mediate Protection against Lethal Influenza Virus Infection. *Journal of virology* **86,** 6792–6803; 10.1128/JVI.07172-11 (2012).

111. Antunes, I. & Kassiotis, G. Suppression of Innate Immune Pathology by Regulatory T Cells during Influenza A Virus Infection of Immunodeficient Mice ▿ †. *Journal of virology* **84,** 12564–12575; 10.1128/JVI.01559-10 (2010).

112. Bedoya, F. *et al.* Viral antigen induces differentiation of Foxp3+ natural regulatory T cells in influenza virus-infected mice. *Journal of immunology (Baltimore, Md. : 1950)* **190,** 6115–6125; 10.4049/jimmunol.1203302 (2013).

113. Belkaid, Y. & Rouse, B. T. Natural regulatory T cells in infectious disease. *Nature immunology* **6,** 353–360; 10.1038/ni1181 (2005).

114. Brincks, E. L. *et al.* Antigen-specific memory regulatory CD4+Foxp3+ T cells control memory responses to influenza virus infection. *Journal of immunology (Baltimore, Md. : 1950)* **190,** 3438–3446; 10.4049/jimmunol.1203140 (2013).

115. Chapman, T. J., Lambert, K. & Topham, D. J. Rapid reactivation of extralymphoid CD4 T cells during secondary infection. *PloS one* **6,** e20493; 10.1371/journal.pone.0020493 (2011).

116. Rogers, P. R., Dubey, C. & Swain, S. L. Qualitative changes accompany memory T cell generation: faster, more effective responses at lower doses of antigen. *Journal of immunology (Baltimore, Md. : 1950)* **164,** 2338–2346; 10.4049/jimmunol.164.5.2338 (2000).

117. Teijaro, J. R. *et al.* Cutting edge: Tissue-retentive lung memory CD4 T cells mediate optimal protection to respiratory virus infection. *Journal of immunology (Baltimore, Md. : 1950)* **187,** 5510–5514; 10.4049/jimmunol.1102243 (2011).

118. Nelson, S. A. *et al.* Intranasal Nanoparticle Vaccination Elicits a Persistent, Polyfunctional CD4 T Cell Response in the Murine Lung Specific for a Highly Conserved Influenza Virus Antigen That Is Sufficient To Mediate Protection from Influenza Virus Challenge. *Journal of virology* **95,** e0084121; 10.1128/JVI.00841-21 (2021).

119. MacLeod, M. K. *et al.* Memory CD4 T cells provide accelerated help to B cell because they express CXCR5. *Journal of immunology (Baltimore, Md. : 1950)* **186,** 2889–2896; 10.4049/jimmunol.1002955 (2011).

120. Schmidt, M. E. & Varga, S. M. The CD8 T Cell Response to Respiratory Virus Infections. *Frontiers in immunology* **9,** 678; 10.3389/fimmu.2018.00678 (2018).

121. Topham, D. J., Tripp, R. A. & Doherty, P. C. CD8+ T cells clear influenza virus by perforin or Fas-dependent processes. *Journal of immunology (Baltimore, Md. : 1950)* **159,** 5197–5200 (1997).

122. Cullen, S. P. & Martin, S. J. Mechanisms of granule-dependent killing. *Cell death and differentiation* **15,** 251–262; 10.1038/sj.cdd.4402244 (2008).

123. Trapani, J. A. & Smyth, M. J. Functional significance of the perforin/granzyme cell death pathway. *Nature reviews. Immunology* **2,** 735–747; 10.1038/nri911 (2002).

124. Trapani, J. A. Granzymes: a family of lymphocyte granule serine proteases. *Genome biology* **2,** REVIEWS3014; 10.1186/gb-2001-2-12-reviews3014 (2001).

125. Brincks, E. L., Katewa, A., Kucaba, T. A., Griffith, T. S. & Legge, K. L. CD8 T cells utilize TRAIL to control influenza virus infection. *Journal of immunology (Baltimore, Md. : 1950)* **181,** 4918–4925; 10.4049/jimmunol.181.7.4918 (2008).

126. Flynn, K. J. *et al.* Virus-specific CD8+ T cells in primary and secondary influenza pneumonia. *Immunity* **8,** 683–691; 10.1016/S1074-7613(00)80573-7 (1998).

127. McMaster, S. R., Wilson, J. J., Wang, H. & Kohlmeier, J. E. Airway-Resident Memory CD8 T Cells Provide Antigen-Specific Protection against Respiratory Virus Challenge through Rapid IFN-γ Production. *Journal of immunology (Baltimore, Md. : 1950)* **195,** 203–209; 10.4049/jimmunol.1402975 (2015).

128. Taylor, P. M. & Askonas, B. A. Influenza nucleoprotein-specific cytotoxic T-cell clones are protective in vivo. *Immunology* **58,** 417–420 (1986).

129. O'Neill, E., Krauss, S. L., Riberdy, J. M., Webster, R. G. & Woodland, D. L. Heterologous protection against lethal A/HongKong/156/97 (H5N1) influenza virus infection in C57BL/6 mice. *The Journal of general virology* **81,** 2689–2696; 10.1099/0022-1317-81-11-2689 (2000).

130. Zens, K. D., Chen, J. K. & Farber, D. L. Vaccine-generated lung tissue-resident memory T cells provide heterosubtypic protection to influenza infection. *JCI insight* **1**; 10.1172/jci.insight.85832 (2016).

131. Sawitzki, B. *et al.* Identification of gene markers for the prediction of allograft rejection or permanent acceptance. *American journal of transplantation : official journal of the American Society of Transplantation and the American Society of Transplant Surgeons* **7,** 1091–1102; 10.1111/j.1600-6143.2007.01768.x (2007).

132. Schumann, J. *et al.* The mitochondrial protein TCAIM regulates activation of T cells and thereby promotes tolerance induction of allogeneic transplants. *American journal of transplantation : official journal of the American Society of Transplantation and the American Society of Transplant Surgeons* **14,** 2723–2735; 10.1111/ajt.12941 (2014).

133. Iwert, C. *et al. TCAIM controls effector T cell generation by preventing Mitochondria-Endoplasmic Reticulum Contact Site-initiated Cholesterol Biosynthesis* (2021).

134. Keeren, K. *et al.* Expression of tolerance associated gene-1, a mitochondrial protein inhibiting T cell activation, can be used to predict response to immune modulating therapies. *Journal of immunology (Baltimore, Md. : 1950)* **183,** 4077–4087; 10.4049/jimmunol.0804351 (2009).

135. Vogel, S. Z. *et al.* TCAIM decreases T cell priming capacity of dendritic cells by inhibiting TLR-induced Ca2+ influx and IL-2 production. *Journal of immunology (Baltimore, Md. : 1950)* **194,** 3136–3146; 10.4049/jimmunol.1400713 (2015).

136. Head, S. A. *et al.* Antifungal drug itraconazole targets VDAC1 to modulate the AMPK/mTOR signaling axis in endothelial cells. *Proceedings of the National Academy of Sciences of the United States of America* **112,** E7276-85; 10.1073/pnas.1512867112 (2015).

137. Aono, Y. *et al.* Sulindac sulfone inhibits the mTORC1 pathway in colon cancer cells by directly targeting voltage-dependent anion channel 1 and 2. *Biochemical and biophysical research communications* **505,** 1203–1210; 10.1016/j.bbrc.2018.10.050 (2018).

138. Salmond, R. J. mTOR Regulation of Glycolytic Metabolism in T Cells. *Frontiers in cell and developmental biology* **6,** 122; 10.3389/fcell.2018.00122 (2018).

139. Powell, J. D. & Delgoffe, G. M. The mammalian target of rapamycin: linking T cell differentiation, function, and metabolism. *Immunity* **33,** 301–311; 10.1016/j.immuni.2010.09.002 (2010).

140. Gnanaprakasam, J. N. R., Sherman, J. W. & Wang, R. MYC and HIF in shaping immune response and immune metabolism. *Cytokine & growth factor reviews* **35,** 63–70; 10.1016/j.cytogfr.2017.03.004 (2017).

141. Gu, Z. Complex heatmap visualization. *iMeta* **1,** e43; 10.1002/imt2.43 (2022).

142. Love, M. I., Huber, W. & Anders, S. Moderated estimation of fold change and dispersion for RNA-seq data with DESeq2. *Genome biology* **15,** 550; 10.1186/s13059-014-0550-8 (2014).

143. Kuleshov, M. V. *et al.* Enrichr: a comprehensive gene set enrichment analysis web server 2016 update. *Nucleic acids research* **44,** W90-7; 10.1093/nar/gkw377 (2016).

144. Korotkevich, G. *et al. Fast gene set enrichment analysis* (2016).

145. Wickham, H. & Sievert, C. *Ggplot2. Elegant graphics for data analysis.* 2nd ed. (Springer, Dordrecht, New York, op. 2016).

146. Satija, R., Farrell, J. A., Gennert, D., Schier, A. F. & Regev, A. Spatial reconstruction of single-cell gene expression data. *Nature biotechnology* **33,** 495–502; 10.1038/nbt.3192 (2015).

147. Ullman-Culleré, M. H. & Foltz, C. J. Body condition scoring: a rapid and accurate method for assessing health status in mice. *Laboratory animal science* **49,** 319–323 (1999).

148. Greenwald, N. F. *et al.* Whole-cell segmentation of tissue images with human-level performance using large-scale data annotation and deep learning. *Nature biotechnology* **40,** 555–565; 10.1038/s41587-021-01094-0 (2022).

149. Wells, M. A., Albrecht, P. & Ennis, F. A. Recovery from a viral respiratory infection. I. Influenza pneumonia in normal and T-deficient mice. *Journal of immunology (Baltimore, Md. : 1950)* **126,** 1036–1041; 10.4049/jimmunol.126.3.1036 (1981).

150. Duan, S. & Thomas, P. G. Balancing Immune Protection and Immune Pathology by CD8(+) T-Cell Responses to Influenza Infection. *Frontiers in immunology* **7,** 25; 10.3389/fimmu.2016.00025 (2016).

151. Enelow, R. I. *et al.* Structural and functional consequences of alveolar cell recognition by CD8(+) T lymphocytes in experimental lung disease. *The Journal of clinical investigation* **102,** 1653–1661; 10.1172/JCI4174 (1998).

152. Dietert, K. *et al.* Spectrum of pathogen- and model-specific histopathologies in mouse models of acute pneumonia. *PloS one* **12,** e0188251; 10.1371/journal.pone.0188251 (2017).

153. Bala, N. *et al.* T cell activation niches—Optimizing T cell effector function in inflamed and infected tissues*. *Immunological reviews* **306,** 164–180; 10.1111/imr.13047 (2021).

154. Bacher, P. & Scheffold, A. Flow-cytometric analysis of rare antigen-specific T cells. *Cytometry. Part A : the journal of the International Society for Analytical Cytology* **83,** 692–701; 10.1002/cyto.a.22317 (2013).

155. Poloni, C. *et al.* T-cell activation-induced marker assays in health and disease. *Immunology and cell biology* **101,** 491–503; 10.1111/imcb.12636 (2023).

156. Georg, P. *et al.* Complement activation induces excessive T cell cytotoxicity in severe COVID-19. *Cell* **185,** 493-512.e25; 10.1016/j.cell.2021.12.040 (2022).

157. Diamond, M. S. & Farzan, M. The broad-spectrum antiviral functions of IFIT and IFITM proteins. *Nature reviews. Immunology* **13,** 46–57; 10.1038/nri3344 (2013).

158. Wein, A. N. *et al.* CXCR6 regulates localization of tissue-resident memory CD8 T cells to the airways. *The Journal of experimental medicine* **216,** 2748–2762; 10.1084/jem.20181308 (2019).

159. Hatok, J. & Racay, P. Bcl-2 family proteins: master regulators of cell survival. *Biomolecular concepts* **7,** 259–270; 10.1515/bmc-2016-0015 (2016).

160. Hentschel, A. *et al.* A Homozygous PPP1R21 Splice Variant Associated with Severe Developmental Delay, Absence of Speech, and Muscle Weakness Leads to Activated Proteasome Function. *Molecular neurobiology* **60,** 2602–2618; 10.1007/s12035-023-03219-9 (2023).

161. Ferreira, M., Beullens, M., Bollen, M. & van Eynde, A. Functions and therapeutic potential of protein phosphatase 1: Insights from mouse genetics. *Biochimica et biophysica acta. Molecular cell research* **1866,** 16–30; 10.1016/j.bbamcr.2018.07.019 (2019).

162. Shimizu, S., Konishi, A., Kodama, T. & Tsujimoto, Y. BH4 domain of antiapoptotic Bcl-2 family members closes voltage-dependent anion channel and inhibits apoptotic mitochondrial changes and cell death. *Proceedings of the National Academy of Sciences of the United States of America* **97,** 3100–3105; 10.1073/pnas.97.7.3100 (2000).

163. Abu-Hamad, S. *et al.* The VDAC1 N-terminus is essential both for apoptosis and the protective effect of anti-apoptotic proteins. *Journal of cell science* **122,** 1906–1916; 10.1242/jcs.040188 (2009).

164. Grayson, J. M., Zajac, A. J., Altman, J. D. & Ahmed, R. Cutting edge: increased expression of Bcl-2 in antigen-specific memory CD8+ T cells. *Journal of immunology (Baltimore, Md. : 1950)* **164,** 3950–3954; 10.4049/jimmunol.164.8.3950 (2000).

165. Garcia, S., DiSanto, J. & Stockinger, B. Following the development of a CD4 T cell response in vivo: from activation to memory formation. *Immunity* **11,** 163–171; 10.1016/S1074-7613(00)80091-6 (1999).

166. Gramaglia, I. *et al.* The OX40 costimulatory receptor determines the development of CD4 memory by regulating primary clonal expansion. *Journal of immunology (Baltimore, Md. : 1950)* **165,** 3043–3050; 10.4049/jimmunol.165.6.3043 (2000).

167. Ishii, N., Takahashi, T., Soroosh, P. & Sugamura, K. OX40-OX40 ligand interaction in T-cell-mediated immunity and immunopathology. *Advances in immunology* **105,** 63–98; 10.1016/S0065-2776(10)05003-0 (2010).

168. Macián, F., López-Rodríguez, C. & Rao, A. Partners in transcription: NFAT and AP-1. *Oncogene* **20,** 2476–2489; 10.1038/sj.onc.1204386 (2001).

169. Han, X. *et al.* ID2 and ID3 are indispensable for Th1 cell differentiation during influenza virus infection in mice. *Eur. J. Immunol.* **49,** 476–489; 10.1002/eji.201847822 (2019).

170. Schwarz, D. A., Katayama, C. D. & Hedrick, S. M. Schlafen, a new family of growth regulatory genes that affect thymocyte development. *Immunity* **9,** 657–668; 10.1016/s1074-7613(00)80663-9 (1998).

171. Baine, I., Basu, S., Ames, R., Sellers, R. S. & Macian, F. Helios induces epigenetic silencing of Il2 gene expression in regulatory T cells. *Journal of immunology (Baltimore, Md. : 1950)* **190,** 1008–1016; 10.4049/jimmunol.1200792 (2012).

172. Neyens, D. *et al.* HELIOS-expressing human CD8 T cells exhibit limited effector functions. *Frontiers in immunology* **14,** 1308539; 10.3389/fimmu.2023.1308539 (2023).

173. Nansen, A., Marker, O., Bartholdy, C. & Thomsen, A. R. CCR2+ and CCR5+ CD8+ T cells increase during viral infection and migrate to sites of infection. *Eur. J. Immunol.* **30,** 1797–1806; 10.1002/1521-4141(200007)30:7<1797::AID-IMMU1797>3.0.CO;2-B (2000).

174. Bakos, E. *et al.* CCR2 Regulates the Immune Response by Modulating the Interconversion and Function of Effector and Regulatory T Cells. *Journal of immunology (Baltimore, Md. : 1950)* **198,** 4659–4671; 10.4049/jimmunol.1601458 (2017).

175. Hutloff, A. *et al.* ICOS is an inducible T-cell co-stimulator structurally and functionally related to CD28. *Nature* **402,** 21–24; 10.1038/35005523 (1999).

176. Humphreys, I. R. *et al.* A critical role for ICOS co-stimulation in immune containment of pulmonary influenza virus infection. *Eur. J. Immunol.* **36,** 2928–2938; 10.1002/eji.200636155 (2006).

177. Takahashi, N. *et al.* Impaired CD4 and CD8 effector function and decreased memory T cell populations in ICOS-deficient patients. *Journal of immunology (Baltimore, Md. : 1950)* **182,** 5515–5527; 10.4049/jimmunol.0803256 (2009).

178. Sancho, M., Diani, E., Beato, M. & Jordan, A. Depletion of human histone H1 variants uncovers specific roles in gene expression and cell growth. *PLoS genetics* **4,** e1000227; 10.1371/journal.pgen.1000227 (2008).

179. Kim, D.-H. *et al.* Regulation of chitinase-3-like-1 in T cell elicits Th1 and cytotoxic responses to inhibit lung metastasis. *Nature communications* **9,** 503; 10.1038/s41467-017-02731-6 (2018).

180. Collins, S. *et al.* Opposing regulation of T cell function by Egr-1/NAB2 and Egr-2/Egr-3. *Eur. J. Immunol.* **38,** 528–536; 10.1002/eji.200737157 (2008).

181. Ross, S. H. & Cantrell, D. A. Signaling and Function of Interleukin-2 in T Lymphocytes. *Annual review of immunology* **36,** 411–433; 10.1146/annurev-immunol-042617-053352 (2018).

182. Cepek, K. L. *et al.* Adhesion between epithelial cells and T lymphocytes mediated by E-cadherin and the alpha E beta 7 integrin. *Nature* **372,** 190–193; 10.1038/372190a0 (1994).

183. Schenkel, J. M. & Masopust, D. Tissue-resident memory T cells. *Immunity* **41,** 886–897; 10.1016/j.immuni.2014.12.007 (2014).

184. Cham, C. M., Driessens, G., O'Keefe, J. P. & Gajewski, T. F. Glucose deprivation inhibits multiple key gene expression events and effector functions in CD8+ T cells. *Eur. J. Immunol.* **38,** 2438–2450; 10.1002/eji.200838289 (2008).

185. Finlay, D. K. *et al.* PDK1 regulation of mTOR and hypoxia-inducible factor 1 integrate metabolism and migration of CD8+ T cells. *The Journal of experimental medicine* **209,** 2441–2453; 10.1084/jem.20112607 (2012).

186. Palazon, A. *et al.* An HIF-1α/VEGF-A Axis in Cytotoxic T Cells Regulates Tumor Progression. *Cancer cell* **32,** 669-683.e5; 10.1016/j.ccell.2017.10.003 (2017).

187. Vallion, R. *et al.* Regulatory T Cell Stability and Migration Are Dependent on mTOR. *Journal of immunology (Baltimore, Md. : 1950)* **205,** 1799–1809; 10.4049/jimmunol.1901480 (2020).

188. Camp, R. L., Scheynius, A., Johansson, C. & Puré, E. CD44 is necessary for optimal contact allergic responses but is not required for normal leukocyte extravasation. *The Journal of experimental medicine* **178,** 497–507; 10.1084/jem.178.2.497 (1993).

189. Savinov, A. Y. & Strongin, A. Y. Defining the roles of T cell membrane proteinase and CD44 in type 1 diabetes. *IUBMB life* **59,** 6–13; 10.1080/15216540601187795 (2007).

190. Nandi, A., Estess, P. & Siegelman, M. Bimolecular complex between rolling and firm adhesion receptors required for cell arrest; CD44 association with VLA-4 in T cell extravasation. *Immunity* **20,** 455–465; 10.1016/S1074-7613(04)00077-9 (2004).

191. Blass, S. L., Puré, E. & Hunter, C. A. A role for CD44 in the production of IFN-gamma and immunopathology during infection with Toxoplasma gondii. *Journal of immunology (Baltimore, Md. : 1950)* **166,** 5726–5732; 10.4049/jimmunol.166.9.5726 (2001).

192. Fu, Q. *et al.* CD44 deficiency leads to decreased proinflammatory cytokine production in lung induced by PCV2 in mice. *Research in veterinary science* **97,** 498–504; 10.1016/j.rvsc.2014.09.012 (2014).

193. Arbonés, M. L. *et al.* Lymphocyte homing and leukocyte rolling and migration are impaired in L-selectin-deficient mice. *Immunity* **1,** 247–260; 10.1016/1074-7613(94)90076-0 (1994).

194. Mohammed, R. N. *et al.* ADAM17-dependent proteolysis of L-selectin promotes early clonal expansion of cytotoxic T cells. *Scientific reports* **9,** 5487; 10.1038/s41598-019-41811-z (2019).

195. Richards, H., Longhi, M. P., Wright, K., Gallimore, A. & Ager, A. CD62L (L-selectin) down-regulation does not affect memory T cell distribution but failure to shed compromises anti-viral immunity. *Journal of immunology (Baltimore, Md. : 1950)* **180,** 198–206; 10.4049/jimmunol.180.1.198 (2008).

196. Yang, S., Liu, F., Wang, Q. J., Rosenberg, S. A. & Morgan, R. A. The shedding of CD62L (L-selectin) regulates the acquisition of lytic activity in human tumor reactive T lymphocytes. *PloS one* **6,** e22560; 10.1371/journal.pone.0022560 (2011).

197. Mrass, P. *et al.* CD44 mediates successful interstitial navigation by killer T cells and enables efficient antitumor immunity. *Immunity* **29,** 971–985; 10.1016/j.immuni.2008.10.015 (2008).

198. Baaten, B. J., Li, C.-R. & Bradley, L. M. Multifaceted regulation of T cells by CD44. *Communicative & integrative biology* **3,** 508–512; 10.4161/cib.3.6.13495 (2010).

199. Goddery, E. N. *et al.* Microglia and Perivascular Macrophages Act as Antigen Presenting Cells to Promote CD8 T Cell Infiltration of the Brain. *Frontiers in immunology* **12,** 726421; 10.3389/fimmu.2021.726421 (2021).

200. Prizant, H. *et al.* CXCL10+ peripheral activation niches couple preferred sites of Th1 entry with optimal APC encounter. *Cell reports* **36,** 109523; 10.1016/j.celrep.2021.109523 (2021).

201. McGill, J., van Rooijen, N. & Legge, K. L. Protective influenza-specific CD8 T cell responses require interactions with dendritic cells in the lungs. *The Journal of experimental medicine* **205,** 1635–1646; 10.1084/jem.20080314 (2008).

202. Heesch, K. *et al.* The function of the chemokine receptor CXCR6 in the T cell response of mice against Listeria monocytogenes. *PloS one* **9,** e97701; 10.1371/journal.pone.0097701 (2014).

203. Agostini, C. *et al.* Role for CXCR6 and its ligand CXCL16 in the pathogenesis of T-cell alveolitis in sarcoidosis. *American journal of respiratory and critical care medicine* **172,** 1290–1298; 10.1164/rccm.200501-142OC (2005).

204. Jayasekera, J. P., Moseman, E. A. & Carroll, M. C. Natural antibody and complement mediate neutralization of influenza virus in the absence of prior immunity. *Journal of virology* **81,** 3487–3494; 10.1128/jvi.02128-06 (2007).

205. Wu, H., Haist, V., Baumgärtner, W. & Schughart, K. Sustained viral load and late death in Rag2-/- mice after influenza A virus infection. *Virology journal* **7,** 172; 10.1186/1743-422X-7-172 (2010).

206. Eichelberger, M., Allan, W., Zijlstra, M., Jaenisch, R. & Doherty, P. C. Clearance of influenza virus respiratory infection in mice lacking class I major histocompatibility complex-restricted CD8+ T cells. *The Journal of experimental medicine* **174,** 875–880; 10.1084/jem.174.4.875 (1991).

207. Mozdzanowska, K., Furchner, M., Maiese, K. & Gerhard, W. CD4+ T cells are ineffective in clearing a pulmonary infection with influenza type A virus in the absence of B cells. *Virology* **239,** 217–225; 10.1006/viro.1997.8882 (1997).

208. Laidlaw, B. J. *et al.* CD4+ T cell help guides formation of CD103+ lung-resident memory CD8+ T cells during influenza viral infection. *Immunity* **41,** 633–645; 10.1016/j.immuni.2014.09.007 (2014).

209. McMaster, S. R. *et al.* Pulmonary antigen encounter regulates the establishment of tissue-resident CD8 memory T cells in the lung airways and parenchyma. *Mucosal immunology* **11,** 1071–1078; 10.1038/s41385-018-0003-x (2018).

210. Zhou, A. C., Batista, N. V. & Watts, T. H. 4-1BB Regulates Effector CD8 T Cell Accumulation in the Lung Tissue through a TRAF1-, mTOR-, and Antigen-Dependent Mechanism to Enhance Tissue-Resident Memory T Cell Formation during Respiratory Influenza Infection. *Journal of immunology (Baltimore, Md. : 1950)* **202,** 2482–2492; 10.4049/jimmunol.1800795 (2019).

211. Lee, B. O. *et al.* CD4 T cell-independent antibody response promotes resolution of primary influenza infection and helps to prevent reinfection. *Journal of immunology (Baltimore, Md. : 1950)* **175,** 5827–5838; 10.4049/jimmunol.175.9.5827 (2005).

212. Moskophidis, D. & Kioussis, D. Contribution of virus-specific CD8+ cytotoxic T cells to virus clearance or pathologic manifestations of influenza virus infection in a T cell receptor transgenic mouse model. *The Journal of experimental medicine* **188,** 223–232; 10.1084/jem.188.2.223 (1998).

213. Yunis, J., Short, K. R. & Di Yu. Severe respiratory viral infections: T-cell functions diverging from immunity to inflammation. *Trends in microbiology* **31,** 644–656; 10.1016/j.tim.2022.12.008 (2023).

6. Appendix

6.1 Configuration LSRFortessa

Table 6-1: Configuration LSRFortessa

Laser	Detector	1. Pass	2. Pass
Blue 488 nm (100 mW)	A	685 LP	695/40 BP
	B	505 LP	525/50 BP
	C	-	488/10 BP
Yellow / green 561 nm (100 mW)	A	750	780/60
	B	685	710/50
	C	635	670/30
	D	600	610/20
	E	-	585/15
	F	-	-
	G	-	-
	H	-	-
Red 639 nm (40 mW)	A	750	780/60
	B	685	710/50
	C	-	670/14
Violet 404 nm (50 mW)	A	705	780/60
	B	685	710/50
	C	635	660/20
	D	600	610/20
	E	505	525/50
	F	-	450/50
	G	-	-
	H	-	-
UV 355 nm (60 mW)	A	505	530/30
	B	-	405/20
	C	-	-

6.2 IMC supplement

Table 6-2: Antibodies used in IMC

Isotope	Antibody	Clone	Company	Dilution
141Pr	Epcam	EPR20532-222	Abcam, Cambridge, UK	1:200
142Nd	B220	RA3-6B2	Biolegend, San Diego, USA	1:800
143Nd	CD3	E4T1B	Dianova, Hamburg, Germany	1:50
144Nd	CD138	polyclonal	Thermo Fisher, Waltham, USA	1:200
145Nd	CD8	4SM15	eBiosciences, San Diego, USA	1:100
146Nd	CD31	SZ31	Dianova, Hamburg, Germany	1:200
147Sm	CD16	SP175	Abcam, Cambridge, UK	1:2000
148Nd	CD206	E6T5J	Cell Signaling Tech., Danvers, USA	1:100
149Sm	CD19	6OMP31	Thermo Fisher, Waltham, USA	1:2000
150Nd	CD11b	M1/70.15	Thermo Fisher Waltham, USA	1:50
151Eu	CD44	IM7	Biolegend, San Diego, USA	1:1000
152Sm	CD68	FA-11	Novus Biologicals, Littleton, USA	1:800
153Eu	CD127	ab95024	Abcam, Cambridge, UK	1:800
154Sm	CD69	Orb13326	Biorbyt, Cambridge, UK	1:400
155Gd	Iba1	E4O4W	Cell Signaling Tech., Danvers, USA	1:500
158Gd	CRTH2	PA5-20333	Thermo Fisher, Waltham, USA	1:800
159Tb	Eomes	Dan11mag	Thermo Fisher, Waltham, USA	1:100
160Gd	Ly6G	1A8	Biolegend, San Diego, USA	1:800
161Dy	CD4	4SM95	Thermo Fisher, Waltham, USA	1:400
162Dy	F4.80	BM8	Thermo Fisher, Waltham, USA	1:400
164Dy	CD25	E9W2J	Cell Signaling, Danvers, USA	1:100
165Ho	MHC II	M5/114.15.2	Thermo Fisher, Waltham, USA	1:200
167Er	CD137	E2J5H	Cell Signaling, Danvers, USA	1:200
168Er	CD45	30-F11	Biolegend, San Diego, USA	1:2400
169Tm	FoxP3	FJK-16s	Thermo Fisher, Waltham, USA	1:200
170Er	KI67	16A8	Biolegend, San Diego, USA	1:2000
171Yb	CD11c	D1V9Y	Cell Signaling, Danvers, USA	1:200
172Yb	CD56	RNL-1	Novus Biologicals, Littleton, USA	1:100
176Yb	Histone	D1H2	Cell Signaling, Danvers, USA	1:1200
191Ir	DNA1		Fluidigm, San Francisco, USA	1:400
193Ir	DNA2		Fluidigm, San Francisco, USA	1:400

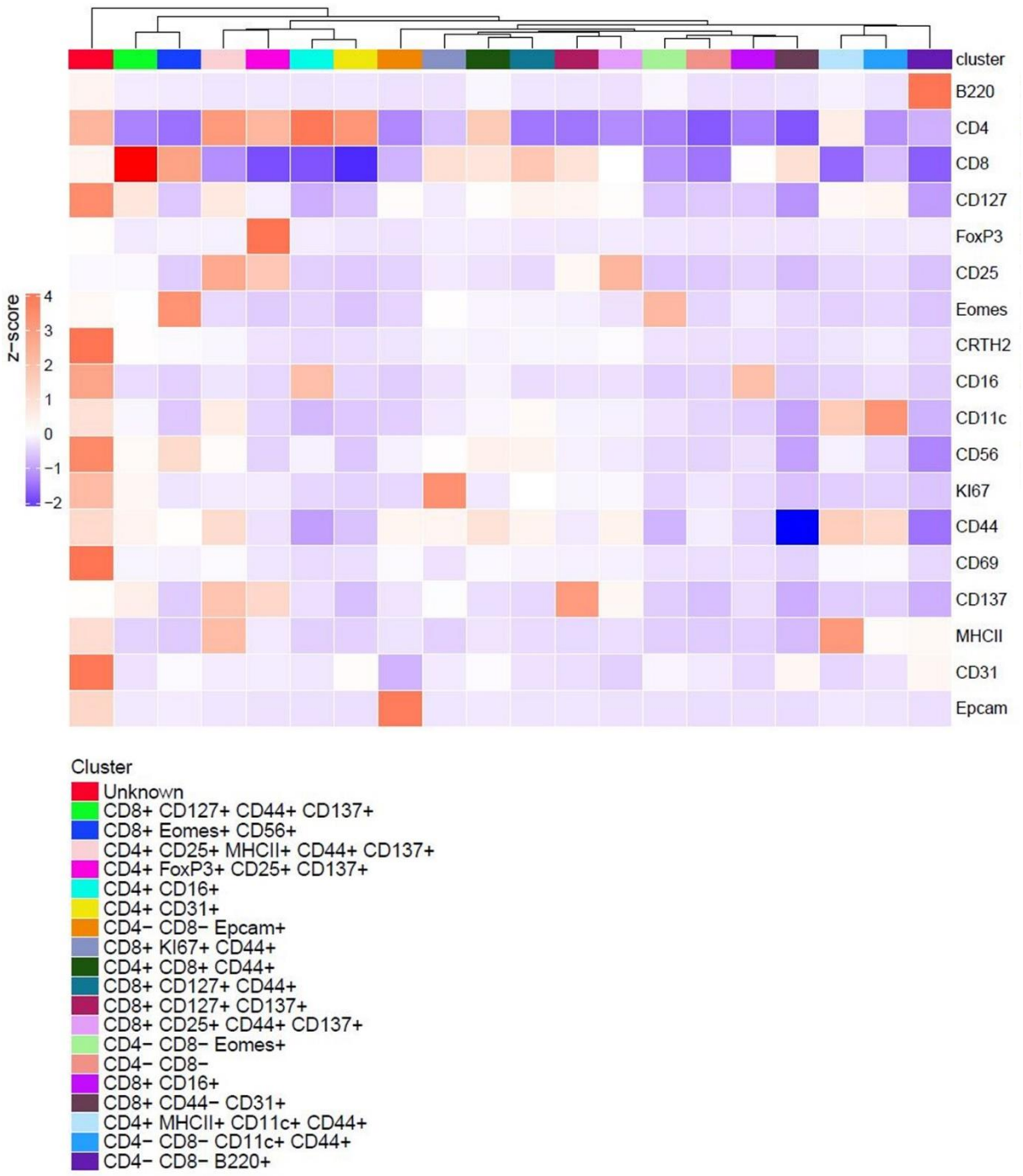

Figure 6-1: IMC annotation heatmap. *The heatmap is showing z-score normalized marker expression of cells within the different clusters acquired using IMC. Based on the marker expression, clusters were annotated as shown below.*

6.3 scRNAseq supplement

Table 6-3: top10 differential expressed genes per cluster

cluster	gene	avg_log2FC	pct.1	pct.2	p_val	p_val_adj
0	Cd8b1	1.433767722	0.826	0.285	0	0
0	Dapl1	1.905070229	0.567	0.17	0	0
0	Ccr7	1.166137044	0.669	0.323	0	0
0	Fam241a	1.922171077	0.482	0.161	0	0
0	Actn1	1.034295286	0.497	0.252	0	0
0	Ccr9	2.103479062	0.133	0.028	1.0729E-273	3.4639E-269
0	Slc6a19	3.806965149	0.07	0.006	6.0404E-246	1.9501E-241
1	Igfbp4	2.487403271	0.511	0.157	0	0
1	Lef1	1.301270489	0.781	0.463	0	0
1	Cd4	1.19348858	0.462	0.173	0	0
1	Ccr7	1.096851597	0.612	0.353	0	0
1	Satb1	1.133722096	0.762	0.509	0	0
1	Rflnb	1.434915938	0.435	0.21	0	0
1	Ly6c1	2.570713054	0.239	0.054	0	0
1	St8sia6	3.030854593	0.166	0.019	0	0
1	Pdlim4	3.770757794	0.127	0.011	0	0
1	Trib2	1.510718227	0.359	0.17	1.3806E-289	4.4574E-285
2	Ly6c2	1.622877509	0.875	0.277	0	0
2	Ccl5	1.191483787	0.851	0.302	0	0
2	Cd8b1	1.005064056	0.847	0.38	0	0
2	Eomes	1.858127338	0.272	0.055	0	0
2	Gzmm	3.20794094	0.201	0.021	0	0
2	1700025G04Rik	1.645722165	0.289	0.078	6.3267E-250	2.0426E-245
2	Plek	1.544450875	0.265	0.07	2.1662E-235	6.9936E-231
2	Rnf138	1.03129572	0.654	0.315	3.7472E-233	1.2098E-228
2	Samd3	1.950654742	0.19	0.04	1.9997E-226	6.4559E-222
2	Ifitm10	1.545169279	0.247	0.064	4.4227E-221	1.4279E-216
3	Ccl5	3.686233329	0.969	0.299	0	0
3	Nkg7	2.631181623	0.961	0.42	0	0
3	S100a6	1.519256348	0.879	0.404	0	0
3	Cd8a	2.500014871	0.721	0.261	0	0

3	Ccl4	4.200842887	0.498	0.056	0	0
3	Cd8b1	1.82891514	0.828	0.387	0	0
3	Itgb1	1.700346743	0.703	0.307	0	0
3	Lgals1	1.486573586	0.799	0.413	0	0
3	Itga1	3.437841238	0.443	0.061	0	0
3	Id2	1.681556558	0.849	0.467	0	0
4	S100a4	1.673439201	0.711	0.243	0	0
4	S100a6	1.171499816	0.807	0.398	0	0
4	Maf	1.804911634	0.596	0.201	0	0
4	Ahnak	1.286508139	0.806	0.468	0	0
4	Lgals1	1.217735698	0.737	0.408	0	0
4	Cd4	1.579494535	0.518	0.204	0	0
4	Rora	1.743540175	0.48	0.181	0	0
4	S100a11	1.171740137	0.779	0.503	0	0
4	Vim	1.301171693	0.751	0.516	0	0
4	S100a10	1.10959074	0.883	0.703	0	0
5	Tbc1d4	2.818172892	0.357	0.077	0	0
5	Ctla4	2.257358592	0.378	0.093	7.0827E-270	2.2866E-265
5	Foxp3	3.101271569	0.178	0.023	1.0605E-252	3.4239E-248
5	Izumo1r	2.528603643	0.368	0.101	2.7066E-239	8.7383E-235
5	Tnfrsf4	2.137640831	0.242	0.053	8.1973E-190	2.6465E-185
5	Ikzf2	2.069242997	0.413	0.148	7.5843E-182	2.4486E-177
5	Cd4	1.539591025	0.52	0.221	2.8632E-174	9.2439E-170
5	Lrrc32	3.522700624	0.07	0.007	3.3536E-118	1.0827E-113
5	Rgs16	2.566098754	0.104	0.022	2.64894E-82	8.55212E-78
5	Gpm6b	3.269511824	0.068	0.011	3.05459E-74	9.86173E-70
6	Tmem176a	3.797066332	0.861	0.091	0	0
6	Tmem176b	3.623579246	0.846	0.099	0	0
6	S100a4	2.764577344	0.968	0.248	0	0
6	Cxcr6	2.27114659	0.811	0.182	0	0
6	Maf	2.065040386	0.826	0.205	0	0
6	Capg	2.690135466	0.754	0.156	0	0
6	Lmo4	3.311984256	0.821	0.233	0	0
6	Ramp1	3.071236225	0.75	0.163	0	0
6	S100a6	2.355153351	0.977	0.406	0	0

6	Ccr2	2.682966314	0.675	0.117	0	0
7	Ifit3	3.509394472	0.819	0.083	0	0
7	Isg15	2.938930554	0.905	0.218	0	0
7	Zbp1	2.686691646	0.817	0.175	0	0
7	Irf7	2.516741332	0.801	0.174	0	0
7	Ly6c2	2.759399348	0.897	0.298	0	0
7	Bst2	2.404999488	0.899	0.303	0	0
7	Rnf213	2.339121568	0.8	0.219	0	0
7	Ifit1	3.160901711	0.65	0.072	0	0
7	Usp18	3.370480267	0.626	0.068	0	0
7	Slfn5	2.52514482	0.708	0.159	0	0
8	Mki67	6.285110939	0.875	0.023	0	0
8	Pclaf	7.260754156	0.856	0.009	0	0
8	Stmn1	4.712842269	0.97	0.126	0	0
8	Birc5	7.308701274	0.814	0.007	0	0
8	Lmnb1	3.643313753	0.863	0.098	0	0
8	Top2a	5.293622293	0.819	0.057	0	0
8	Cks1b	4.77526614	0.789	0.033	0	0
8	Hmgn2	3.049594749	0.91	0.182	0	0
8	Cdca8	6.085586085	0.729	0.012	0	0
8	Hist1h1b	6.14947986	0.716	0.029	0	0
9	Ccl5	1.90274595	0.966	0.326	0	0
9	Ly6c2	1.712210014	0.853	0.308	0	0
9	Klre1	2.766261106	0.359	0.044	0	0
9	Klra7	4.470358581	0.299	0.018	0	0
9	Klra6	4.354502192	0.157	0.01	0	0
9	Klra1	4.230084183	0.149	0.008	0	0
9	Xcl1	2.355921928	0.389	0.068	3.1588E-294	1.0198E-289
9	Klrc2	2.541439266	0.37	0.064	3.3566E-284	1.0837E-279
9	Il2rb	1.635309524	0.794	0.315	1.6253E-250	5.2474E-246
9	Klrk1	2.184778615	0.467	0.111	1.1496E-248	3.7114E-244
10	Il2rb	2.381274839	0.861	0.314	0	0
10	Ifng	2.565005043	0.58	0.112	0	0
10	Xcl1	3.57132305	0.527	0.065	0	0
10	Klrk1	2.718403648	0.545	0.109	0	0

10	Klrb1c	5.159755066	0.445	0.017	0	0
10	Klrc2	2.826548584	0.406	0.063	0	0
10	Mmp9	5.116932293	0.263	0.008	0	0
10	Gm36723	3.545708696	0.257	0.021	0	0
10	Atp8a2	4.022304886	0.197	0.013	0	0
10	Cxcr6	1.890359946	0.715	0.202	9.7971E-304	3.163E-299
11	Ifit3	4.360696292	0.791	0.096	0	0
11	Ifit1	4.442100494	0.752	0.078	0	0
11	Isg15	4.015926813	0.901	0.229	0	0
11	Slfn5	3.970615416	0.803	0.165	0	0
11	Isg20	4.089137217	0.725	0.1	0	0
11	Irf7	3.338450164	0.793	0.185	0	0
11	Zbp1	3.130400919	0.78	0.187	0	0
11	Bst2	3.30110311	0.868	0.314	0	0
11	Rnf213	2.906739346	0.76	0.23	0	0
11	Iigp1	4.303530691	0.576	0.064	0	0
12	Tnfrsf4	4.878723963	0.777	0.052	0	0
12	Ikzf2	3.755854398	0.833	0.151	0	0
12	Ctla4	3.760262814	0.773	0.097	0	0
12	Foxp3	4.91024103	0.548	0.023	0	0
12	Il1rl1	5.591224362	0.211	0.007	0	0
12	Itgb8	5.614509171	0.132	0.003	0	0
12	Rgs16	4.121221579	0.299	0.022	4.8109E-289	1.5532E-284
12	Ptpn5	5.880972983	0.084	0.001	1.4871E-269	4.801E-265
12	Tnfrsf9	4.444856114	0.276	0.02	4.1298E-266	1.3333E-261
12	Ttn	4.447116837	0.174	0.01	7.3295E-205	2.3663E-200
13	Dntt	9.086883582	1	0.006	0	0
13	Arpp21	10.93302369	0.951	0.001	0	0
13	Mki67	5.709076312	0.963	0.038	0	0
13	Ly6d	7.495033332	0.951	0.027	0	0
13	Endou	10.39044402	0.914	0.001	0	0
13	Pclaf	5.956944697	0.926	0.024	0	0
13	Marcks	5.307781142	0.926	0.03	0	0
13	Hist1h1b	5.020480998	0.914	0.04	0	0
13	Birc5	5.822712454	0.877	0.021	0	0

13	Cdca7	5.910457973	0.864	0.024	0	0
14	Trdc	5.513515763	0.973	0.051	0	0
14	Cd163l1	8.097019193	0.883	0.009	0	0
14	Tcrg-C1	5.640785659	0.901	0.045	0	0
14	Tmem176a	3.787448734	0.905	0.115	0	0
14	Trdv4	9.75176955	0.786	0.003	0	0
14	Tmem176b	3.763776309	0.901	0.122	0	0
14	S100a4	2.576783114	0.966	0.272	0	0
14	Cxcr6	2.710593205	0.886	0.201	0	0
14	Maf	2.429585139	0.873	0.224	0	0
14	Capg	2.841165961	0.803	0.174	0	0

Table 6-4: GSEA gene list

Name	Genes included
HALLMARK_INTERFERON_ALPHA_RESPONSE (systematic name: MM3877) Pubmed 30224793	Trim25 Il15 Stat2 Procr Wars1 Psma3 Il4ra Ly6e Trim21 Elf1 Irf9 Psme2 Psme1 Ifit3 Casp8 Ifi27 Trim26 Csf1 Samd9l Usp18 Psmb9 Psmb8 Uba7 Cxcl10 Eif2ak2 C1s1 Isg15 Irf7 Cxcl11 Nub1 Txnip Adar Ripk2 Ifitm3 Gmpr Lap3 Herc6 Lpar6 Ube2l6 Rtp4 Epsti1 Tmem140 Ifitm1 Bst2 Ifi35 Ifih1 Pnpt1 Ogfr Parp14

	Ccrl2 Mvb12a Cmtr1 Batf2 Trim14 Sp110 Trafd1 Gbp3 Nmi Isg20 Rsad2 Dhx58 Parp9 Ifitm2 Rnf31 Ifi30 Tdrd7 Parp12 Slc25a28 Oasl1 Oas1a Ddx60 Helz2 Lamp3 Ifi44 Ncoa7 Tent5a Trim12c B2m Cnp Plscr1 Ifi44l Cd74 Casp1 Il7 Irf1 Irf2 Cd47 Mov10 Mx2 Sell Tap1 Ifit2 Lgals3bp Cmpk2
GOBP_LEUKOCYTE_ADHESION_TO_VASCULAR_ENDOTHELIAL_CELL (GO:0061756) PMID:23897866	Ccl21b Ccl21d Pawr Add2 Alox5 Rhoa Capn1

	Ccr2 Cx3cr1 Ext1 Fut4 Fut7 Fut9 Gcnt1 Gp1ba Icam1 Irak1 Il6 Itga4 Itgam Itgb1 Itgb2 Itgb7 Klf4 Lep Madcam1 Mdk Ccl21a Ptafr Rela Rock1 Ccl25 Cxcl12 Sele Sell Selp Selplg St3gal4 Spn Tnf Traf6 Vcam1 Ets1 Chst4 Podxl2 Elane Chst2 Nfat5 Ccl28 Golph3 Jam2 Slc39a8 Zdhhc21 Lrg1